




Universitetet  
i Stavanger

**FACULTY OF SCIENCE AND  
TECHNOLOGY**

## **MASTER'S THESIS**

Study programme/specialisation:  Petroleum Geoscience Engineering	Spring semester, 2019  Open
Author: Olav Josefsen	 ..... (signature of author)
Supervisor:  Dora Luz Marin Restrepo	
Title of the master's thesis:  Origin of anticline structure in the southern Hammerfest Basin and their impact in sedimentation and coarse-grained distribution	
Credits: 30	
Keywords: Hammerfest Basin Anticline Syncline Turbidites Syn-rift	Number of pages: 81  Stavanger, 15/06-2019

Copyright

By

Olav Josefsen

2019

**Origin of anticline structure in the southern Hammerfest Basin and their  
impact in sedimentation and coarse-grained distribution**

by

Olav Josefsen

**Master thesis**

Presented to the Faculty of Science and Technology  
The University of Stavanger

**The University of Stavanger**

June 2019

## Acknowledgment

I want to express my sincere gratitude to my supervisor Dora Luz Marin Restrepo for her valuable guidance and expertise throughout this thesis. I would also thank Nestor Cardozo and Alejandro Escalona for their feedbacks and constructive discussions during this project, which were much appreciated. Credits to Jennifer Elisabeth Cunningham, Luis Alberto Rojo Moraleda and Andreas Habel for their technical support, knowledge, and input about the different geological software's used in this thesis. The computer programs used were Landmark Decision Space (Halliburton), 3DMove (Midland Valley), Petrel (Schlumberger), GeoTeric and StructureSolver. Lastly, I would like to thank my fellow students, especially Thomas Meldahl Olsen and Ville August Aarseth. These five years would not have been the same without you.

## Abstract

### **Origin of anticline structure in the southern Hammerfest Basin and their impact in sedimentation and coarse-grained distribution.**

Olav Josefsen

University of Stavanger, 2019

Supervisor: Dora Luz Marin Restrepo

This thesis shows how extensional fault-related folding holds a fundamental control on basin physiography and syn-kinematic sediments. The study has used two- and three-dimensional seismic data in combination with a stratigraphic attribute, well data and forward modeling to investigate an anticline structure in the southern part of the Hammerfest Basin, SW Barents Sea. The fault geometry changes significantly along the ENE –WSW striking Troms-Finnmark Fault Complex, suggesting different kinematic evolution alongside the same fault zone. From the forward modeling and the distinctive hanging-wall deformation patterns, the extensional fault-related anticline structure was developed by ramp-flat-ramp geometry during the Late Jurassic – Early Cretaceous rifting period. In response to the anticline development, a syncline was formed, which affected a major submarine fan system within the Knurr Formation. These structures controlled the depositional architecture of the syn-rift sediments. As the syncline developed, the turbidite deposition shifted from a northern to a north-eastern direction.

## Table of Contents

Acknowledgment.....	IV
Abstract .....	V
List of Tables.....	VIII
List of Figures .....	IX
1. Introduction .....	1
2. Geological setting.....	5
2.1 Structural Framework.....	6
2.2 Stratigraphic Framework.....	9
2.3 Main structural elements .....	12
2.3.1 Hammerfest Basin .....	12
2.3.1 Finnmark Platform.....	13
2.3.2 Troms-Finnmark Fault Complex .....	13
2.3.3 Ringvassøy-Loppa Fault Complex.....	14
3. Data and Methodology .....	15
3.1 Seismic well tie .....	16
3.2 Seismic approach.....	17
3.3 Forward Modelling.....	18
4. Results and observations .....	21
4.1 Structural Style .....	21
4.1.1 Main fault .....	23
4.1.2 NNE – SSW trend .....	23
4.1.3 E – W trend.....	25
4.2 Time thickness maps .....	27
4.3 Hanging-wall folds.....	29
4.4 Forward Modelling.....	38
Section AA' .....	38
Section BB' .....	38
Section CC' .....	41
Section DD' .....	41
Section EE' .....	44
Section FF' .....	44
4.4 Wells.....	47
4.5 Iso-slices and rms amplitude .....	49
5. Interpretation .....	52
5.1 Late Jurassic to Early Cretaceous extension and structural styles.....	52

5.2	Anticline development and fault geometry .....	53
5.3	Stratigraphy .....	55
5	Discussion .....	56
5.1	Comparison with other mechanisms and extensional fault-fold systems .....	56
5.1.1	Roll-over and ramp-flat-ramp.....	56
5.1.2	<i>Inversion</i> .....	59
5.1.3	<i>Other mechanisms</i> .....	59
5.2	Evolutionary model along Troms-Finnmark Fault Complex .....	62
5.3	Anticline and syncline development and its impact on coarse-grained sediments.....	64
	Conclusion.....	66
	Future work .....	66
	References .....	67

## List of Tables

<b>Table 1.</b> Petrophysical data available in this study .....	16
<b>Table 2.</b> Time depth table from well 7120/10-1, 7120/12-2 and 7120/12-4 used in the depth conversion process. ....	18



## List of Figures

<b>Fig. 1.</b> Geometries associated with extensional fault-related folds. (a) Fault propagation fold (modified from Schlische, 1995). (b) Reverse drag folds (modified from Barnett et al., 1987). (c) Listric fault (modified from Rykkelid and Fossen, 2002). (d) Transverse folding (Schlische, 1995). (e) Compaction (Skuce, 1996). (f) Inversion (Indrevær et al., 2016).....	1
<b>Fig. 2.</b> Four main growth basin geometries associated in the extensional setting. (a) Fault-tip monocline. (b) Standard growth basin. (c) Rollover basin. (d) Fault-bend synclinal basin. (Serck and Braathen, 2019) .....	2
<b>Fig. 3.</b> a) Bathymetric map of the Arctic Ocean (Jakobsson et al., 2012). (b) Geological elements of the Hammerfest Basin, main structural features, well location, and the data used in this study. Green rectangle displays the location of the Goliat anticline. (Modified from Marin et al., 2017).....	3
<b>Fig. 4.</b> a) Time depth converted section for regional line BSS01-112 close to the Troms-Finnmark Fault Complex. The alternative interpretations suggest (b) listric, (c) listric with a pronounced ramp-flat-ramp geometry or (d) Stepped planar segments. The orange, purple, light blue and green color correspond to Paleozoic, Triassic, Jurassic, and Cretaceous respectively. (Mulrooney et al., 2017).....	4
<b>Fig. 5.</b> Main structural elements of the greater Barents Sea (Henriksen et al., 2011).....	5
<b>Fig. 6.</b> Major structural elements in the Barents Sea shelf during the Carboniferous and Permian. Elevated highs marked in green and subsided basins marked with yellow. Stippled areas indicate later developing structures. (Worsley and Nøttvedt, 2008).....	6
<b>Fig. 7.</b> Main structural elements of the western Barents Sea and adjacent areas. Colors reflect the focus of the tectonic activity. Modified from Faleide et al. (2008) & Faleide et al. (2010). .....	8
<b>Fig. 8.</b> Norwegian Barents Sea stratigraphic chart of the main lithologies in the Hammerfest Basin, Bjarmeland Platform, Nordkapp Basin, and Finnmark Platform. Summary of the structural history is shown in the right column. (Ohm et al., 2008).....	9
<b>Fig. 9.</b> Stratigraphy chart of the Lower Cretaceous succession in the Hammerfest Basin, showing seven sequences correlated with well 7120/10-2. The sequences used in this study are sequence (S0) and sequence 2 (S2). (Marin et al., 2017).....	10
<b>Fig. 10.</b> Sedimentological log of well 7120/10-2 interpreted by Marin et al. (2017) based on cores places the lower section turbidites in a slope setting, before prograding into a proximal setting. The uppermost core section is situated in lobe fringe/off axis environment. ....	11
<b>Fig. 11.</b> Structural elements of the Hammerfest Basin. Current oil (green) and gas (red) fields are displayed throughout the Hammerfest Basin. Troms-Finnmark Fault Complex (TFFC) to the south and Ringvassøy-Loppa Fault Complex (RLFC) to the west. Stippled lines displaying selected cross-section of fig.12 and 13. (Mulrooney et al., 2017). ....	12
<b>Fig. 12.</b> Interpreted cross-section of the Hammerfest Basin, extending from the Finnmark Platform in the south to the Loppa High in the north shows the main structures. See fig.11 for location. Modified from Gabrielsen et al. (1990).....	13
<b>Fig. 13.</b> Interpreted cross-section of Troms-Finnmark Fault Complex in the area of study. Tromsø Basin to the NW and Finnmark Platform to the SE. See fig.11 for location. Modified from Gabrielsen et al (1990).....	14
<b>Fig. 14.</b> Map displaying the extent of the 3D seismic (in red), the additional 2D lines (grey lines) and different well location. Modified from Marin et al., (2017).....	15
<b>Fig. 15.</b> a) Synthetic seismogram showing Base Cretaceous Unconformity (BCU) and the underlying Stø Fm from well 7120/10-1. b) Wavelet, amplitude, and phase .....	16
<b>Fig. 16.</b> a) Section displaying two different fault geometries with key horizons. b) Forward modeling from StructureSolver displaying a bad fit model between the interpreted beds and projected beds. c) Forward modeling displaying a best-fit model between the interpreted and projected beds. ....	20

<b>Fig. 17.</b> Variance map to the left, structural map to the right showing the structural style. (a) Stø Fm (b) BCU (c) S0 (d) S2. Structural map of Stø displaying the location of the cross-sections of fig.18, 19 and 20. Maps in ms.....	22
<b>Fig. 18.</b> Uninterpreted vs. interpreted section, display the main fault to the south and secondary faulting northwards. See fig.17a for location. Vertical exaggeration (VE) = 2.....	24
<b>Fig 19.</b> Uninterpreted vs. interpret section, showing NNE – SSW fault trends. See fig.17a for location. VE=2 .....	25
<b>Fig. 20.</b> Uninterpreted vs. interpret section, showing E – W fault trends. See fig.17a for location. VE=2 .....	26
<b>Fig. 21.</b> Time thickness map of Upper Jurassic strata (Hekkingen Fm). Red arrows indicating substantially thickness increase .....	27
<b>Fig. 22.</b> Time thickness map of a) S0 b) S2. Red arrows indicating substantially thickness increase..	28
<b>Fig. 23.</b> Map view of the extent of the anticline and syncline. Section AA', BB', CC', DD', EE' and FF' displayed along the Troms-Finnmark Fault Complex. The dotted line between the syncline and anticline show the projected structure. ....	29
<b>Fig. 24.</b> Uninterpreted vs. Interpreted section of section AA' in depth (m). Dotted rectangle show fig.26. No vertical exaggeration. See fig.23 for location. ....	30
<b>Fig. 25.</b> Uninterpreted vs. Interpreted section of section BB' in depth (m). No vertical exaggeration. See fig.23 for location. ....	31
<b>Fig. 26.</b> Zoomed in AA' cross-section (fig.25) showing stratigraphic onlaps within the S0 unit. VE=2 .....	32
<b>Fig. 27.</b> Uninterpreted vs. interpreted. CC' section (BSS01-102) showing anticline structure in the hangingwall of the main fault with one large secondary fault offsets the succession with a varying throw. No vertical exaggeration. See fig.23 for location.....	34
<b>Fig. 28.</b> Uninterpreted vs. interpreted. DD' section (BSS01-103) showing anticline structure in the hanging-wall with antithetic and synthetic subsidiary faulting. No vertical exaggeration. See fig.23 for location. ....	35
<b>Fig. 29.</b> Uninterpreted vs. interpreted. EE' section (BSS01-104) display a rollover structure. No vertical exaggeration. See fig.23 for location.....	36
<b>Fig. 30.</b> Uninterpreted vs. interpreted. FF' section (BSS01-105) show syncline where S0 increase the thickness in both towards the fault and syncline. No vertical exaggeration. See fig.23 for location. ...	37
<b>Fig. 31.</b> Upper figure display section AA' of the interpreted top horizons, whereas the underlying show the best-fit modeling result. The section shows an overall good fit until top S0 and S2. See fig.23 for location. ....	39
<b>Fig. 32.</b> Upper figure display section AA' of the interpreted top horizons, whereas the underlying show the best-fit modeling result. The best-fit model has limitations basinward close to the secondary fault. See fig.23 for location. ....	40
<b>Fig. 33.</b> Upper figure displaying the interpret CC' section, while the lower figure shows the comparison of the modeled beds and interpret intra and top horizons of the best-fit model. An overall good best-fit model. See fig.23 for location. ....	42
<b>Fig. 34.</b> Upper figure displaying the interpreted DD' section, while the middle figure shows the comparison of the modeled beds and interpret intra and top horizons of the best-fit model. The lowermost figure shows alternative modeling. Both modeling have limitations. See fig.23 for location. ....	43
<b>Fig. 35.</b> Upper figure displaying the interpret EE' section, while the lower figure shows the comparison of the projected beds and interpret intra and top horizons of the best-fit model. The best-fit model shows an overall good correlation. See fig.23 for location. ....	45

<b>Fig. 36.</b> Upper figure displaying the interpret FF' section, while the lower figure shows the comparison of the projected beds and interpret intra and top horizons of the best-fit model. See fig.23 for location. ....	46
<b>Fig. 37.</b> a) Well correlation of four wells in the area display thickness differences between Hekkingen Fm and S0. (b) Time structural map for the top Stø Fm. GG' show the correlated trend. ....	47
<b>Fig. 38.</b> GR response within the Knurr Fm. Green and blue color indicate an increase in GR-response, whereas yellow and orange points to low responses. ....	48
<b>Fig. 39.</b> a) Location of the area that underwent iso-slices and rms attribute. b) Cross section of the traced iso-slices within the S0 interval. NB, the polarity is reversed in this section c) Iso-slice of lowermost area. d) Isoslice of the lower part. Well 7120/10-2 location is marked with a red circle and stippled lines indicate geological features. ....	50
<b>Fig. 40.</b> Iso-slices of the S0 interval. a) Middle part b) Upper part. c) Uppermost part. Well 7120/10-2 location is marked with a red circle and stippled lines indicate geological features. See fig.39 for location. ....	51
<b>Fig. 41.</b> Forced fold (i.e., anticline) develops above the 'flat' in relation to extensional movements. (Vazquez et al., (2018) ....	58
<b>Fig. 42.</b> Section illustrating the structural style associated along October Fault Zone in Gulf of Suez. From Rotevatn and Jackson (2014).....	61
<b>Fig. 43.</b> Conceptual 3D model of the fault-related hanging wall deformation of the Troms-Finnmark Fault Complex in the southwestern-most area of Hammerfest Basin. Section AA', BB' and CC is located in a ramp-flat-ramp structure', whereas DD' is located in a flat. Section EE' is situated in a listric fault shape, while FF' has a more planar fault structure. ....	63
<b>Fig. 44.</b> Conceptual model of how the turbidite system shifted from a northern direction towards a northeastern due to the syncline development.....	65

## 1. Introduction

The majority of folds in extensional tectonic setting are associated with normal fault systems over a wide range of factors such as fault-propagation folds, drag folds, reverse drag folds, rollovers and transverse folding which exert distinctive characteristics in terms of folding and dipping geometries (fig.1; Schlische, 1995). However, other mechanisms that could control the folding structure are differential compaction (Hedberg, 1926; Skuce, 1996) and inversion (Mitra, 1993).

In an extensional setting, fault-related folds form above propagating normal fault and is a continuous form of deformation associated with fault interaction (Withjack, Olson, & Peterson, 1990). These structures exert a fundamental control on the sedimentary architecture (Prosser, 1993; Gawthorpe, Fraser, & Collier, 1994; Ravnås & Steel, 1997) which changes over time with increasing fault displacement, fault linkage and fault terminations. Forced folding during early stages of rifting could hold key control on basin physiography, synrift stratal architecture and facies development (Jackson & Leeder, 1994; Gawthorpe et al., 1997; Maurin & Niviere, 1999; Corfield & Sharp, 2000; Gawthorpe et al., 2003; Ford, Veslund, & Bourgeois, 2007; Lewis et al., 2015).

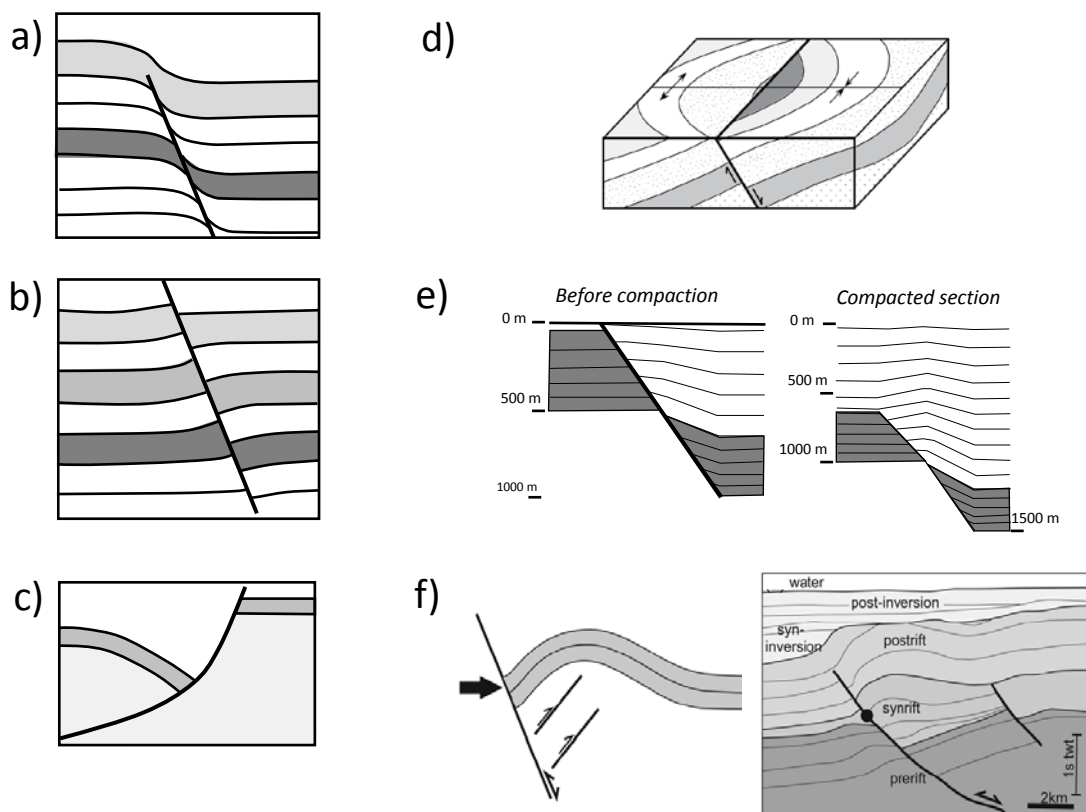


Fig. 1. Geometries associated with extensional fault-related folds. (a) Fault propagation fold (modified from Schlische, 1995). (b) Reverse drag folds (modified from Barnett et al., 1987). (c) Listric fault (modified from Rykkelid and Fossen, 2002). (d) Transverse folding (Schlische, 1995). (e) Compaction (Skuce, 1996). (f) Inversion (Indrevær et al., 2016).

The extensional fault-related folds are widely observed in rift systems such as North Sea (Corfield & Sharp, 2000), offshore Australia (Deng & McClay, 2019), offshore New Zealand (Conneally, Childs, & Nicol, 2017), Gulf of Suez (Gawthorpe et al., 1997) and the Barents Sea (Serck & Braathen, 2019). Understanding fold and fault geometry in extensional setting is important because these structures directly influence the physiography and form petroleum traps (Rotevatn & Jackson, 2014). Synrift units, deposited on the flanks of fault-related folds may be attractive exploration target in rift systems, but carry a large degree of risk in terms of predicting synrift reservoir presence and continuity (Lewis et al., 2015).

A wide range of fold styles (Serck & Braathen, 2019) develops in this setting (fig.2), which influence transport direction of sediments, accommodation generation and sedimentary architecture (Schlische, 1995; Gawthorpe & Leeder, 2000; Rotevatn & Jackson, 2014). The distinct style of surface deformation gives rises to significantly different stratigraphic responses (Gawthorpe et al., 1997). During the initial extension, forced folds (fig.2a) are formed ahead of the blind fault propagation. The stratal units form a basinward-thickening wedge that onlaps and thin toward the monocline (Gawthorpe et al., 1997; Lewis et al., 2015). Planar faults (fig.2b), which have propagated through the forced folds, results in a thickening strata unit toward the fault plane (Gawthorpe et al., 1997).

Along a single fault segment, the two tectonostratigraphic styles (fig.2a and 2b) coincide as the fault propagate along the strike, with a varying throw and plunging towards the fault tip (Gawthorpe et al., 1997; Corfield & Sharp, 2000). Listric faulting (fig.2c) is related to rollover basins (Xiao & Suppe, 1992), resulting in the collapse of the hanging wall. Growth units will fill the void above the folding towards the fault plane. A ramp-flat-ramp fault will develop fault-bend synclinal basins (fig.2d), which will trigger anticline-syncline pairs (Xiao & Suppe, 1992; Serck & Braathen, 2019). The listric segment above the ramp-flat will form a rollover anticline, while the lower listric segment (flat-ramp) develops a syncline structure (Xiao & Suppe, 1992).

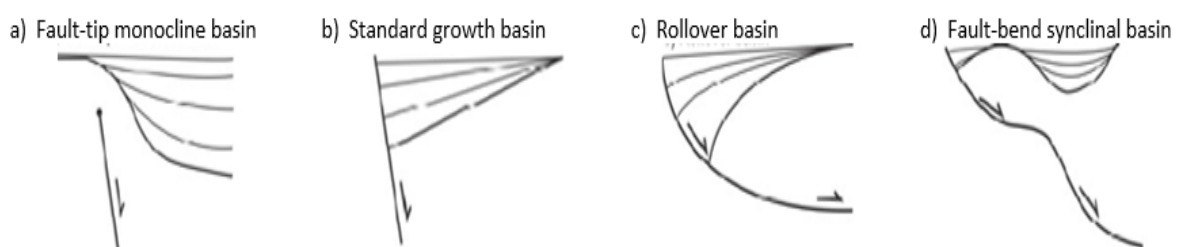


Fig. 2. Four main growth basin geometries associated in the extensional setting. (a) Fault-tip monocline. (b) Standard growth basin. (c) Rollover basin. (d) Fault-bend synclinal basin. (Serck and Braathen, 2019)

The Hammerfest Basin, which is located in the south-western Barents Sea (fig.3) has undergone several phases of extensional tectonism, comprised by numerous tectonic pulses since the Caledonian orogeny (Faleide, Vågnes, & Gudlaugsson, 1993). In response to the rifting periods, the basin has developed anticlinal structures along the hanging-wall of the Troms-Finnmark Fault Complex (Berglund et al., 1986; Gabrielsen et al., 1990; Indrevær, Gabrielsen, & Faleide, 2016; Mulrooney, Leutscher, & Braathen, 2017).

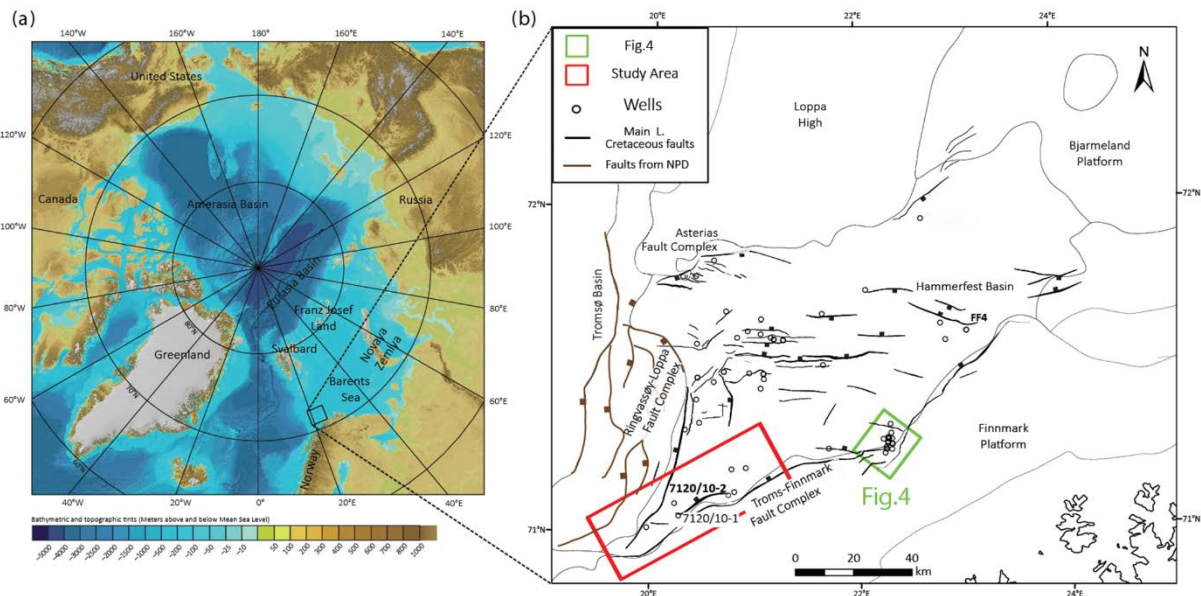


Fig. 3. a) Bathymetric map of the Arctic Ocean (Jakobsson et al., 2012). b) Geological elements of the Hammerfest Basin, main structural features, well location, and the data used in this study. Green rectangle displays the location of the Goliat anticline. (Modified from Marin et al., 2017)

The Goliat anticline (fig.4) is located in the hanging wall of the Troms-Finnmark Fault Complex. This anticline has previously been described as formed by a listric fault (fig.4b; Gabrielsen, 1984; Gabrielsen et al., 1990) where the hanging wall strata have rotated and created a rollover structure. Indrevær et al. (2015) described the structure as a listric fault with marked ramp-flat-ramp geometry (fig.4c), while Mulrooney et al. (2017) concluded that two planar segments formed the anticline (fig.4d). Regional studies (Rønnevik & Jacobsen, 1984; Gabrielsen & Færseth, 1989; Indrevær et al., 2016) suggest that inversion and strike-slip movements along the Troms-Finnmark Fault Complex were additional mechanisms affecting the region.

The thesis will examine an anticlinal fold that developed in the hanging wall along the Troms-Finnmark Fault Complex close to the Ringvassøy-Loppa Fault Complex in the Hammerfest Basin (fig.3b). The anticline is located further south compared to the Goliat anticline. Mulrooney et al. (2017) did not perform cross-section restoration or other modelling technique

to discern the viability of these interpretations. Therefore, the thesis will do simple forward modelling, trying to explain the origin of the structure in the study area.

Also, the previous studies have focused on understanding the evolution of these anticlines, but they have not studied how the evolution of these structures affected the sedimentation and coarse-grained distribution. The Lower Cretaceous Knurr sandstone (Sequence 0 from Marin et al., 2017) forms an attractive play (Seldal, 2005; Sattar et al., 2017; NPD, 2019) in the Hammerfest Basin, along the fault boundary of Troms-Finnmark Fault Complex and southern slope of Loppa High. Within the study area, well 7120/10-2 penetrated well-sorted turbidites (Marín et al., 2017), showing the potential of this play. The turbiditic sandstone has been interpreted as a syn-rift succession, but they do not exhibit the standard wedge shape geometry (fig.1b). Instead, they thicken slightly basinward similar to fig.1a.

The main objective of this thesis is to understand the mechanism responsible for the development of the anticline structure in the SW parts of the Hammerfest Basin. In addition, explain the impact the evolution of this structure had on the input and distribution of the coarse-grained sediment in the basin. The study utilises seismic data to (i) do simple forward modelling in order to highlight the mechanisms responsible for the development of the anticlinal structure, (ii) use stratigraphic attributes to identify geological features in the Lower Cretaceous and (iii) explain the impact the origin of the anticline had on the syn-rift sedimentation and the coarse-grained distribution.

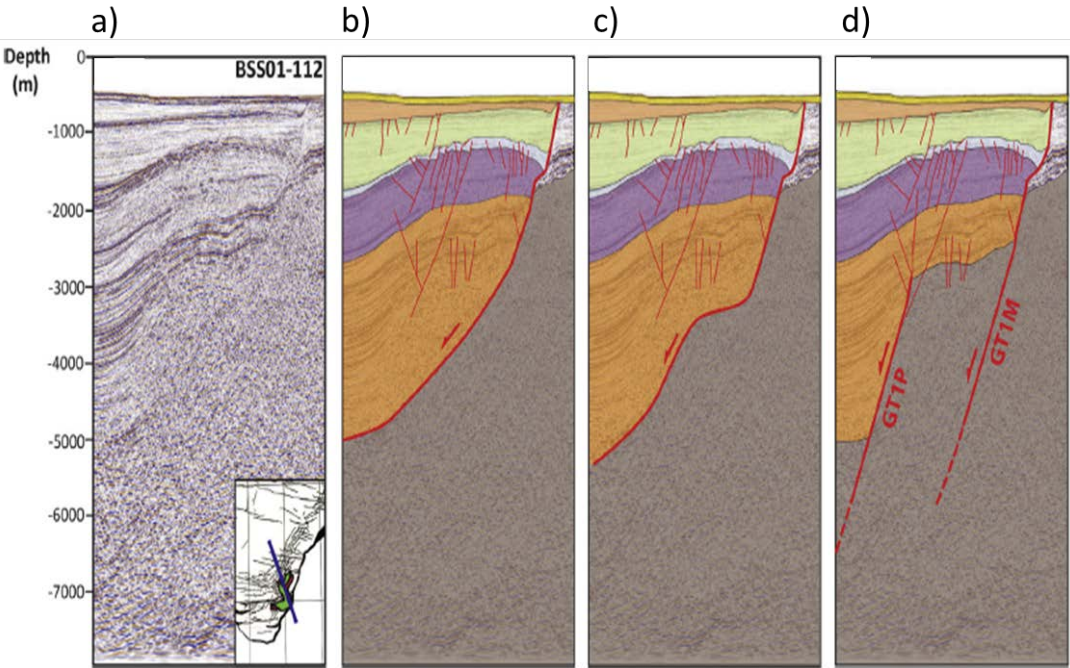


Fig. 4. a) Time depth converted section for regional line BSS01-112 close to the Troms-Finnmark Fault Complex. The alternative interpretations suggest (b) listric, (c) listric with a pronounced ramp-flat-ramp geometry or (d) Stepped planar segments. The orange, purple, light blue and green color correspond to Paleozoic, Triassic, Jurassic, and Cretaceous respectively. (Mulrooney et al., 2017).

## 2. Geological setting

The Barents Sea is situated outside the northern coast of Norway and covers the western part of the Russian mainland in an intracratonic setting (Faleide et al., 1993). The Barents Sea is bounded by Svalbard and Franz Josef Land in the north, whereas the Novaya Zemlya confines the eastern border, while the deeper waters in the Norwegian-Greenland Sea defines the western margin (fig.5). The geological framework of the Barents Sea is complex and extends back to Paleoproterozoic Svecofennian orogeny (Smelror et al., 2009). The regional geology of the western Barents Sea is extensively studied (Rønnevik, Beskow, & Jakobsen, 1982; Faleide, Gudlaugsson, & Jacquart, 1984; Berglund et al., 1986; Sund et al., 1986; Gabrielsen et al., 1990; Henriksen et al., 2011; Gernigon et al., 2014) and the development of the regional geological framework is well established. The western and eastern regions have been influenced differently by the tectonic history and can be divided into two different provinces. The two provinces hold different characteristics where the eastern region has large basins, while smaller basins, several highs, and widespread platform areas distinguish the western side (fig.5; Henriksen et al., 2011)

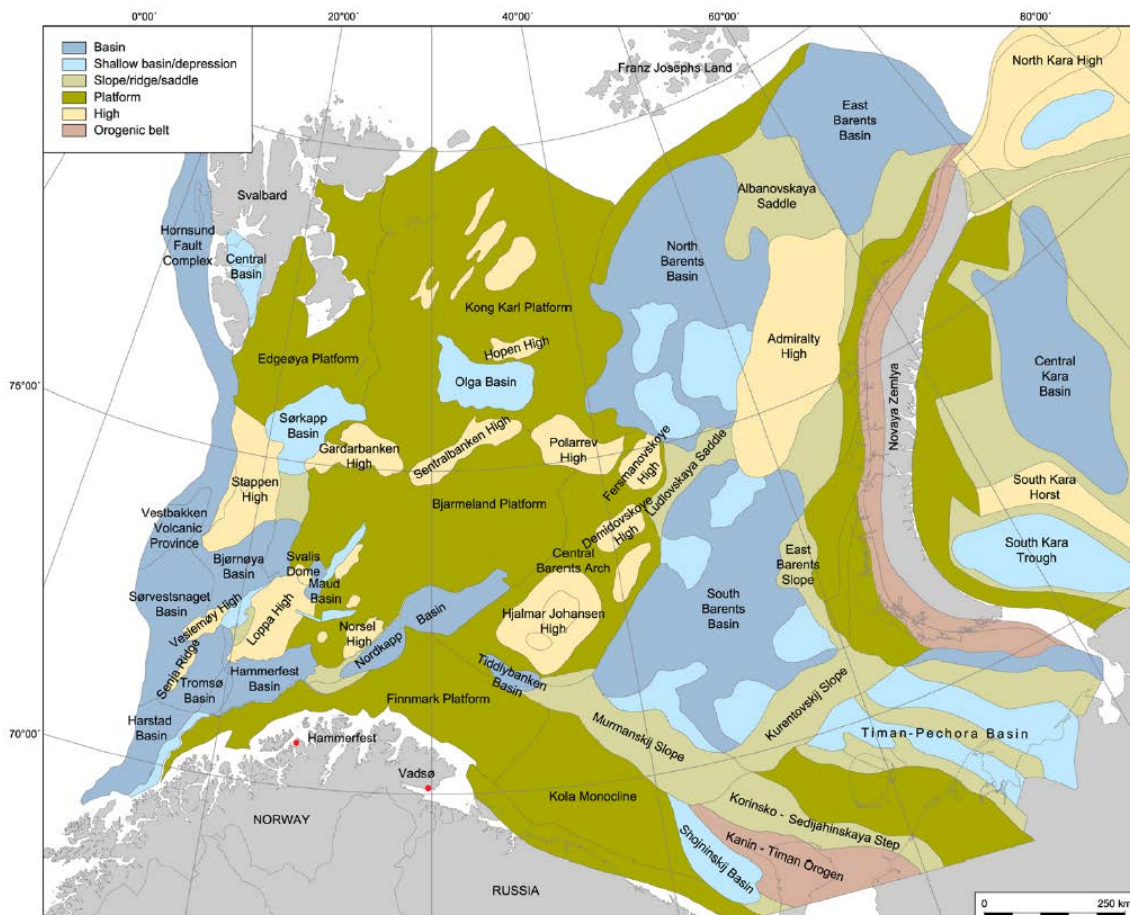


Fig. 5. Main structural elements of the greater Barents Sea (Henriksen et al., 2011)



## 2.1 Structural Framework

Since the convergence of Laurentia, Greenland, and Baltica, resulting in the Caledonian orogeny Fossen et al., 2008, the western Barents Sea has undergone three major extensional rift phases. These extensional periods were in Late Devonian – Carboniferous, Late Jurassic – Early Cretaceous and Late Cretaceous – Early Cenozoic (Faleide et al., 1993).

The first period of extension started due to the initiation of the Paleozoic-Mesozoic pre-opening that developed the North Atlantic (Smelror et al., 2009). Several rift basins started to develop, both in Svalbard and on the western Barents Sea shelf (fig.6). Some of the active fault zones were bounded by older fracture zones formed by the Caledonian orogeny (Worsley & Nøttvedt, 2008). The onset of the Uralian orogeny in the Late Paleozoic, led to a pronounced change in basin physiography with high subsidence, especially in the east towards the basin flanks of Novaya Zemlya (Worsley, 2008; Worsley & Nøttvedt, 2008; Henriksen et al., 2011). By the Middle to Late Permian, the extension activity waned and the Barents Sea evolved into platform dominated setting (Worsley, 2008).

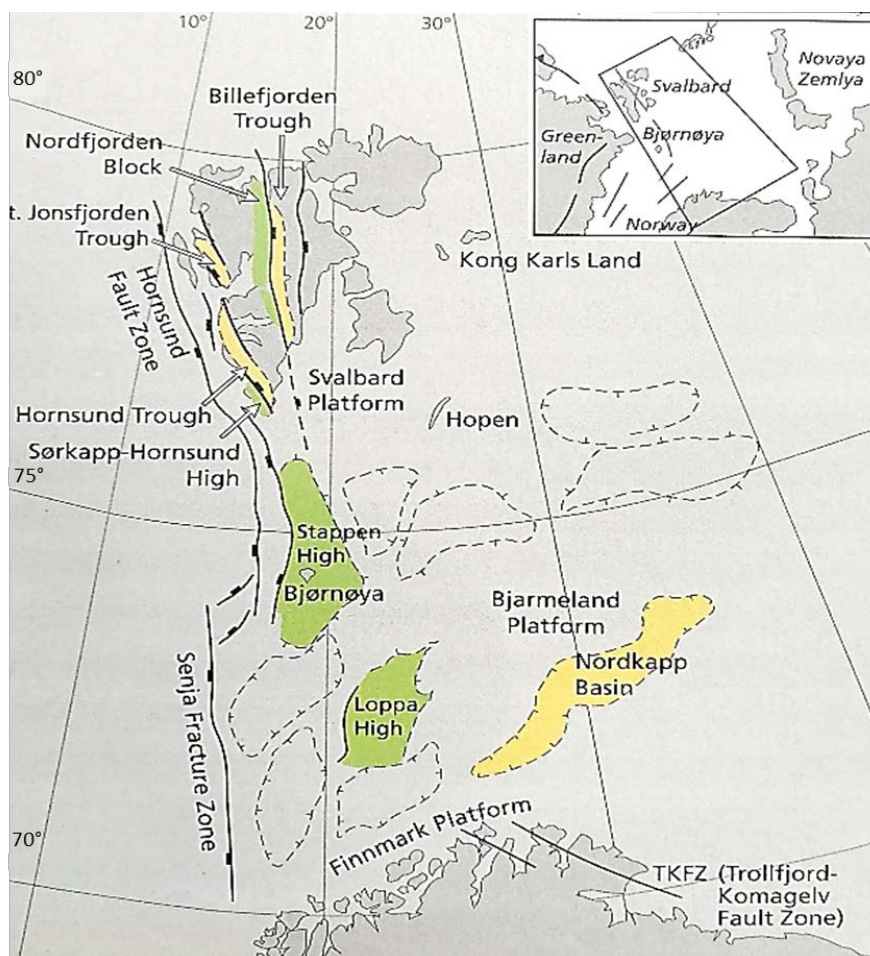


Fig. 6. Major structural elements in the Barents Sea shelf during the Carboniferous and Permian. Elevated highs marked in green and subsided basins marked with yellow. Stippled areas indicate later developing structures. (Worsley and Nøttvedt, 2008)

The Triassic is characterized by tectonic quiescence (Nystuen et al., 2008), although local zones of fault activity around the Loppa High, Hopen High, and eastern Svalbard have been interpreted (Gabrielsen, 1984; Anell et al., 2013; Mahajan, Gabrielsen, & Faleide, 2014). Nevertheless, the Barents Sea continued being a relatively stable platform throughout the Early and Middle Jurassic (Nøttvedt & Johannessen, 2008; Smelror et al., 2009).

The extension period in Late Jurassic to Early Cretaceous influenced the western Barents Sea with the establishment of the present day structural architecture of basins and highs (Nøttvedt & Johannessen, 2008; Henriksen et al., 2011). The tectonic activity affected the central and western parts (fig.7), forming the Hammerfest, Sørvestnaget, and Bjørnøya Basin. It contributed to the development of structural highs such as the Loppa, Stappen, and Sentralbanken High (Nøttvedt & Johannessen, 2008). Successive rifting episodes during the Cretaceous led to rapid subsidence and created deep basins in Harstad, Tromsø, and Sørvestnaget (Smelror et al., 2009). Extensive uplift and erosion of Cretaceous sediments are also evident across the Barents Sea and are associated with a major volcanic event that occurred around Franz Josef Land and Karl Land (Smelror et al., 2009).

The Late Cretaceous to Paleocene rifting is linked to the subsequent breakup between Norway and Greenland. The tectonic activity consisted of strike-slip movement and deformation in the westernmost part of the Barents Sea (fig.7; Faleide et al., 2008; Smelror et al., 2009). On a regional scale, extension affected the western Barents Sea, but reverse faulting and inversion transpired (Gabrielsen et al., 1990) affecting basin physiography. The final phase of the separation between Norway and Greenland is associated with the development of the passive margin along the western Barents shelf (Berglund et al., 1986).

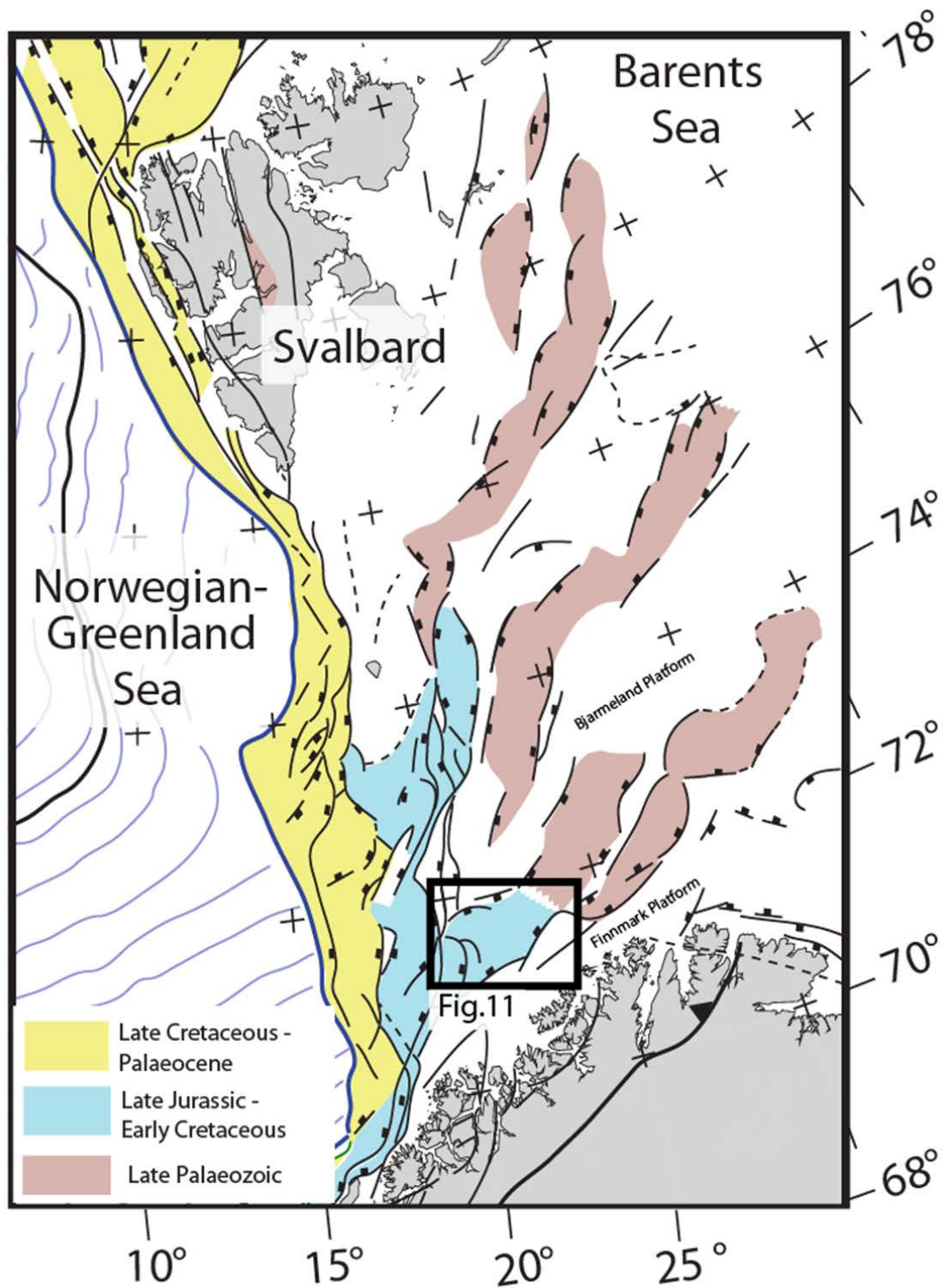


Fig. 7. Main structural elements of the western Barents Sea and adjacent areas. Colors reflect the focus of the tectonic activity. Modified from Faleide et al. (2008) & Faleide et al. (2010).

## 2.2 Stratigraphic Framework

From the Early Carboniferous to the Middle Permian the Barents Sea region passed several climatic zones (i.e. semiarid to arid), depositing a highly contrasting sedimentary succession (i.e. Ugle, Falk, Ørn and Isbjørn Fm) of continental red bed overlain by shallow marine carbonate and evaporates (fig.8; Worsley & Nøttvedt, 2008).

The Triassic period is marked by the onset of mud and sand deposits by alternating deltaic sequences (Nystuen et al., 2008; Ohm, Karlsen, & Austin, 2008). The deltaic sequences prograded across the entire Barents Sea region, sourced by the recently uplifted Uralides (Glørstad-Clark et al., 2010; Glørstad-Clark et al., 2011; Anell, Midtkandal, & Braathen, 2014; Klausen, Nyberg, & Helland-Hansen, 2019). At the end of the Triassic, alluvial plains occupied large parts of the Barents Sea region, depositing sandstones (Johannessen & Nøttvedt, 2008).

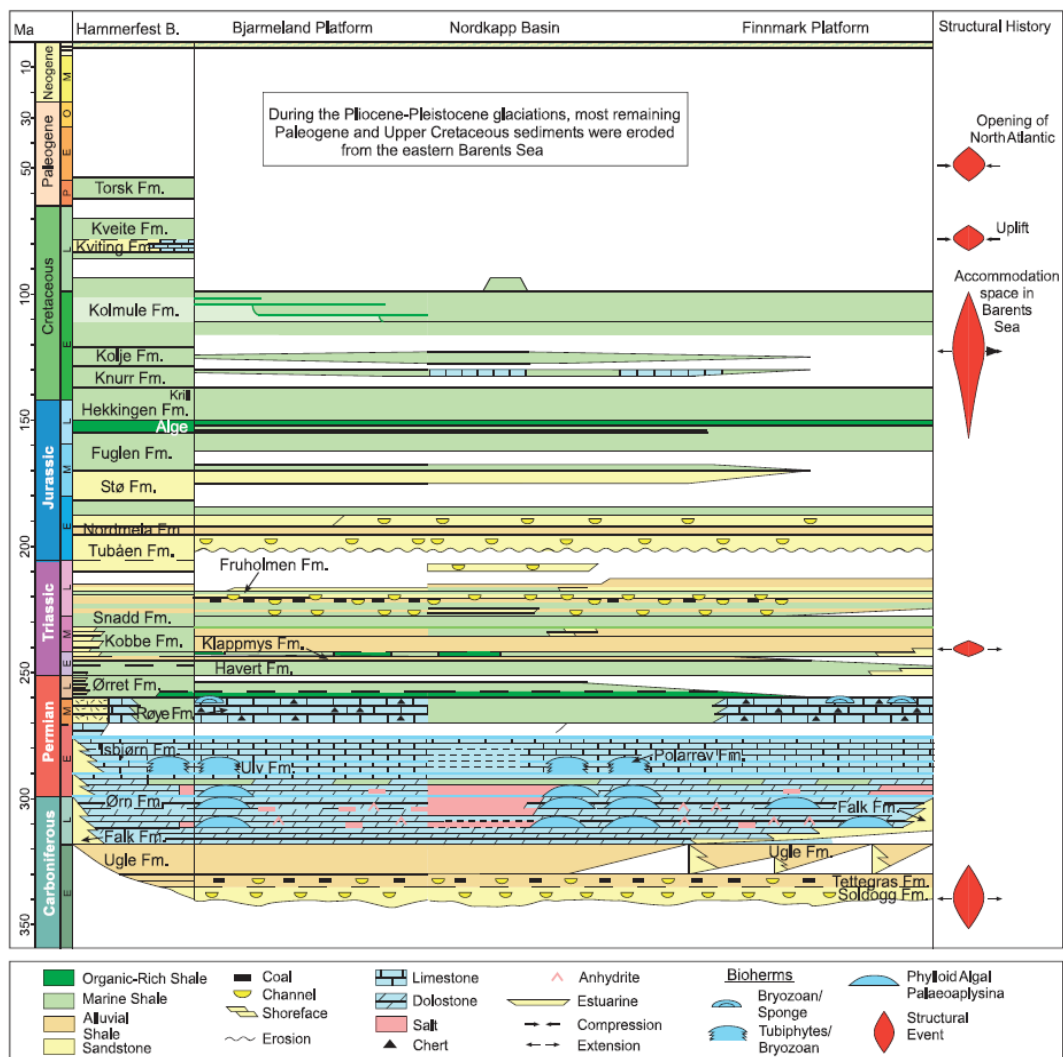


Fig. 8. Norwegian Barents Sea stratigraphic chart of the main lithologies in the Hammerfest Basin, Bjarmeland Platform, Nordkapp Basin, and Finnmark Platform. Summary of the structural history is shown in the right column. (Ohm et al., 2008)

The Barents Sea gradually became submerged during the Early Jurassic, and coastline retreated across the older alluvial plains depositing laterally extensive sandbodies (i.e., Tubåen Fm). The Hammerfest Basin region was subjected to increased subsidence resulting in thick marine sand unit (i.e., Stø Fm). Sea level rise during Middle Jurassic had regional implications, turning the Barents Sea into a shallow- to deep-marine setting (Nøttvedt & Johannessen, 2008) depositing organic-rich marine shale throughout the remaining period (i.e., Fuglen and Hekkingen Fm).

The subsidence influenced by the Early Cretaceous rifting, increased rapidly where marine mudstone continued being deposited in the Early Cretaceous. A regional unconformity, known as Base Cretaceous Unconformity (BCU), separate the Lower Cretaceous succession from the Jurassic (Mørk et al., 1999). The Lower Cretaceous succession consists of fine-grained, deep marine sedimentary rocks with sandstone interbeds and is divided into Knurr, Kolje, and Kolmule formations (fig.9; Mørk et al., 1999). The Knurr, Kolje and Kolmule sandstone beds formed wedges along the margins of the Hammerfest Basin. The sandstones are laterally discontinuous, suggesting a major variability in the depositional environment (Mørk et al., 1999; Seldal, 2005).

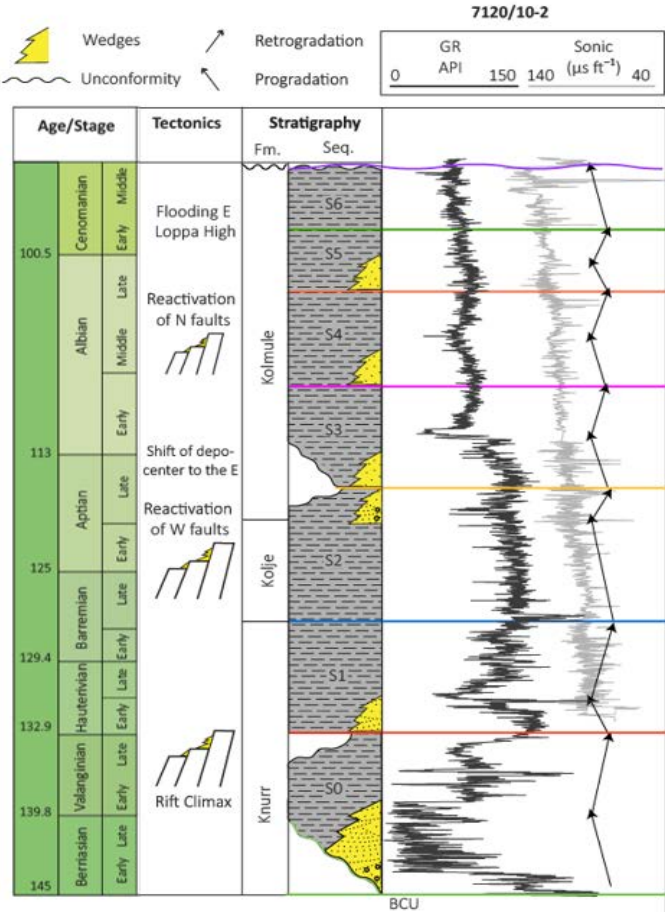


Fig. 9. Stratigraphy chart of the Lower Cretaceous succession in the Hammerfest Basin, showing seven sequences correlated with well 7120/10-2. The sequences used in this study are sequence (S0) and sequence 2 (S2). (Marin et al., 2017).

The depositional environment of these wedges varies from fan deltas in a shallow marine setting to submarine fan system in deep marine setting (Seldal, 2005; Marín et al., 2017). Marín et al. (2017) have defined six sequences (fig.9) based on flooding surfaces, stacking patterns in the Gamma Ray (GR) and lap terminations on seismic data. These sequences are correlated throughout the basin and represent a period of 5-10 million years between them. Core analysis (fig.10) of well 7120/10-2 place the Knurr sandstone as turbidite deposits in a deep marine setting (Marín et al., 2017), where the lower core section is situated in a slope setting with distal/off axis lobe environment due to the heterolithic sandstone units. The middle section is located in a proximal setting with high-density turbidite currents, before shifting to a lobe fringe/off axis environment in the upper part.

During Neogene, the Barents Sea region became uplifted and was subjected to severe erosion (Martinsen & Nøttvedt, 2008), which is evident in the stratigraphic framework where massive Cenozoic sediments are missing (fig.8).

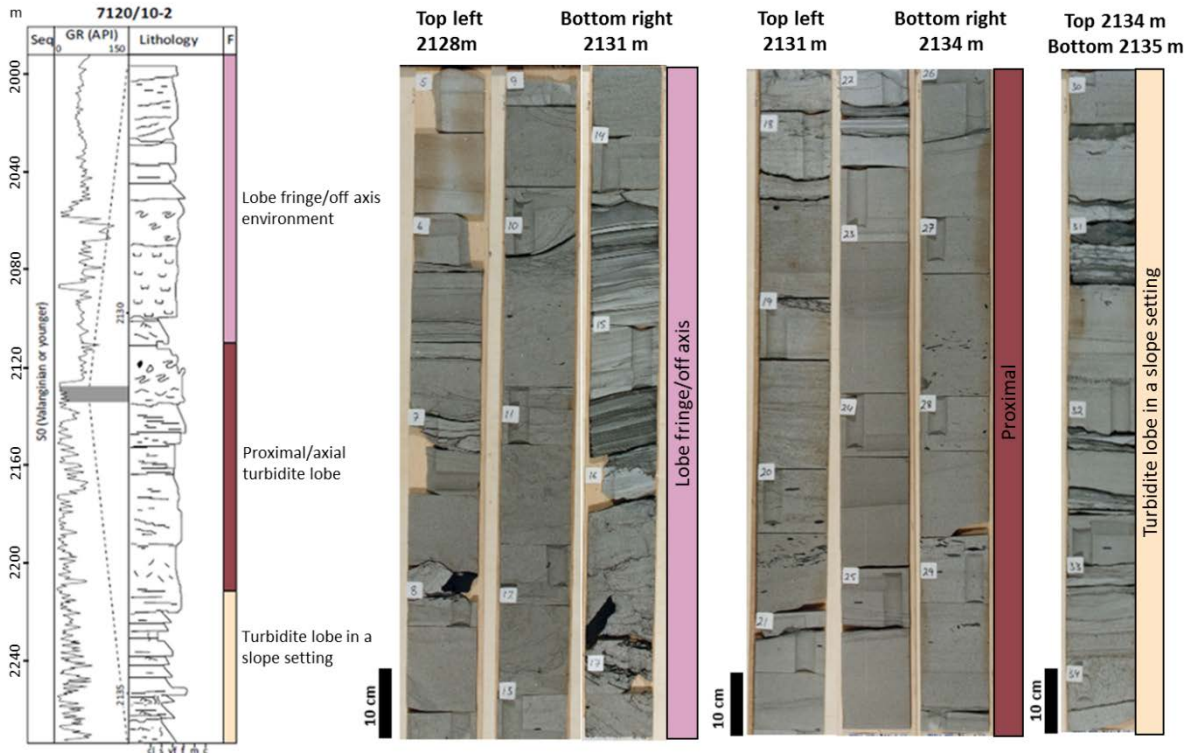


Fig. 10. Sedimentological log of well 7120/10-2 interpreted by Marín et al. (2017) based on cores places the lower section turbidites in a slope setting, before prograding into a proximal setting. The uppermost core section is situated in lobe fringe/off axis environment.

## 2.3 Main structural elements

### 2.3.1 Hammerfest Basin

The Hammerfest basin (fig.11) is major Mesozoic and Cenozoic east-northeast-to-west-southwest rift basin that is approximately 70 km wide and 150 km long (Berglund et al., 1986; Sund et al., 1986; Mulrooney et al., 2017). The basin (fig.12) is separated from the Finnmark Platform to the south by the Tromsø-Finnmark Fault Complex (TFFC), and from the Loppa High in the north by the Asterias Fault Complex (AFC). The Ringvassøy-Loppa Fault Complex (RLFC) defines the western border to the deeper Tromsø Basin, while the structural relief to the eastern border shallows and flexes to become the Bjarmeland Platform (Berglund et al., 1986; Gabrielsen et al., 1990).

The basin was part of a regional intracratonic basin (Berglund et al., 1986) before the outline was established during the Late Jurassic and continued developing into the Cretaceous (Gabrielsen et al., 1990; Faleide et al., 1993). However, some faults formed in this event were conditioned by Caledonian basement structure (Gabrielsen et al., 1990). The basin development culminated in the late Early Cretaceous, where RLFC started to separate the Hammerfest and Tromsø Basin (Berglund et al., 1986). The Loppa High and Finnmark Platform were topographical highs throughout the Cretaceous, and several reactivations along the main fault zones resulted in uplift and erosion (Gabrielsen et al., 1990).

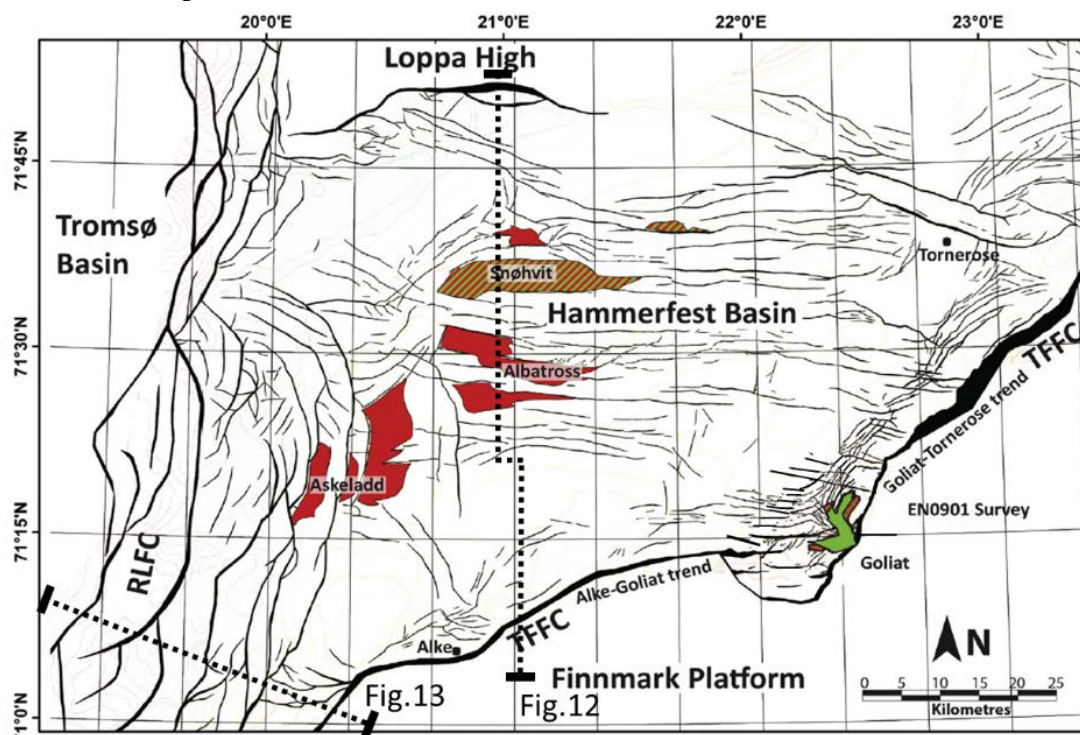


Fig. 11. Structural elements of the Hammerfest Basin. Current oil (green) and gas (red) fields are displayed throughout the Hammerfest Basin. Troms-Finnmark Fault Complex (TFFC) to the south and Ringvassøy-Loppa Fault Complex (RLFC) to the west. Stippled lines displaying selected cross-section of fig.12 and 13. (Mulrooney et al., 2017).

The basin has an internal fault system composed of E – W, ENE – WS, and WNW – ESE trending faults (fig.11; Gabrielsen, 1984). Ziegler, Doery, and Scott (1986) divided the basin into a western and an eastern subbasin. The eastern part of the basin is generally less affected by faulting and hold the characteristics of a sag basin (Gabrielsen et al., 1990).

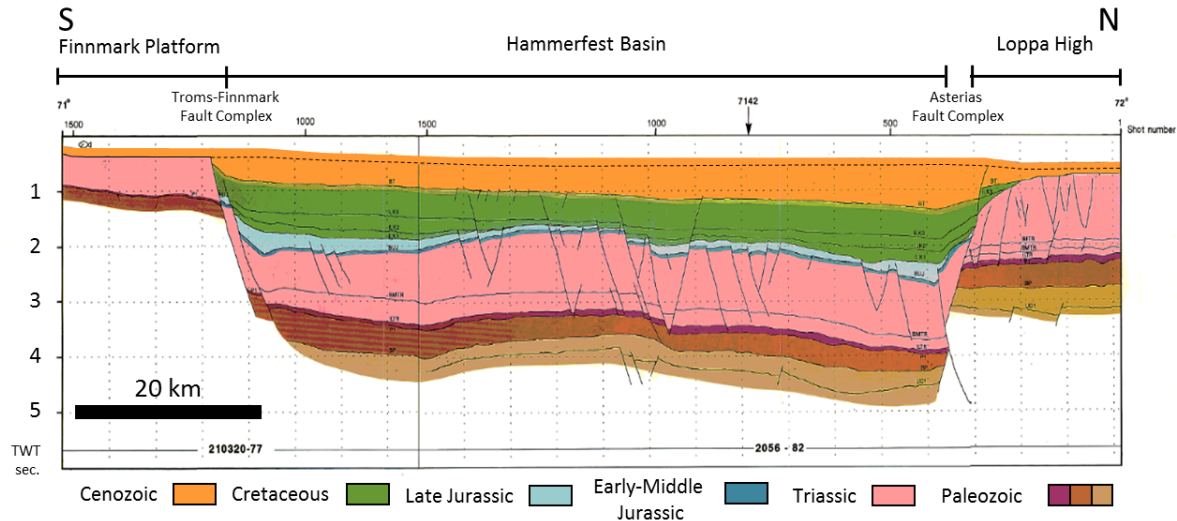


Fig. 12. Interpreted cross-section of the Hammerfest Basin, extending from the Finnmark Platform in the south to the Loppa High in the north shows the main structures. See fig.11 for location. Modified from Gabrielsen et al. (1990).

### 2.3.1 Finnmark Platform

Since the development in the Late Carboniferous, the Finnmark Platform has been stable. The transition from a pre-platform to platform development is defined by the Early Carboniferous clastics and Late Carboniferous carbonates (Gabrielsen et al., 1990). The platform is bounded to the south by the Caledonides of the Norwegian mainland, while the Troms-Finnmark Fault Complex and the Nordkapp Basin (fig.5) defines the western and northwestern boundary. The platform consists of a thin Cenozoic succession overlying thick Triassic and Paleozoic rocks, where Cretaceous and Jurassic rocks usually are absent due to massive erosion (Gabrielsen et al., 1990).

### 2.3.2 Troms-Finnmark Fault Complex

The Troms-Finnmark Fault Complex (TFFC) separate the Finnmark Platform from the basinal areas (Harstad Basin, Tromsø Basin, and Hammerfest Basin) to the north and northwest (Gabrielsen et al., 1990). The TFFC is a major basement involved fault system that utilizes a Caledonian trend (Faleide et al., 1984; Worsley, 2008) and terminates to the northeast, against the Trollfjord-Komagelv Fault Zone (Mulrooney et al., 2017). The structure consists of several hard linked segments with NNE – SSW to NE – SW trends in the south and ENE – WSW trend towards the north (Gabrielsen et al., 1990; Mulrooney et al., 2017). The fault complex has several periods of activity, where the northeastern segment can be traced back to the pre-



Permian sequence (Berglund et al., 1986), and reactivation took place until Eocene where the most prominent subsidence along the fault system is dated to Late Jurassic and Early Cretaceous (Gabrielsen et al., 1990).

### 2.3.3 Ringvassøy-Loppa Fault Complex

The Ringvassøy-Loppa Fault Complex strikes N – S and is situated in the transition zone between the Hammerfest Basin and the Tromsø Basin (fig.13; Gabrielsen et al., 1990). The northern part delineates the Loppa High to the west (fig.11). The fault complex is characterized by large penetrating normal faults with rotated fault blocks, dipping towards the deep Tromsø Basin (fig.13).

Reactivation of post-Caledonian fault system formed the RLFC during the subsidence of the Tromsø Basin in the Late Jurassic (Sund et al., 1986). The extension period accelerated the subsidence and accumulation of thick Cretaceous succession (Indrevær et al., 2016).

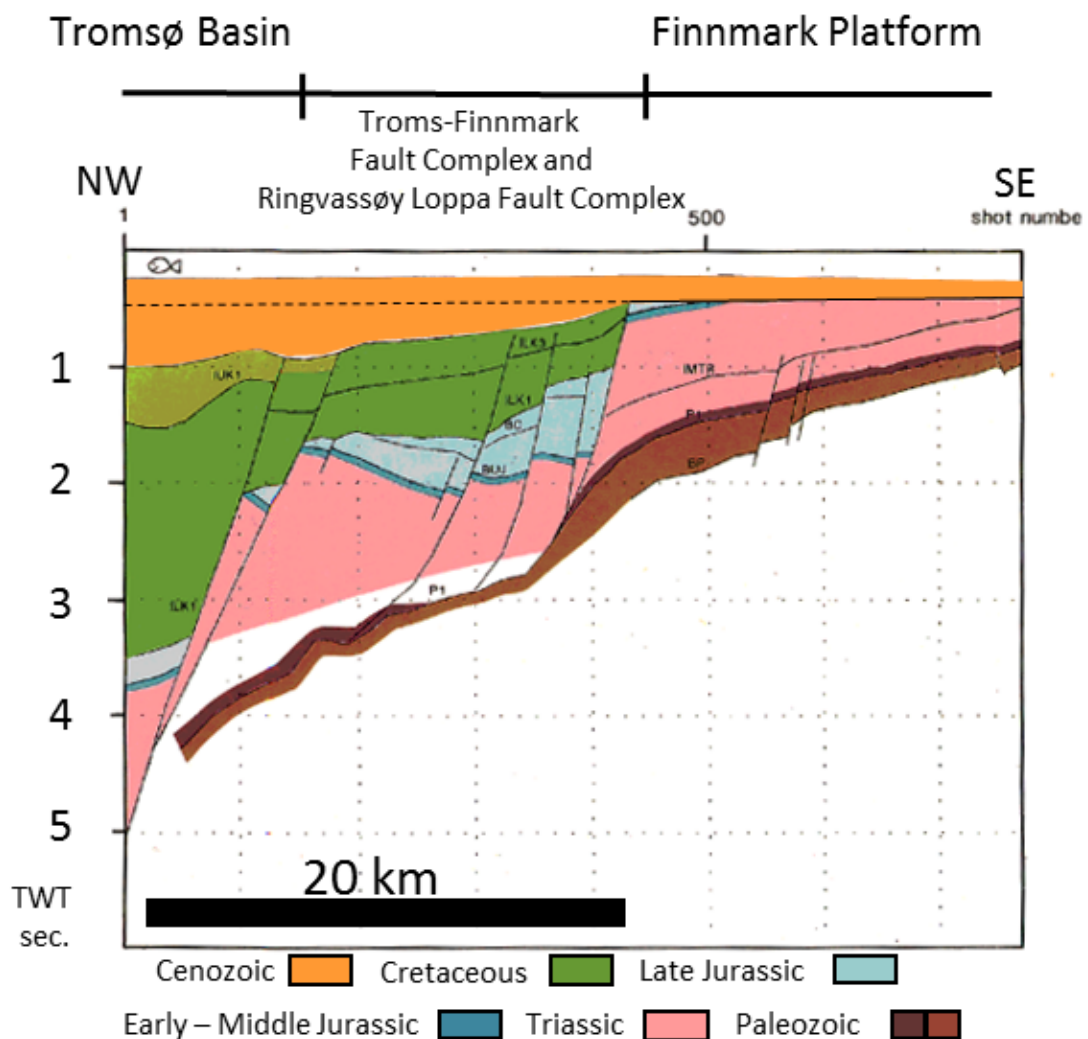


Fig. 13. Interpreted cross-section of Troms-Finnmark Fault Complex in the area of study. Tromsø Basin to the NW and Finnmark Platform to the SE. See fig.11 for location. Modified from Gabrielsen et al (1990).

### 3. Data and Methodology

The study was conducted in the southwestern part of the Hammerfest Basin using a three-dimensional seismic survey (fig.14), ST09M03, provided from the Norwegian DISKOS database. The seismic survey was acquired in 2009 and cover an area of approximately 600 km<sup>2</sup>. Additionally, four 2D lines (BSS01-102, BSS01-103, BSS01-104, and BSS01-105) were used in the study to show and analyze the hanging wall deformation along the fault boundary separating the Finnmark Platform with the Hammerfest Basin. The seismic has normal polarity, where an increase in acoustic impedance (i.e., hard kick) is represented as a peak (positive) reflector. The seismic data provide imagery down to 6000 ms, and the quality varies significantly downwards, where the frequencies ranging from 20 to 45 Hz.

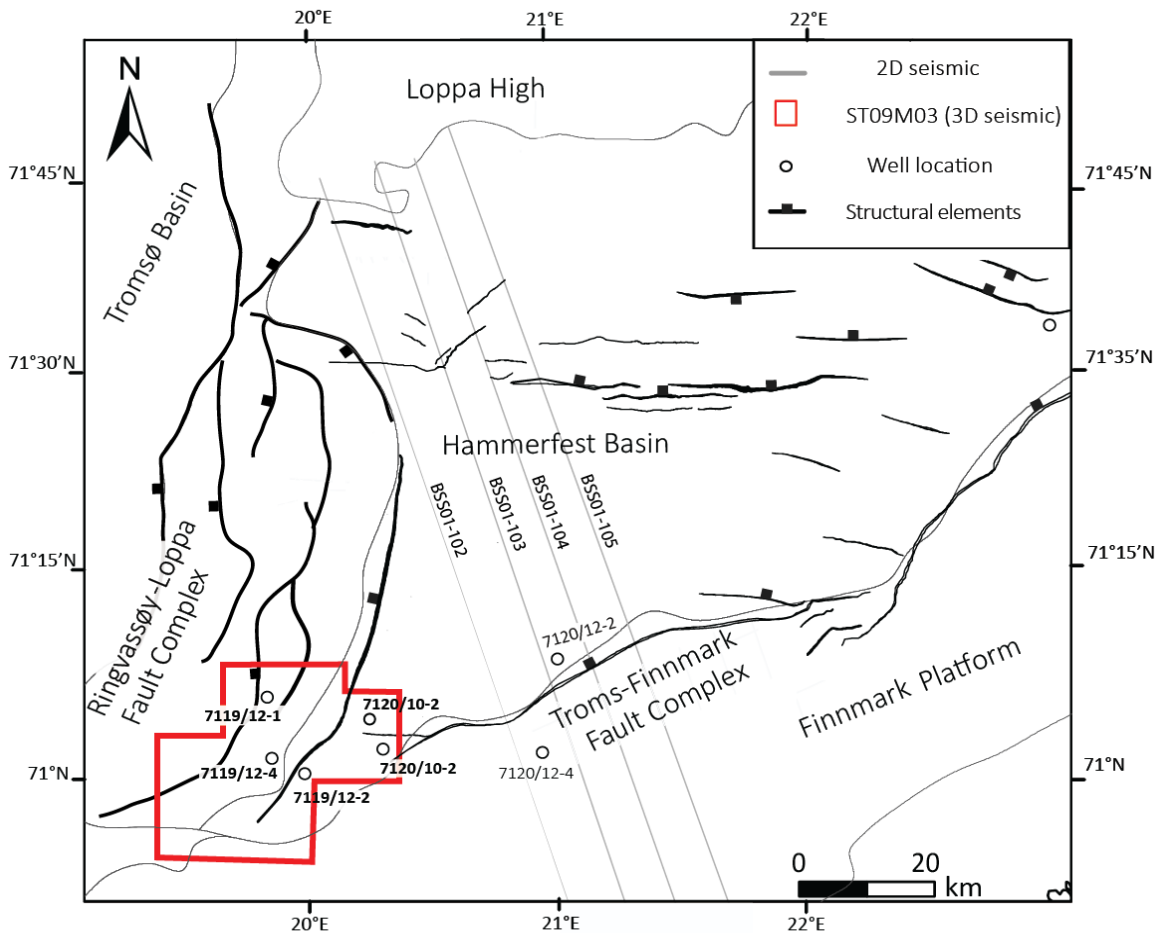


Fig. 14. Map displaying the extent of the 3D seismic (in red), the additional 2D lines (grey lines) and different well location. Modified from Marin et al., (2017).

Five exploration wells (i.e., 7119/12-1, 7119/12-2, 7119/12-4, 7120/10-1 and 7120/10-2) have been drilled within the cub, and a full suite of logs was available except for 7119/12-4, where petrophysical data were missing (Table 1). In addition, a seven-meter sedimentological log (fig.10) description of well 7120/10-2 from Marin et al. (2017) was accessible. The

tectonostratigraphic analysis of southwestern Hammerfest Basin has been carried out utilizing both seismic and well data.

Table 1. Petrophysical data available in this study.

Well	7119/12-1	7119/12-2	7119/12-4	7120/10-1	7120/10-2
Target	Middle – Early Jurassic Late Triassic	Middle – Early Jurassic Late Triassic	Middle – Early Jurassic	Middle – Early Jurassic	Lower Cretaceous
Oldest penetrated age	Early Jurassic	Late Triassic	Late Triassic	Late Triassic	Late Jurassic
Gamma Ray	X	X	-	X	X
Sonic	X	X	-	X	X
Density	X	X	-	X	X
Caliper	X	X	-	X	X
Neutron	X	X	-	X	X
Resistivity	X	X	-	X	X

### 3.1 Seismic well tie

Synthetic seismogram was generated from check-shot using sonic and density logs in Landmark DecisionSpace (fig.15). The key horizons from the wells were correlated with the seismic. A zero-phase Ricker wavelet (fig.15b) with a dominant frequency at 20 Hz was used. To get a good correlation, a time shift of – 21 ms was implemented.

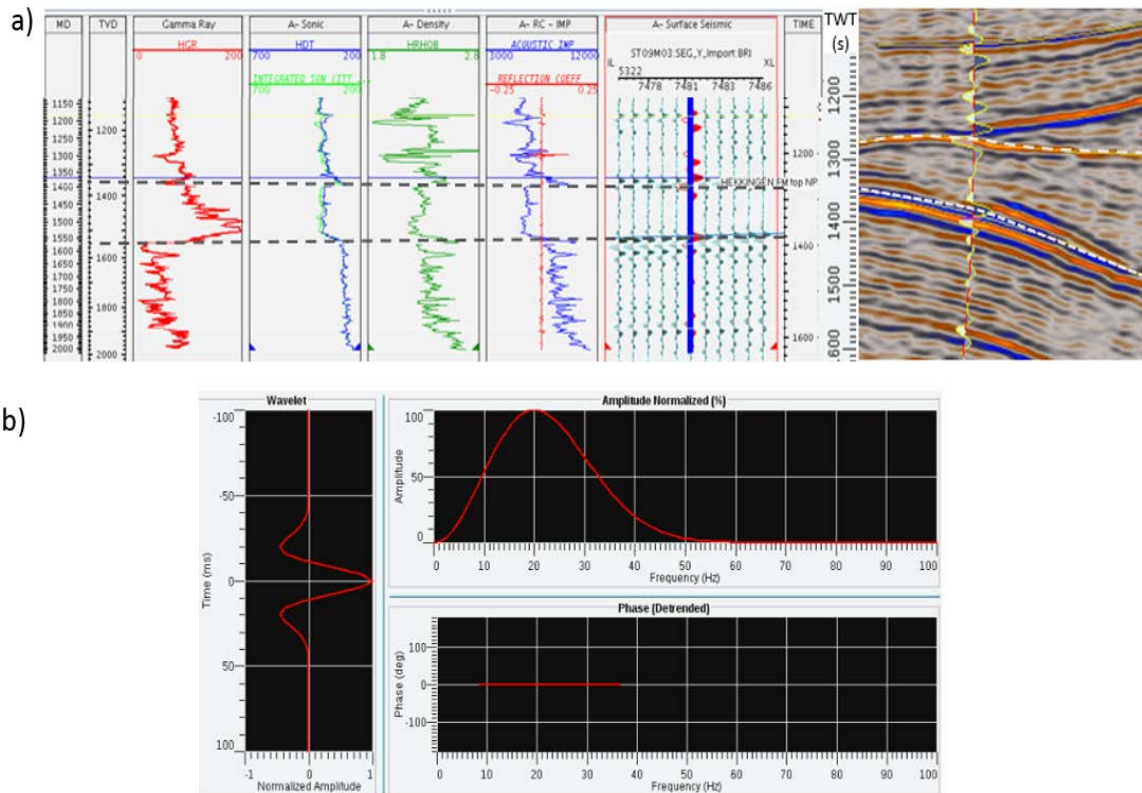


Fig. 15. a) Synthetic seismogram showing Base Cretaceous Unconformity (BCU) and the underlying Stø Fm from well 7120/10-1. b) Wavelet, amplitude, and phase

### 3.2 Seismic approach

Four key bounding horizons (i.e., Stø Fm, BCU, S0, and S2) were interpreted to get a detailed stratigraphic and structural mapping of the 3D seismic area. The S0 and S2 correspond to the Top Valanginian and Intra Aptian age in the Lower Cretaceous (see fig.9). The surface outline of the different horizons was mapped before detailed tracing of main faults and reflectors began. A structural attribute, such as *Variance*, was used to enhance the visualization of fault complexity in the area. The attribute calculates the amplitude difference between neighboring seismic traces and is used for fault identification (Chopra & Marfurt, 2007).

The stratigraphic unit of interest was located within the S0 since the sequence has been interpreted as syn-rift deposits and consist of turbidites. In between the unit, the interval was subjected to iso-proportional slicing where *rms amplitude* were run on each slice. The iso-proportional slices generate maps at interval spacing between two non-parallel horizons (i.e., S0 and BCU). Five slices were created within the sequence in the software GeoTeric. The *rms amplitude* highlights the magnitude of the amplitude response over a certain footprint and is a powerful aid in visually enhance geological features (Chopra & Marfurt, 2007).

In order to construct the forward modelling, it was necessary to make a time-depth conversion of some selected seismic lines. For seismic facies and sequence stratigraphy, seismic interpretation in the time domain is usually fine, because their interpretation remains mostly the same with changing the structure. However, structural modeling in the time domain is a riskier business because it means that the interpreter accepts the risk of assuming of a constant velocity model, which can create structural ambiguities (Etris et al., 2001).

The reflectors for Base Nordland Gp (~23 Ma, Neogene), Triassic (~201 Ma) and Top Paleozoic (~251 Ma) were identified in the basin to make a 2D time-depth conversion to get a general velocity increase downwards. From well 7120/10-1, velocities were assigned to the lithostratigraphic units, and a time-depth table was created (Table 2). However, neither wells within the study area penetrated deeper than Top Triassic. Therefore, the Top Paleozoic reflector was identified in the Goliat area from Mulrooney et al. (2017) and traced back to the 3D cube. The velocity for Top Permian was assigned from well 7120/12-2 (fig14) and not from Goliat because the basin deepens westward and would provide a more accurate velocity for the Permian unit in the study area. Since the stratigraphic well correlation on the Finnmark Platform is limited in the study area, it had to be generated from well 7120/12-4 (fig.14), which is located approximately 20 km from the 3D seismic. The reflectors were identified and traced back to

the footwall cutoffs. In addition, a new velocity for the Triassic had to be calculated from well 7120/12-4 for the Finnmark Platform since the Triassic velocity from the basin created a distinctive pull-up effect after depth converting. The time-depth conversion took place in the software Move, where the interval velocities were assigned to the different interpreted horizons. The depth-converted sections were compared with both Gernigon et al. (2014) and Mulrooney et al. (2017), where the selected sections seemed reasonable. Also, the depth corrected section BB' (fig.25) correspond relatively well with the stratigraphic depths of well 7120/10-1 (Table 2), where the well is located at the footwall margin of the secondary fault. However, it should be noted that there exist variations between the depth (~700-800m) of Top Paleozoic in well 7120/12-2 and the depth converted 2D line BSS01-103 (located few km from the well) with the interpreted Top Paleozoic horizon in the anticline.

Table 2. Time depth table from well 7120/10-1, 7120/12-2 and 7120/12-4 used in the depth conversion process.

<b>Well 7120/10-1</b>			
<i>TVD (m)</i>	<i>Lithostrat. Unit</i>	<i>V<sub>interval</sub> (m/s)</i>	<i>V<sub>n</sub></i>
185	Seafloor	1571	V <sub>1</sub>
418	Base Nordland Gp (Base Neogene)	2234	V <sub>2</sub>
1162	Sequence 2	2698	V <sub>3</sub>
1337	Sequence 0	2880	V <sub>4</sub>
1370	BCU (Upper Jurassic)	3291	V <sub>5</sub>
1533	Stoe (Middle-Lower Jurassic)	3263	V <sub>6</sub>
1886	Top Triassic	3748	V <sub>7</sub>
	Top Paleozoic		V <sub>8</sub>
<b>Well 7120/12-2</b>			
3616	Top Paleozoic	4081	V <sub>8</sub>
<b>Well 7120/12-4</b>			
435	Top Triassic	2439	V <sub>7</sub>

### 3.3 Forward Modelling

Forward modelling is an interactive tool for analyzing structural geology, which helps validate the interpretation (fig.16). The forward modelling was done in StructureSolver. The geometries of deformed structural surfaces in the software are computed based on established kinematic models of fault-related folding. The software incorporates the scientific principles from Xiao and Suppe (1992) to model the folding that takes place in the hanging walls where the shapes of the hanging wall geometries are controlled by different variables. The variables include (i) the fault shape, (ii) the history of sedimentation rate relative to fault slip (iii) total slip after each bed is deposited, (iv) direction of relative rock motion in hanging wall collapse.

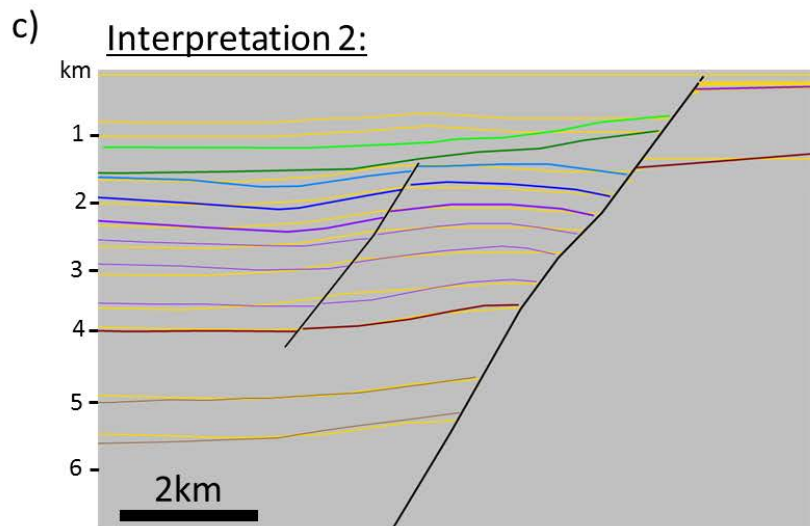
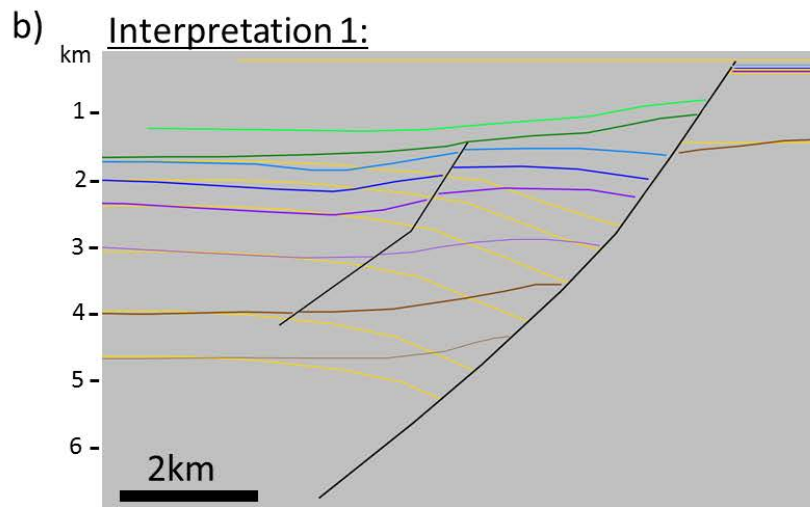
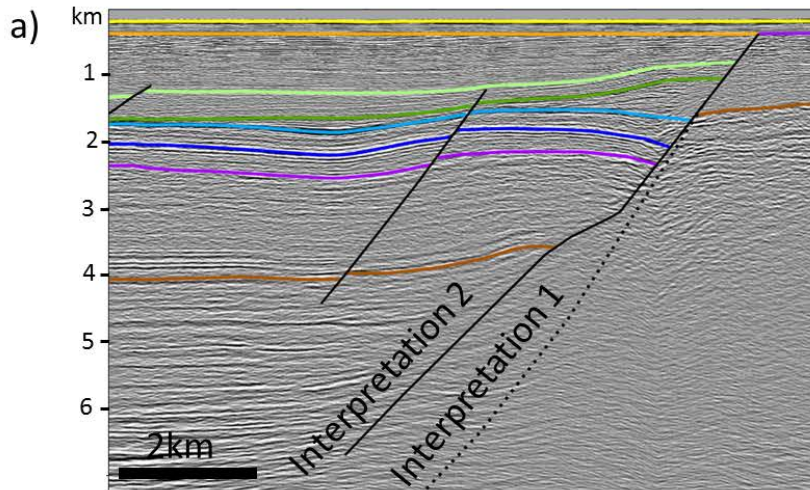
The software does not include compaction. Neglecting compaction in modelling studies are debatable (Skuce, 1996). However, Xiao and Suppe (1992) showed that under certain common

conditions, the history of compaction could be neglected since the compaction changes relatively smoothly in horizontal and vertical directions.

In the thesis, the idea with the forward modelling is to construct simple models trying to reproduce the fault geometry to understand how the hanging wall anticline was formed. It should be noted that several variables exist that the software does not incorporate such as dragging effect, unconformities, and variation in sediment input that could restrict the ability to replicate the structure. The modelling will try to fit the pre-growth horizons, where the anticline is mainly located. It will not take into consideration thick syn-rift sediments that affect the bedding geometries.

The sections are perpendicular to the main fault, and every section was calibrated with their horizontal and vertical scale. The key horizons, intra horizons, and the interpreted fault were digitized into the software (fig.16a). Structural surfaces were linked to the fault and positioned to correspond with all the hanging wall and footwall cutoffs of the already digitized horizons. A datum had to be set and was placed to the sea bottom. The software then predicted the structural surfaces based on the fault geometry (fig. 16a and b). By changing the fault geometry, the projected beds will adjust accordingly, trying to get the best-fit model of each section. In addition, one could adjust each modelled bed when modifying the fault shape to get a better link with the interpreted horizons. Due to the extensive erosion of the footwall, Cretaceous and Jurassic succession were missing. Their structural surfaces were placed right above the Top Triassic to get the minimum throw of the beds. A high shear angle or axial surface (i.e., ~80 – 85 degree) had to be implemented in order to replicate the sections in the best way, which differs from the default setting for extensional setting (~67 degrees) based on the findings from Xiao and Suppe (1992). In the result chapter, the forward modelling will only display the best-fit model of each selected cross section. The first section in every figure will show the interpreted master fault based on the seismic features, whereas the section underneath will be the best forward modelling result. As an example, fig.16a with interpretation 2 and fig.16c will be displayed since it is the best-fit model where the correlation seems to match.

It is important to emphasize that the StructureSolver has limitations in creating forward modelling structures when secondary faults with noticeable displacement are present, and the bedding between the faults is non-horizontal.



Sea Bottom S2 S0 Top Jurassic  
 Middle-Lower Jurassic Triassic Intra Triassic  
 Top Paleozoic Intra Paleozoic Projected beds

Fig. 16. a) Section displaying two different fault geometries with key horizons. b) Forward modeling from StructureSolver displaying a bad fit model between the interpreted beds and projected beds. c) Forward modeling displaying a best-fit model between the interpreted and projected beds.

## 4. Results and observations

### 4.1 Structural Style

The main structural architecture in the southwestern part of the Hammerfest Basin consist of several fault patterns. The distinctive irregularities in the variance map (fig.17) display areas with high lateral variation in reflectors (darker colors), while lateral reflection continuity of the horizons is shown in white. The largest areas of continuity are present in the southwestern and the northeastern-most region. The irregularities in the variance map correspond with the faulted regions throughout the study area except for fig. 17d. This horizon has the most lateral variation from the variance map, yet less observable faulting.

Two major fault populations are identified in the region. These fault populations consist of NNE – SSW, and E – W striking faults. The southeastern NNE – SSW fault (stippled line) changes strike towards an ENE – WSW trend. This fault has the most significant heave offset and is prominent throughout the structural maps. Structural highs are represented by red to yellow colors, whereas areas with blue to purple color display deeper areas. Between the NNE – SSW fault segments, significant changes in elevation are observable. A minimum of -1000 ms drop in elevation takes place from the structural highs in the south towards the northwestern region. On the eastern side, the E – W striking faults have a gradual decrease in elevation from the southern to the northern region. In addition, fig.17 show distinctive U-shape topographies in the northeastern part of Stø, BCU, and S0. The structural map of Stø FM (fig.17a; Middle – Lower Jurassic) is the horizon where the number of faults observed is the greatest. The faulting is less pronounced in the southwestern part where only minor faulting is present within the 3D cube. The BCU and S0 (fig.17b and c) show similar fault patterns as Stø Fm, but the fault complexity decreases slightly where the heave offset reduces. The E – W striking faults are less pronounced in S2 (fig.17d), where only some faults are present in the eastern region. The fault linkages in the area are also less evident compared to the other surfaces.



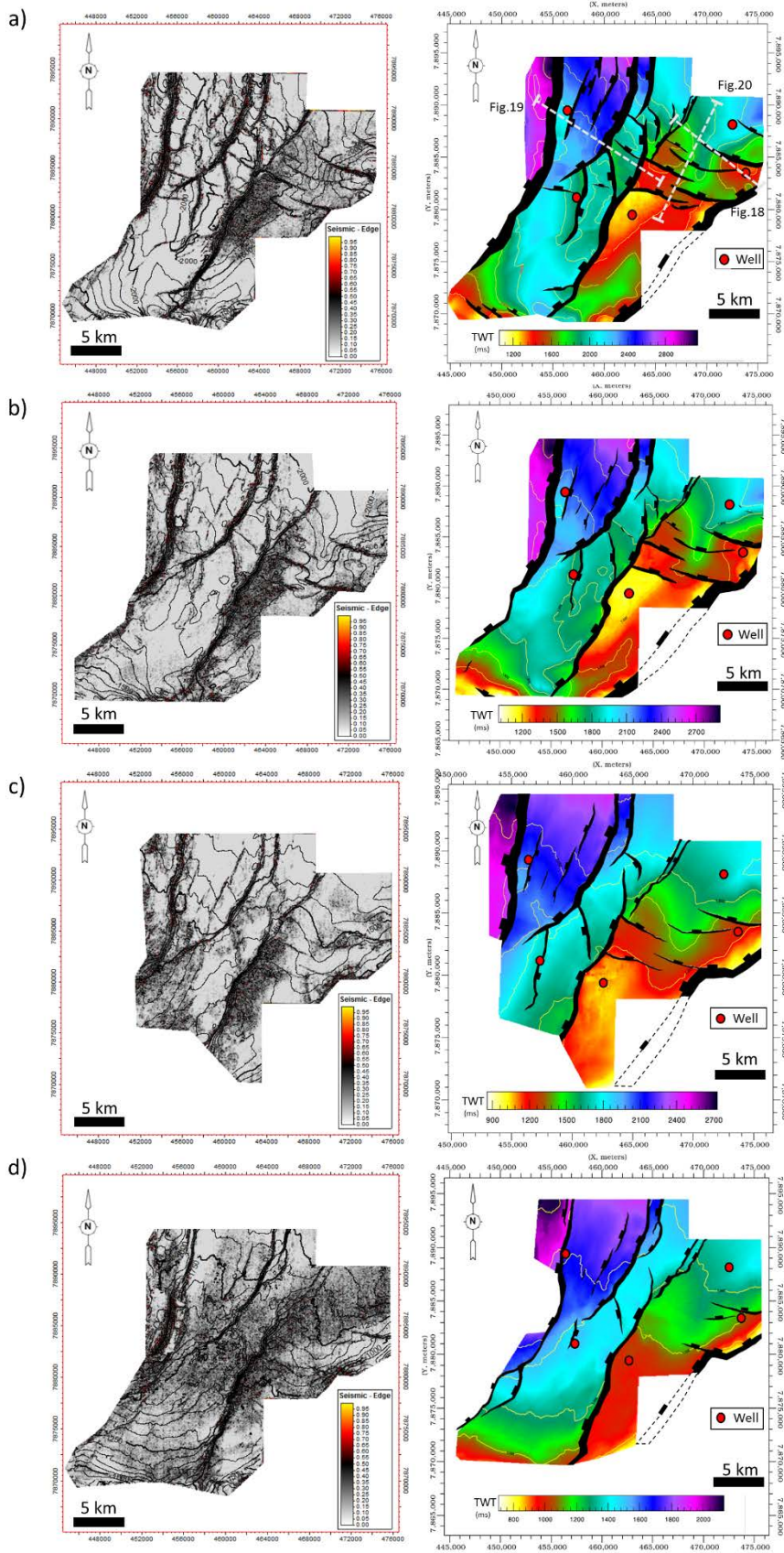


Fig. 17. Variance map to the left, structural map to the right showing the structural style. (a) Stø Fm (b) BCU (c) S0 (d) S2. Structural map of Stø displaying the location of the cross-sections of fig.18, 19 and 20. Maps in ms.

#### 4.1.1 Main fault

The main fault located in the southern part of the study area delineates the Hammerfest Basin from the Finnmark Platform and correspond to the ENE – WSW striking fault from the structural maps (fig.17). This fault has a large vertical offset that varies slightly along the strike within the study area but is represented by a throw of approximately -1500 ms in fig.18, between the footwall and hanging-wall cutoffs of the Top Paleozoic. The other faults display considerably smaller offset compared to the main fault, where the most basinward fault has a throw of approximately -300ms. Based on the lithostratigraphic units from well 7120/12-4, the Finnmark Platform consists of Paleozoic, Triassic and uppermost part of Cenozoic (Neogene) rocks, where Cretaceous and Jurassic rocks are missing. The Triassic succession in the basin consists of uniform thickness throughout the area. The Lower – Middle Jurassic unit also displays constant thickness but is considerably thinner compared to the Triassic. A slight increase in the thickness of the Upper Jurassic unit is observed towards the faults, except the fault located around the anticline. The S0 unit is very thin basinward, whereas the unit thickens significantly towards the main fault plane. However, the unit also thickens slightly in the syncline. The S2 has no thickness increase towards the main fault plane, but rather thickens basinward. This is also observable in the Cretaceous-Paleogene unit. The Neogene rock overlies both the hanging-wall and footwall rocks and is not faulted.

#### 4.1.2 NNE – SSW trend

The NNE – SSW faults (fig.19) dips northwest, towards the Tromsø Basin. The fault population consists of several pronounced and minor planar faults, where the most prominent offset deeply into the Triassic and propagate to the upper part of the Cretaceous-Paleogene unit. The two large faults located towards the southeast in fig.19, have variation in throw along the faults. The offset of the Jurassic units are approximate - 600ms and decreases to -300-400ms at the upper part of S2. The minor faults are limited to the lowermost half of S2 and continue down to the upper Triassic succession with a smaller offset between - 200-300ms in the Jurassic. The throw decreases significantly around S0, with offsets lower than -100ms. The Lower – Middle Jurassic unit has a constant thickness throughout the section, while the Upper Jurassic has slightly thicker packages towards the fault planes. A subsidiary fault that is antithetic compared to the NNE – SSW trend has developed a horst structure in the northwestern area. The thickness of the Upper Jurassic and the S2 units on the horst, are substantially thinner than their corresponding hanging-wall succession. Both S2 and Cretaceous-Paleogene units thicken substantially towards the northwest.

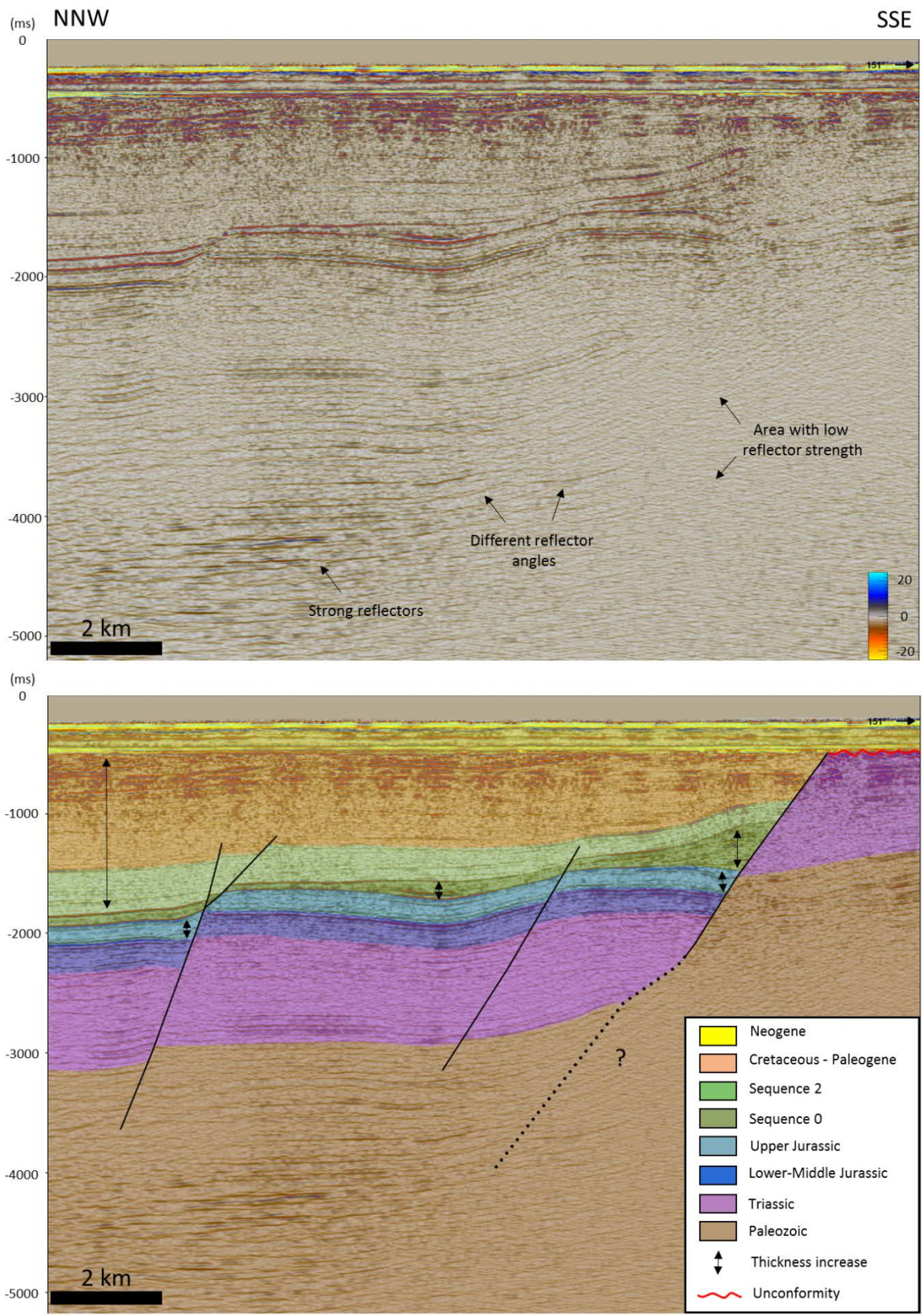


Fig. 18. Uninterpreted vs. interpreted section, display the main fault to the south and secondary faulting northwards. See fig.17a for location. Vertical exaggeration (VE) = 2

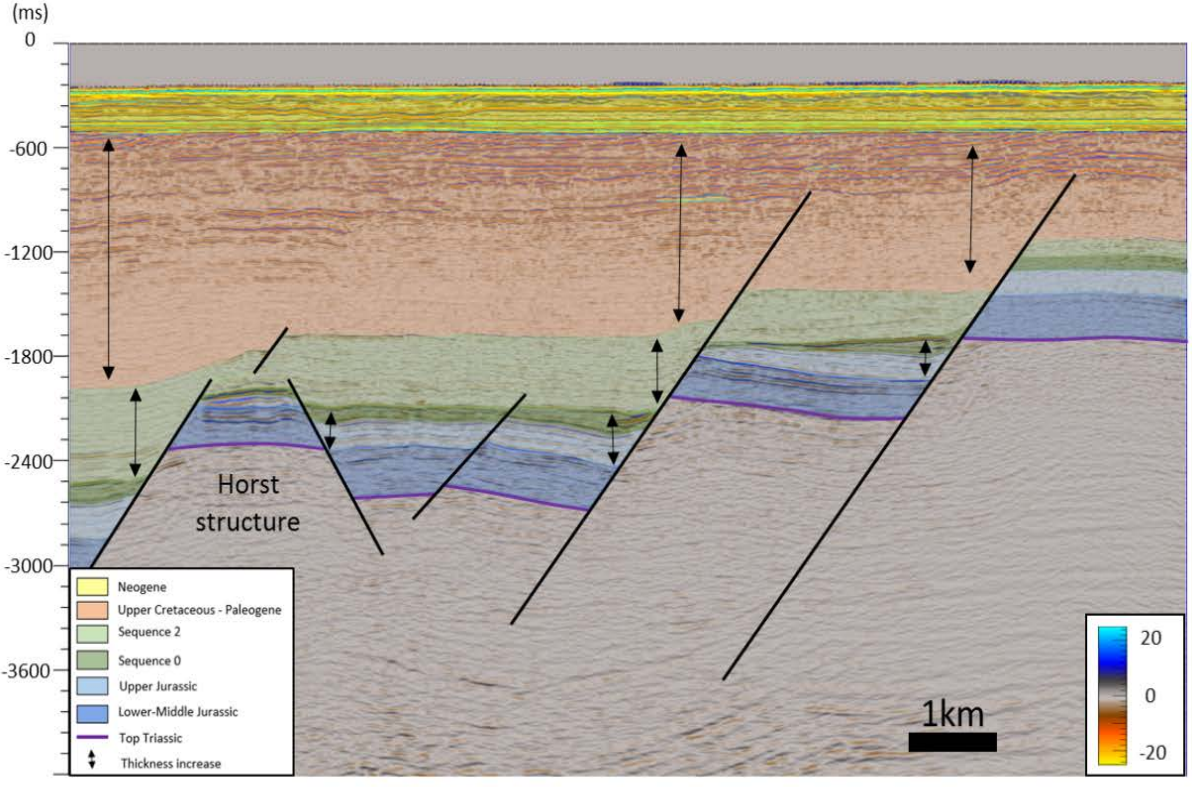
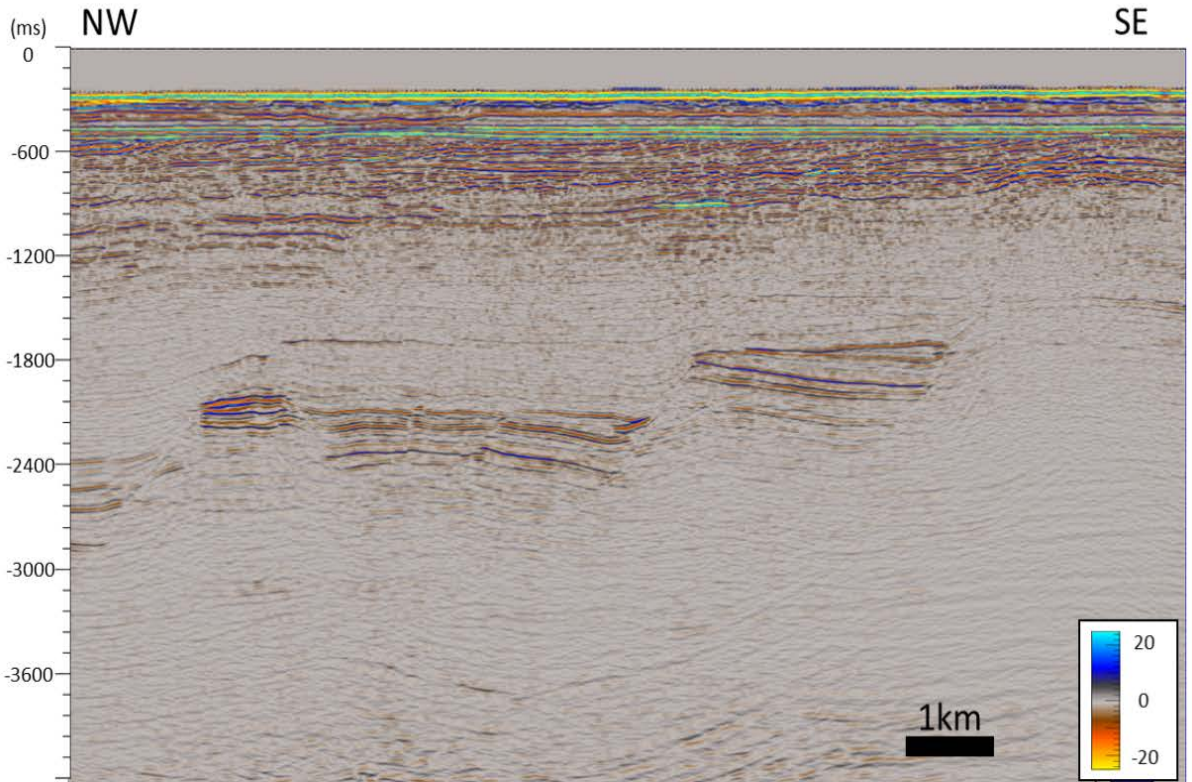


Fig 19. Uninterpreted vs. interpret section, showing NNE – SSW fault trends. See fig.17a for location. VE=2

#### 4.1.3 E – W trend

The other major fault population is the E – W striking faults, which are most prominent on the eastern side of the 3D seismic (fig.17). It consists of planar rotated fault blocks (fig.20) with significantly smaller fault displacement compared to the NNE – SSW trending faults (fig.19). The throw of these faults are around -200ms in the Lower – Middle Jurassic unit, where it decreases to -50ms in the upper part of S0. The faults are also much smaller in terms of propagation. They offset only the uppermost section of Triassic and pierce the top of S0 unit barely. The whole Jurassic unit seems to have a constant thickness throughout the section. However, the Cretaceous units show similarities with the previous section in terms of having slight thickening packages towards the fault. The S2 unit is much thinner in the northern area compared to the northeastern region (fig.20). Same thickness trend is observed in the Cretaceous-Paleogene unit, but with a considerably thicker unit.

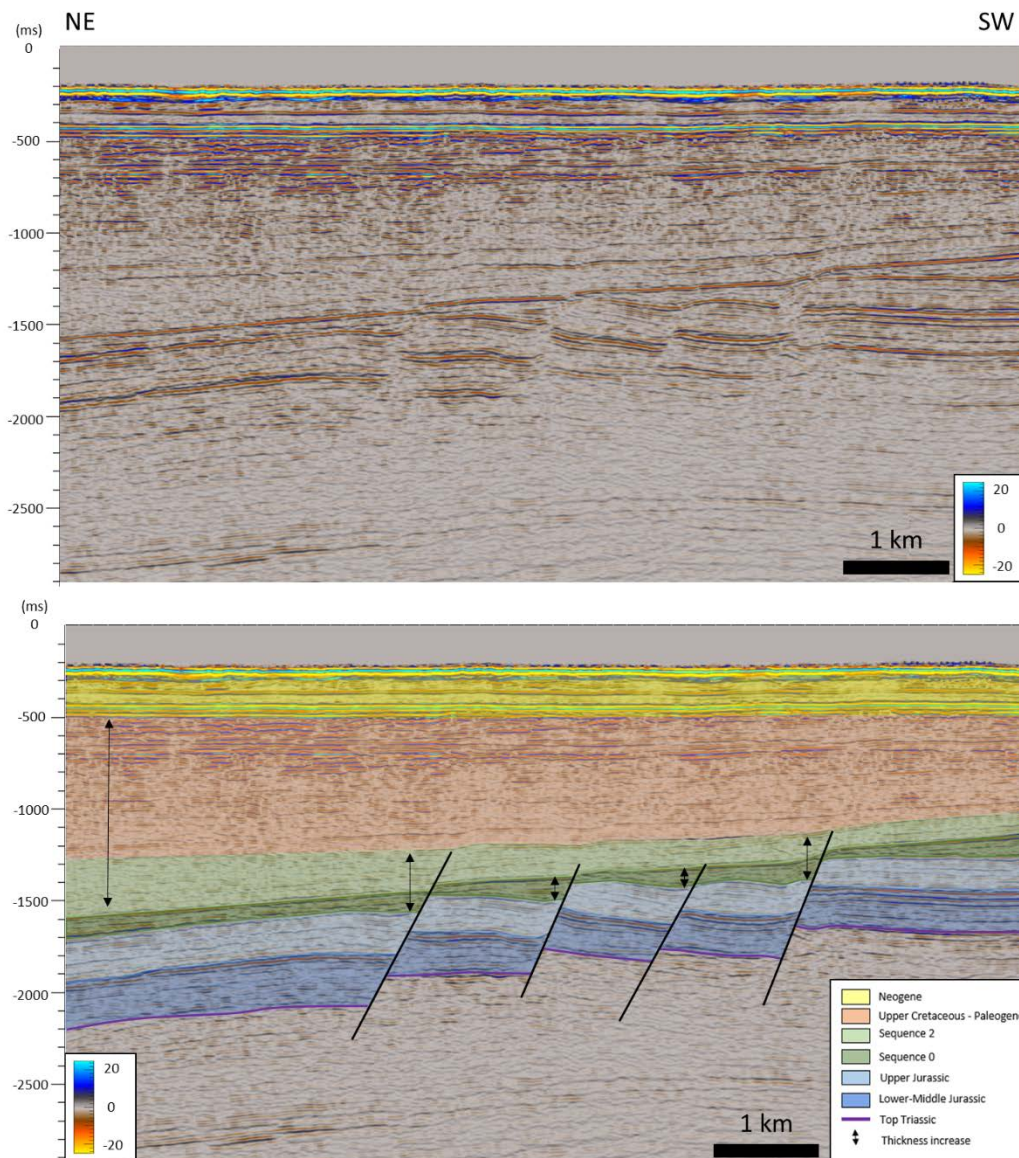


Fig. 20. Uninterpreted vs. interpret section, showing E – W fault trends. See fig.17a for location. VE=2

## 4.2 Time thickness maps

The Upper Jurassic (fig.21) succession show a significant escalation in thickness (i.e., blue to purple color) in the southern areas along the main fault, compared to adjacent areas. The unit also displays a slight thickness increase in the hanging-wall of the NNE – SSW faults. Nevertheless, the unit has a comparatively similar thickness in the center and northwestern areas with minor differences. However, noticeably thickness variations are observed in the northeastern region adjacent to the two wells.

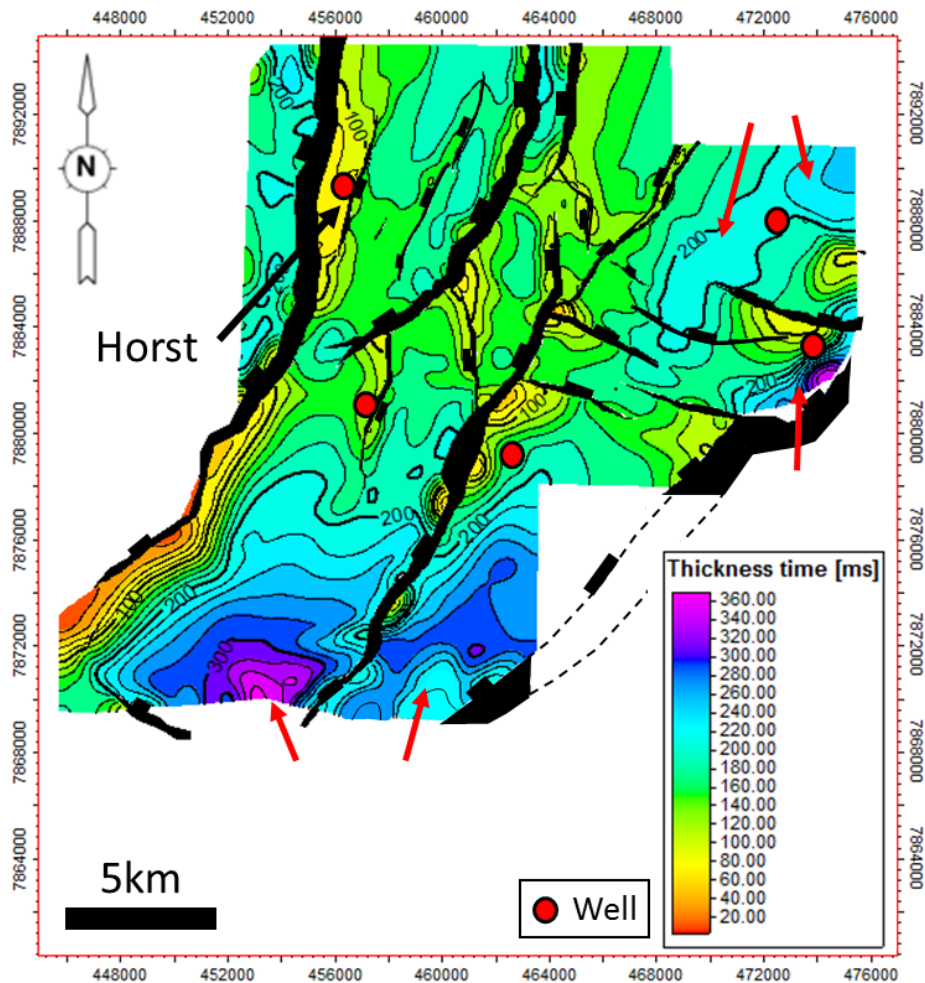


Fig. 21. Time thickness map of Upper Jurassic strata (Hekkingen Fm). Red arrows indicating substantially thickness increase

In general, very thin interval thickness (red to yellow color) of S0 (fig.22a) is present in the footwall areas in both NNW – SSW and E – W striking faults. Minor thickness differences are observable in the NNW – SSW faults. The sequence is thickening towards the main fault, but display thicker packages compared to the Upper Jurassic unit in the southeastern region (see red arrows). A noteworthy thickness variation is located between the E – W fault trend in the northeastern region where the flanks are considerably thinner than the elongated thicker zone. This trend diminishes in the thickness map of S2 (fig.22b), where a general increase in thickness is observed towards the north and northwest. The S2 is thinnest in the southeastern area.

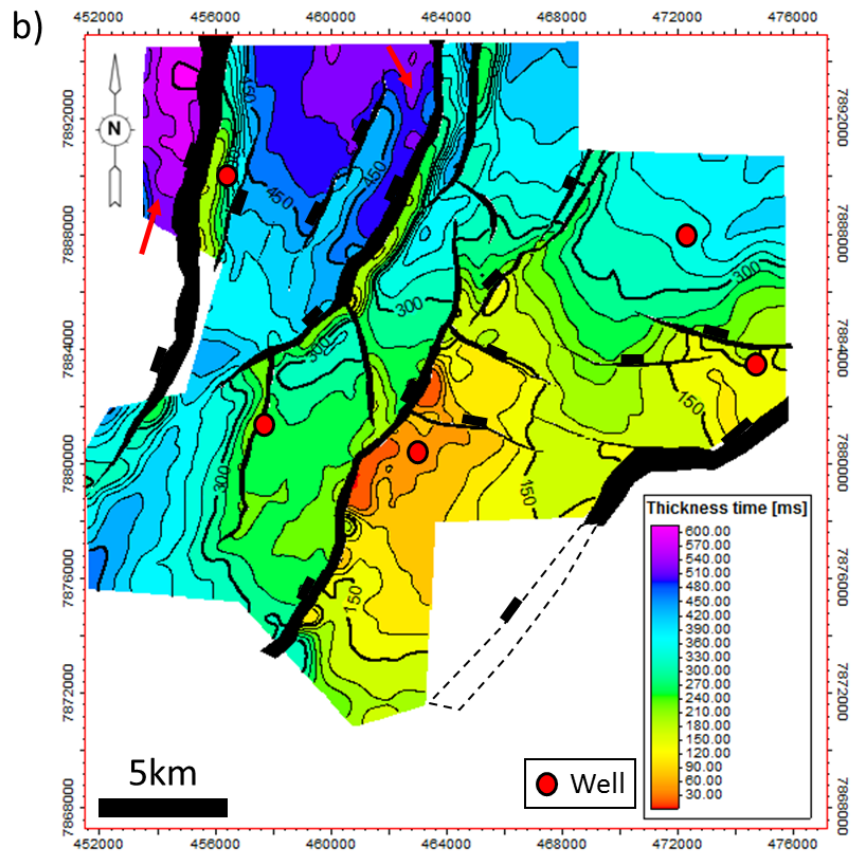
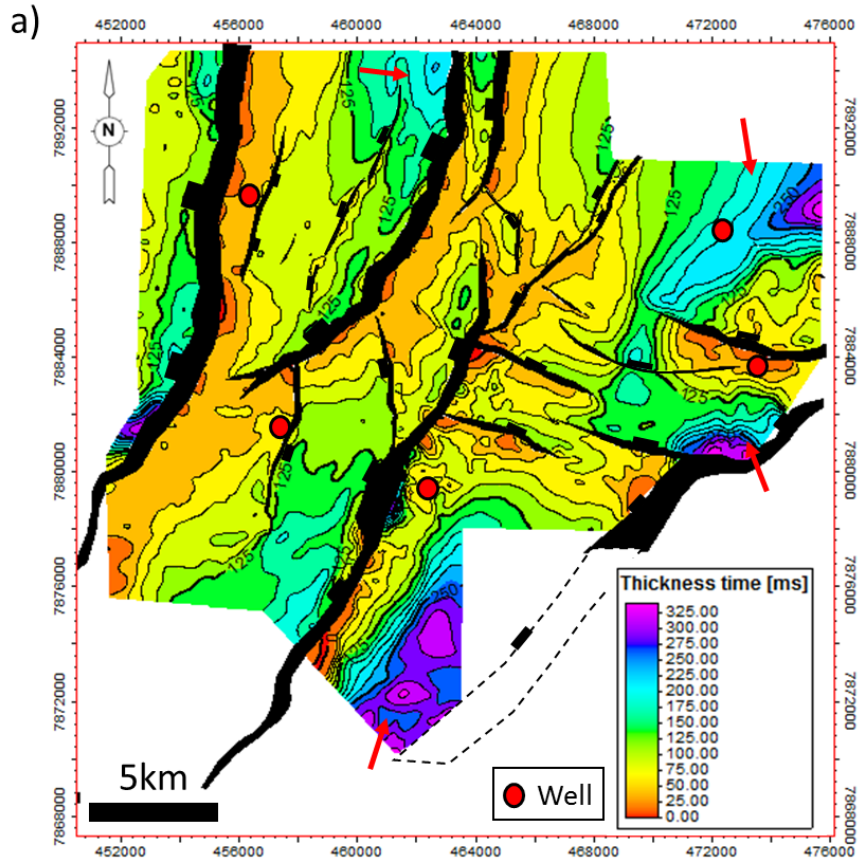


Fig. 22. Time thickness map of a) S0 b) S2. Red arrows indicating substantially thickness increase

### 4.3 Hanging-wall folds

Deformation of the hanging wall of the main fault is characterized by an anticline followed by a syncline (fig. 18 and 23). The anticline is only observable on the eastern side of the given 3D cube before it fades south-westwards. The structure is detected 15-20 km north-eastwards along the main fault before it diminishes (fig.23). The syncline is prominent on the eastern side of the 3D cube but is less pronounced towards the northeast, around section CC' and DD'.

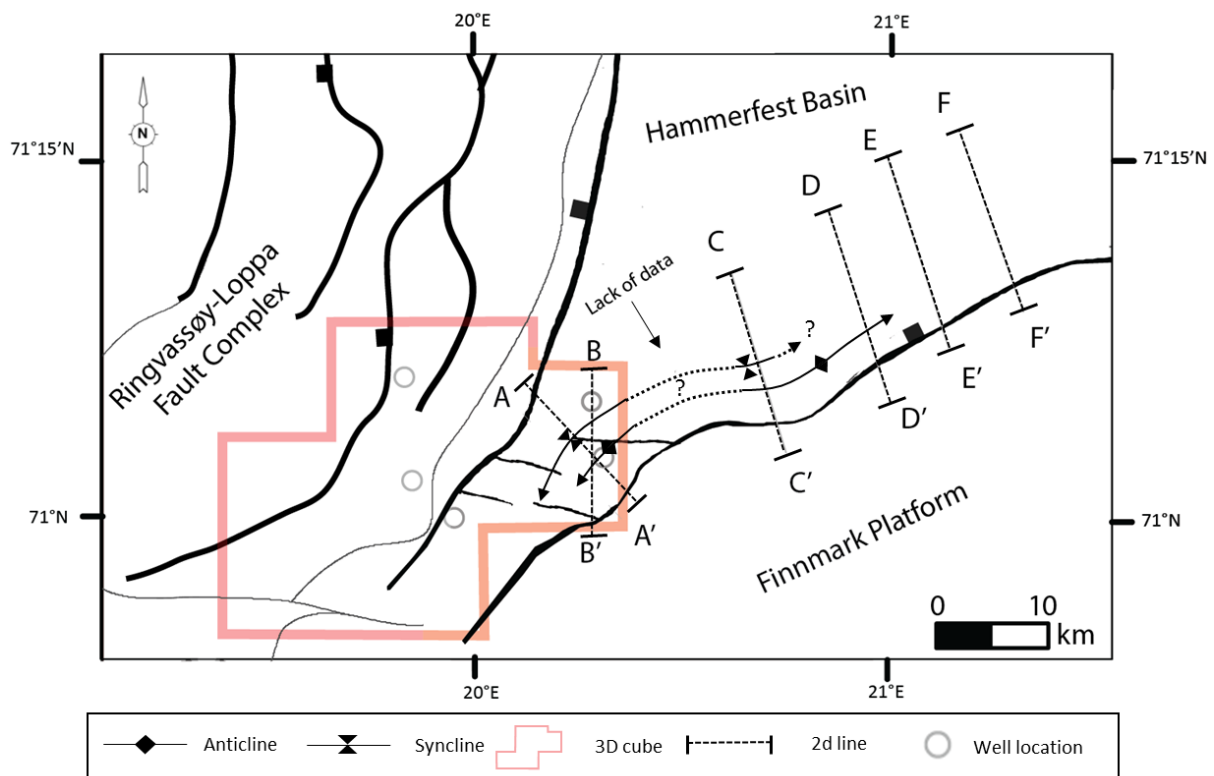


Fig. 23. Map view of the extent of the anticline and syncline. Section AA', BB', CC', DD', EE' and FF' displayed along the Troms-Finnmark Fault Complex. The dotted line between the syncline and anticline show the projected structure.

The width of the anticline is approximately 5-6 km in the study area (fig.24 and 25). The anticline structure is symmetrical (fig.24), where the axial plane is slightly tilted, and the limbs have different dipping angle. The forelimb has a gentler angle where the beds are dipping synthetic to the master fault, while the backlimb has a slightly steeper angle. The anticline structure has larger dimensions compared to the syncline. The fold amplitude of Top Triassic to Top Jurassic is around 300m, where the syncline has a lower amplitude of 100 – 150 m. Stratigraphic onlaps within the syncline of S0 are also observed (fig.26). The S0 and S2 do not exhibit the same folding structure as the underlying layers and have antithetic dipping beds towards the main fault (fig.24 and 25). One prominent secondary fault striking E - W is noticeable within the anticline structure (fig.25) which is terminating towards the west (fig.23 and 24). Smaller subsidiary faulting within the structure are few and not widespread.



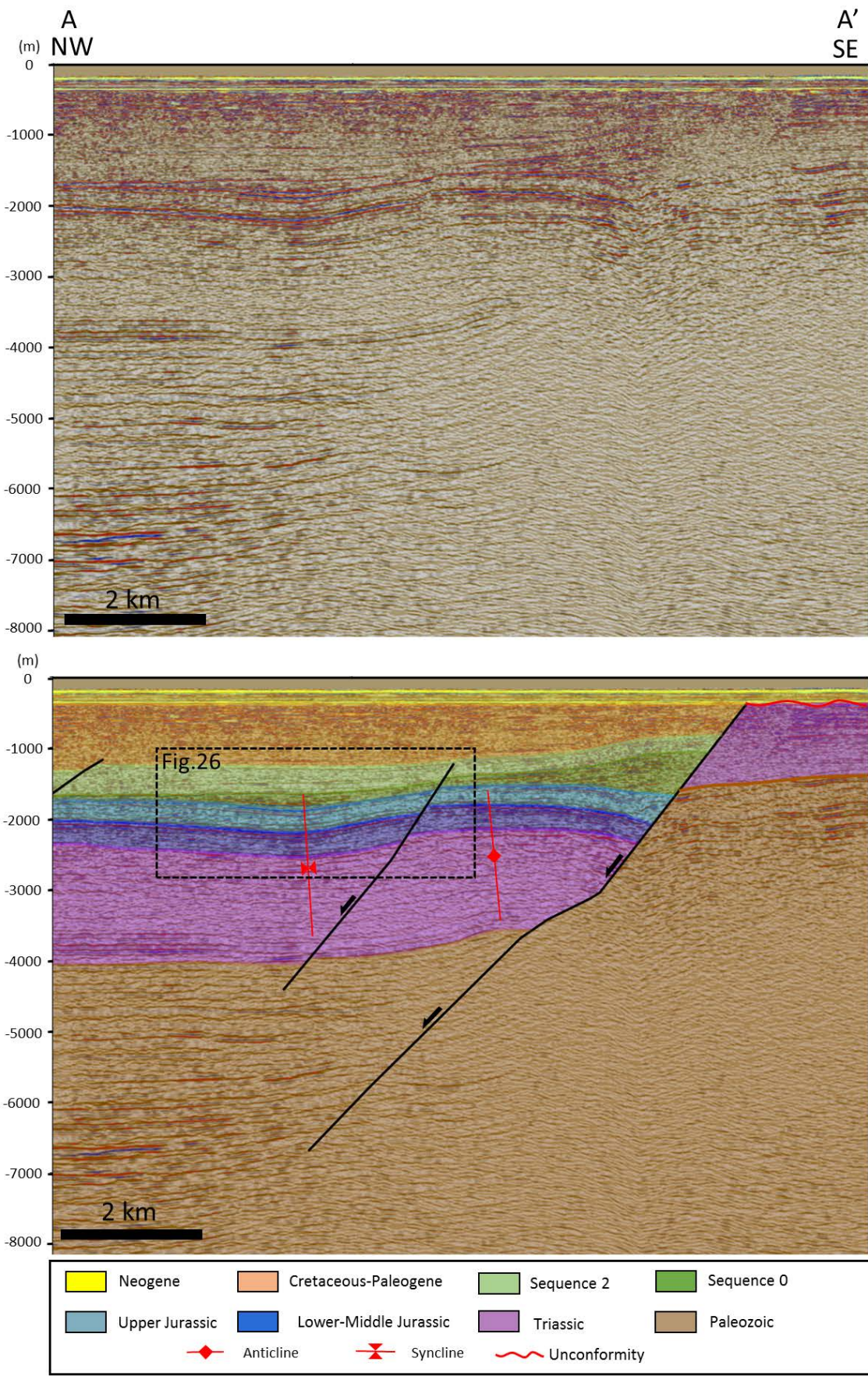


Fig. 24. Uninterpreted vs. Interpreted section of section AA' in depth (m). Dotted rectangle show fig.26. No vertical exaggeration. See fig.23 for location.

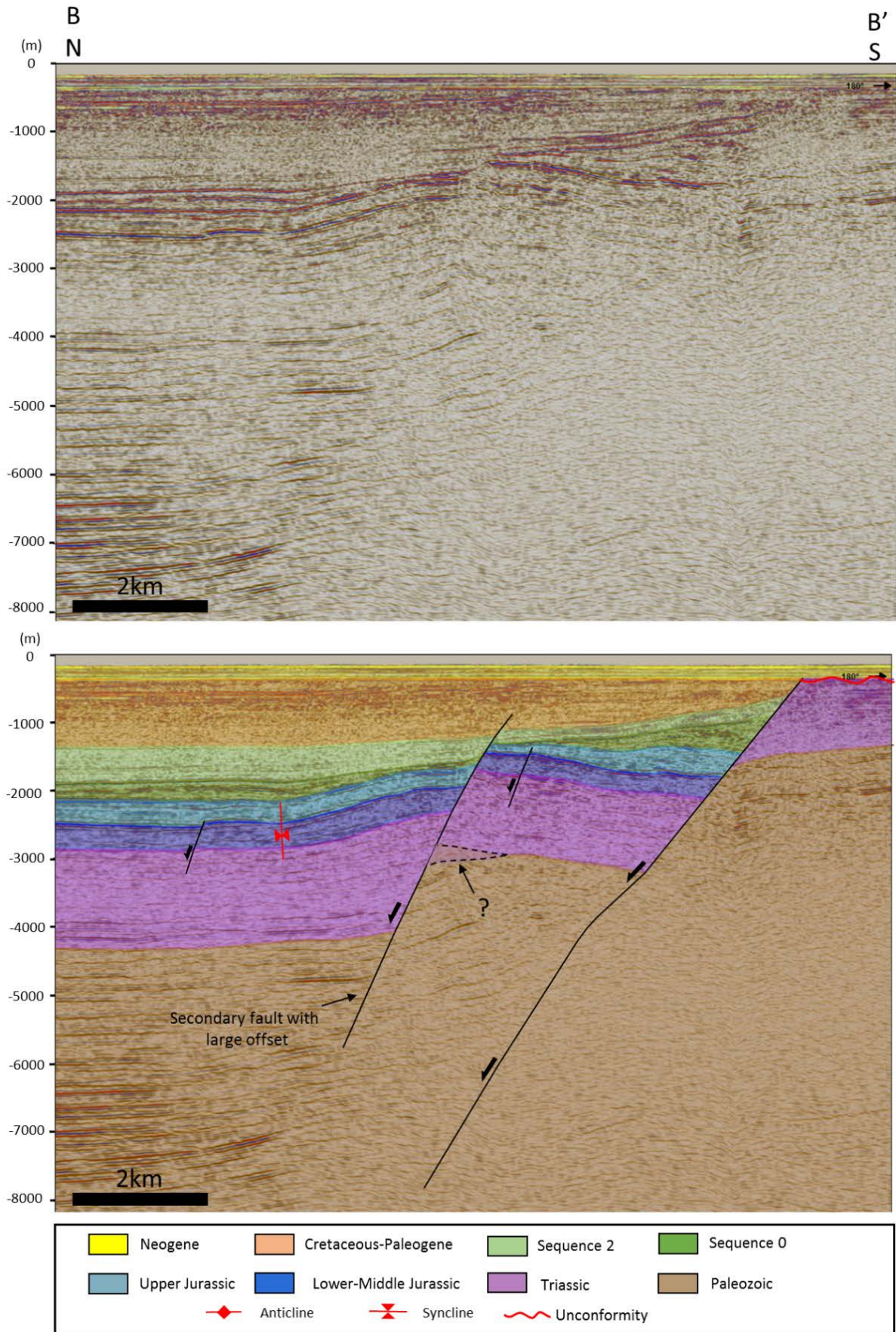


Fig. 25. Uninterpreted vs. Interpreted section of section BB' in depth (m). No vertical exaggeration. See fig.23 for location.

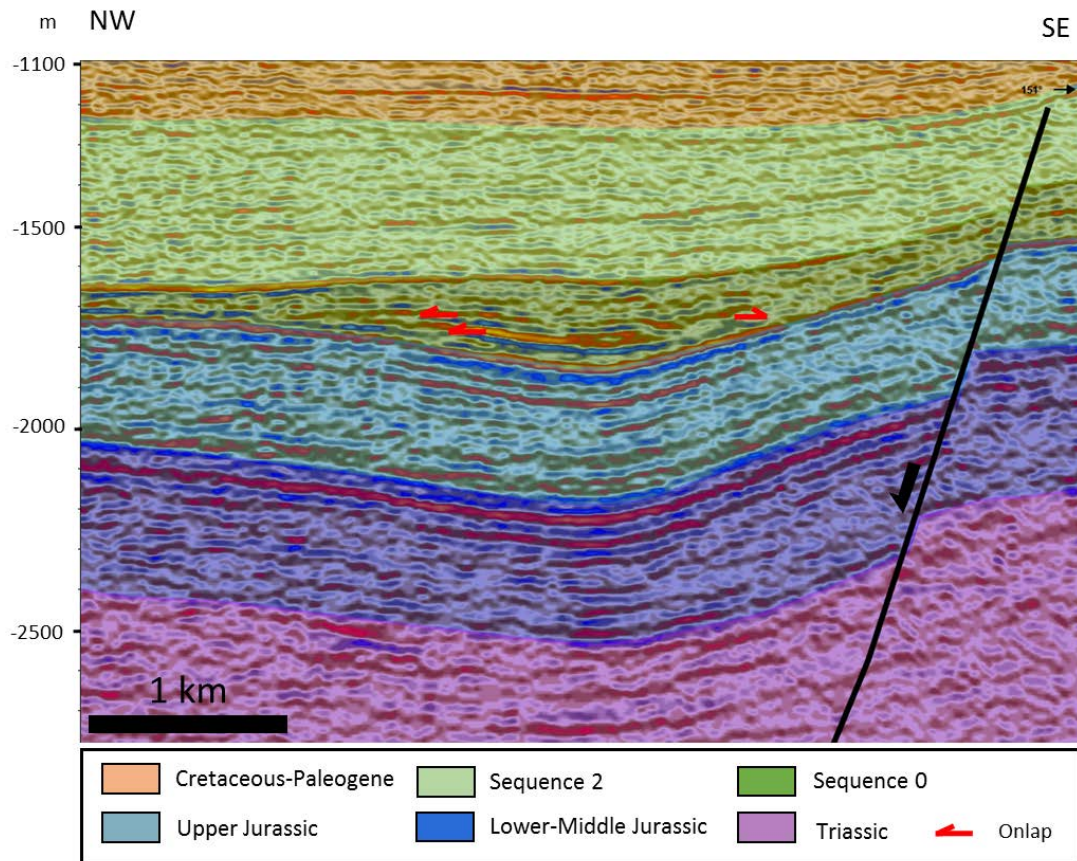


Fig. 26. Zoomed in AA' cross-section (fig.25) showing stratigraphic onlaps within the S0 unit. VE=2

The stratigraphic units in the Finnmark Platform of the selected cross sections (fig. 27- 30) are based on the lithostratigraphy from well 7120/12-4 (see fig.14 for location). Therefore, the Jurassic and Cretaceous rocks are assumed to be missing. Sections CC' (fig.27) and DD' (fig.28) display similar hanging wall geometry of the main fault as the 3D cube, whereas EE' (fig.29) and FF' (fig.30) show other characteristics. Only the Triassic succession has similar thicknesses throughout the sections with some differences, whereas the overlying units exhibit variable thicknesses and dip orientation depending on the sections.

The Triassic and Lower – Middle Jurassic units of section CC' (fig.27) display constant thickness throughout the section, while the Upper Jurassic and S0 units thicken toward the main fault. The Upper Jurassic also thickens against the secondary fault. The S0 does not show this tendency, but is considerably thinner around the anticline and rather thickens in the surrounding areas. The large secondary fault is comparable with BB' in fig.25 but displays smaller displacement. The most significant vertical offset of the secondary fault is located in the Top Paleozoic, Triassic, and Middle – Lower Jurassic rocks with a displacement of ~500m displacement, where the throw decreases significantly towards Upper Jurassic and S0 (< 100m displacement). The anticline in section CC' (fig.27) display similarities with section AA' and

BB' (fig.24 and 25) in terms of width and fold amplitude in both the syncline and anticline. The thickness distribution throughout the units are also similar to both AA' (fig.24) and BB' (fig.25), but the bedding orientation of the Cretaceous succession towards the main fault differs. The S0 and S2 have antithetic dipping beds compared to the synthetic dipping beds within the area of the 3D seismic.

Several minor antithetic and synthetic planar faults are visible in the anticline of section DD' (fig.28). These faults mainly offset the Lower – Middle Jurassic, and some of these faults offset into the S0 and S2. The well-defined syncline seen in fig. 24, 25, and 27 are not evident in the area (fig.28). The Middle – Lower Jurassic unit has a constant thickness throughout the section, but consist of thinner succession compared to CC' (fig.27). Upper Jurassic unit increases the thickness towards both the main fault and the subsidiary faults. The S0 unit situated towards the main fault is significantly thicker than the previous sections (AA', BB' and CC'), whereas S2 has comparable thickness characteristics. Both S0 and S2 have synthetic dipping beds, whereas the underlying units have synthetic beds. These beds also have slightly higher dip angle.

Although the anticline is absent, some degree of folding in the hanging wall of section EE' (fig.29) is observable. Throughout the section, the Triassic and Lower-Middle Jurassic units have a constant thickness and display similar thickness features as section DD' (fig.28). The Upper Jurassic and S2 units thicken towards the main fault. However, the increase is less significant than fig.28. These two units are very thin basinward and display no thickness variation in the hanging-wall of the secondary faults. The whole section has synthetic dipping beds close to the main fault.

Section FF' (fig.30) is located furthest northeast along the strike (fig.23). The folding of the hanging wall has developed a syncline. Subsidiary faulting is present close to the main fault and further out in the basin with a very low throw. The faults close to the main fault offset mainly the Jurassic and are present in the uppermost of Triassic, while the faulting located basinward offset deeper Triassic succession. No significant changes within the Triassic and Jurassic units are present in the section, but the Upper Jurassic unit seems to thin slightly towards the main fault. The S0 unit thickens close to the main fault and at the syncline. Similar synthetic dipping beds as section EE' (fig.29), are present. However, the dipping angle of the beds in FF' seem to be steeper.

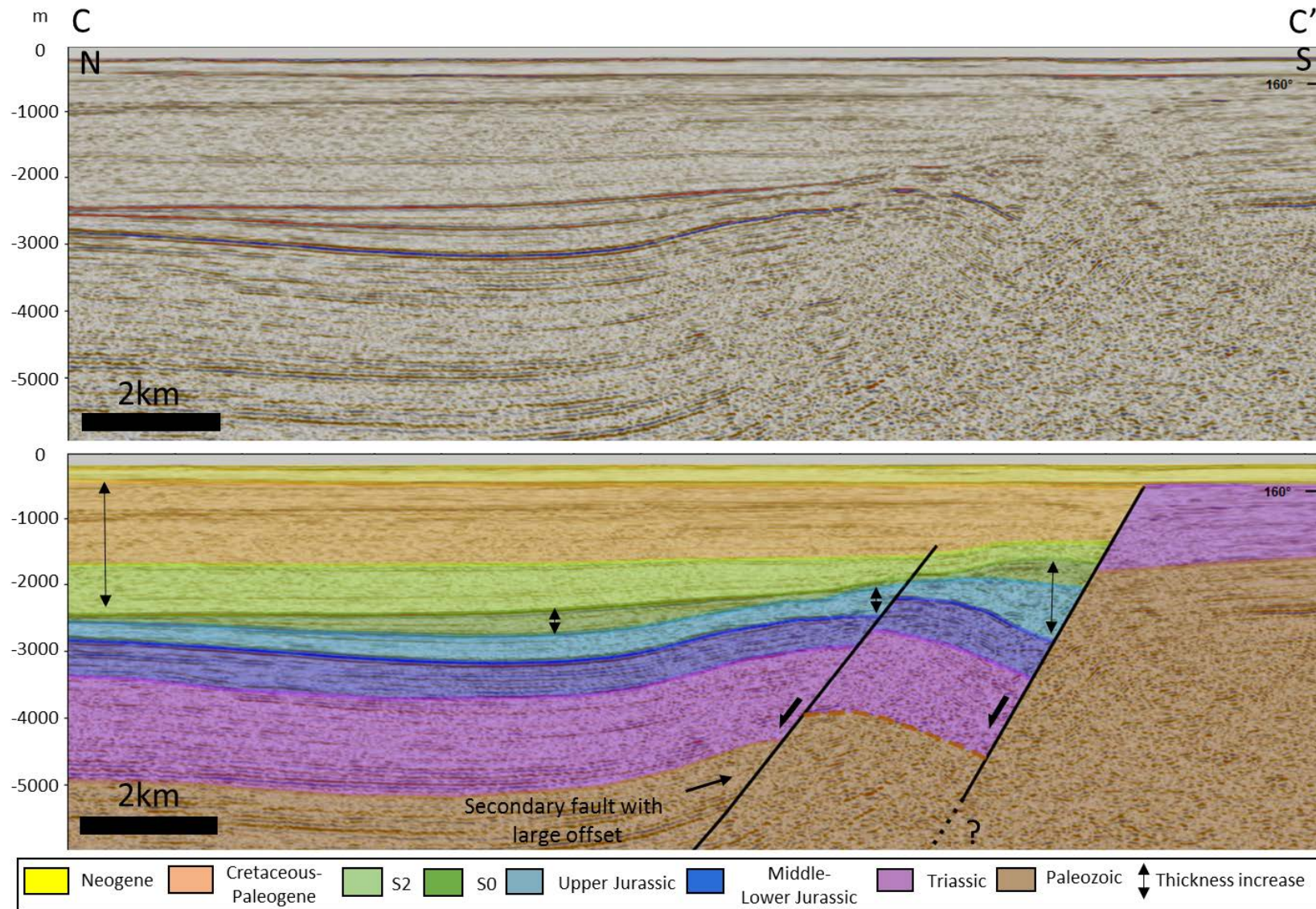


Fig. 27. Uninterpreted vs. interpreted. CC' section (BSS01-102) showing anticline structure in the hangingwall of the main fault with one large secondary fault offsets the succession with a varying throw. No vertical exaggeration. See fig.23 for location.

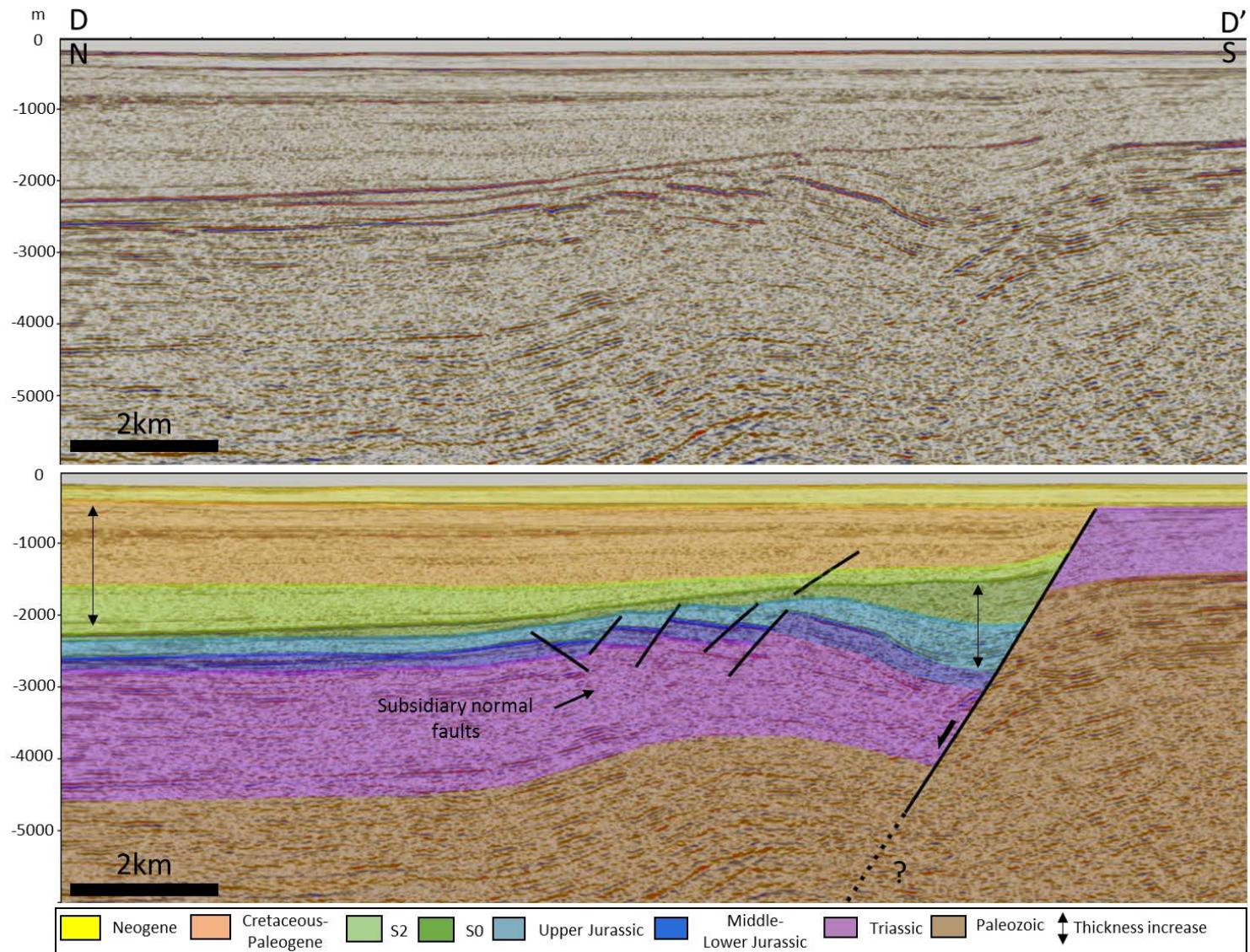


Fig. 28. Uninterpreted vs. interpreted. DD' section (BSS01-103) showing anticline structure in the hanging-wall with antithetic and synthetic subsidiary faulting. No vertical exaggeration. See fig.23 for location.

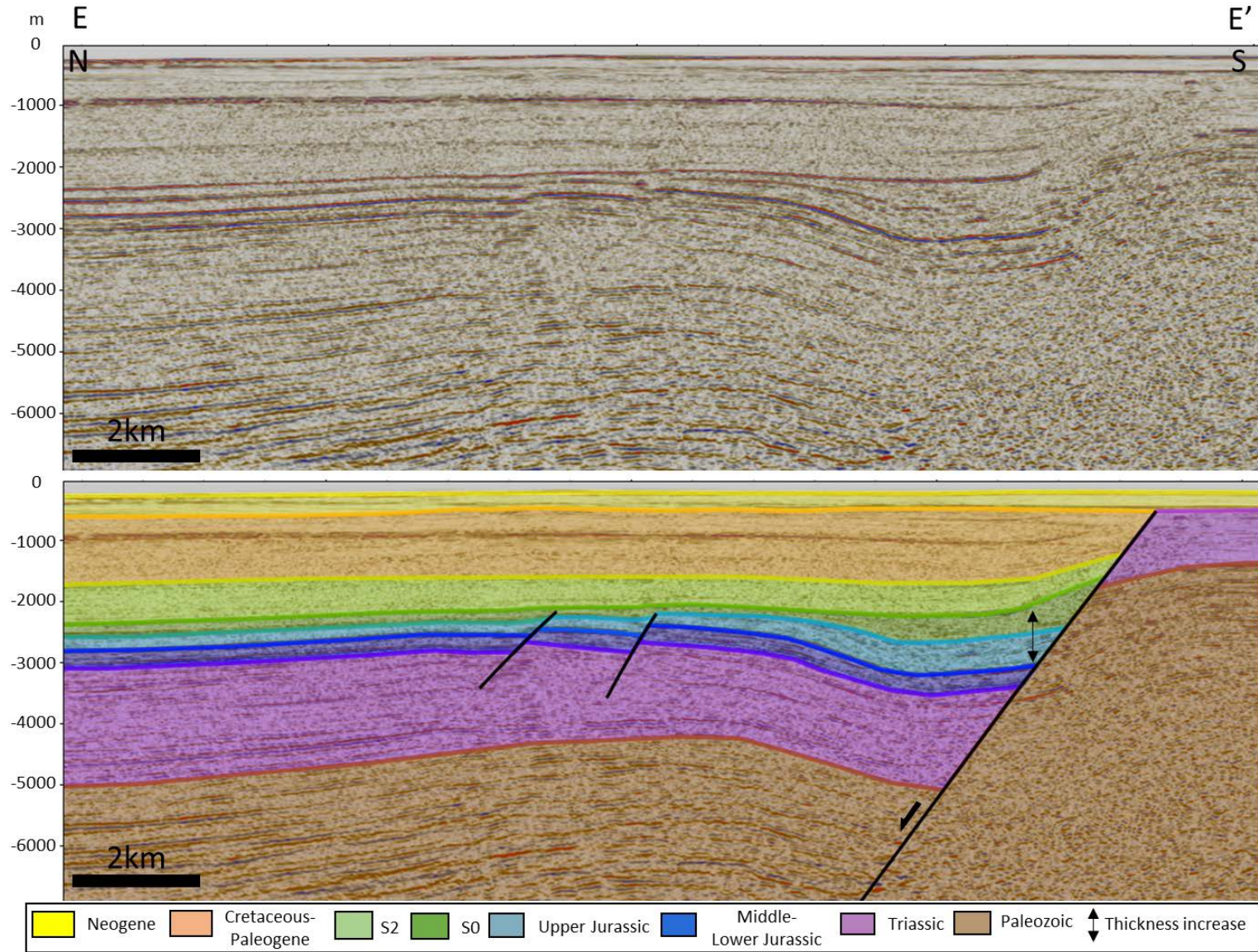


Fig. 29. Uninterpreted vs. interpreted. EE' section (BSS01-104) display a rollover structure. No vertical exaggeration. See fig.23 for location.

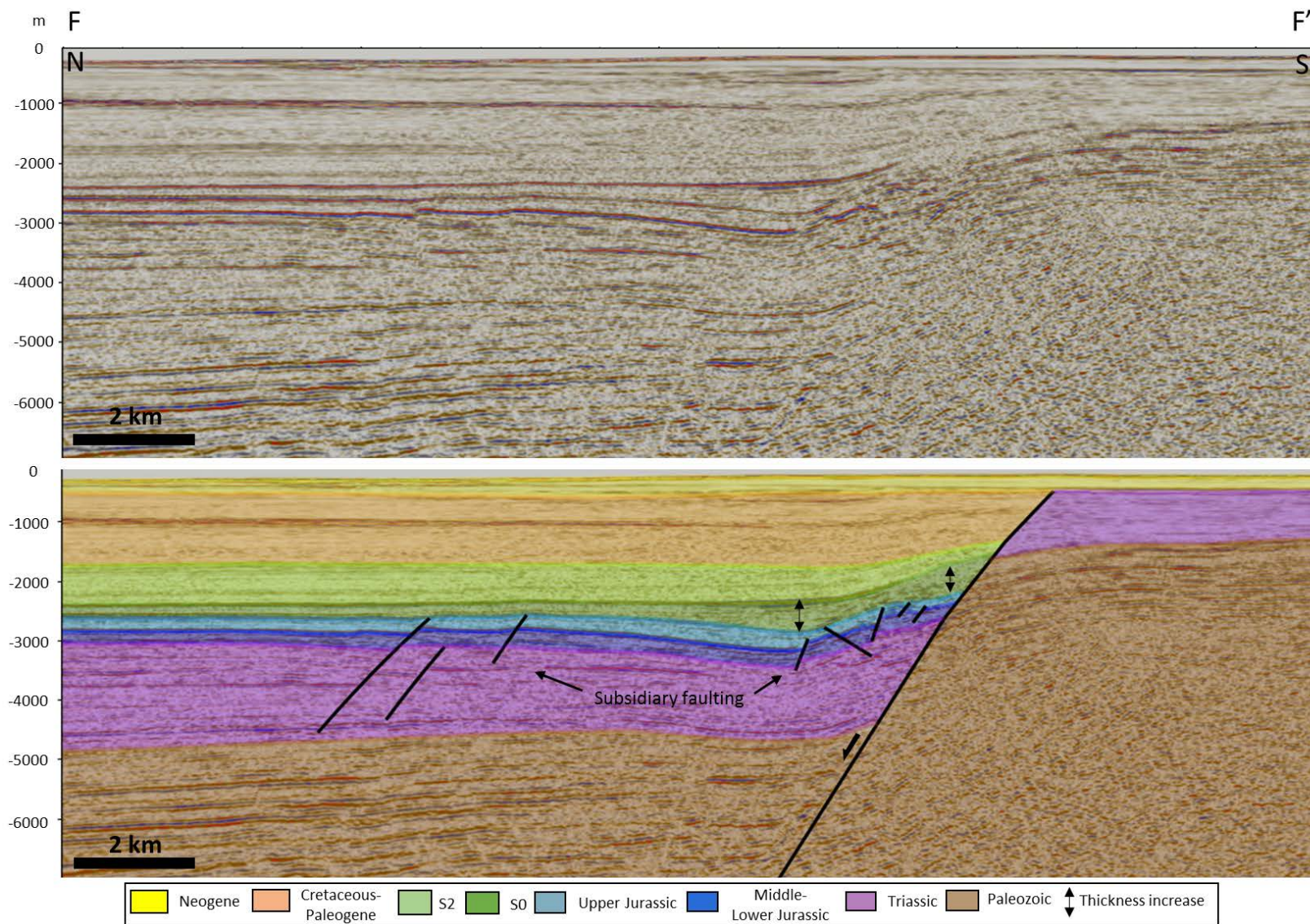


Fig. 30. Uninterpreted vs. interpreted. FF' section (BSS01-105) show syncline where S0 increase the thickness in both towards the fault and syncline. No vertical exaggeration. See fig.23 for location.



#### 4.4 Forward Modelling

In the following chapter, best-fit forward modelling results from section AA' to FF' will be presented. The first section in every figure in this chapter will show the interpreted master fault based on the seismic features, whereas the underneath section will be forward modelling result. The best-fit models do not always coincide with the original interpreted fault to replicate the bedding structure.

##### Section AA'

Fig.31 display section AA' with the originally interpreted horizons. The seismic response beneath 3000 m around the major fault shows little variations in seismic amplitude compared to adjacent areas towards the basin. The interpreted fault has a fold bend at a depth of 4 km. In the modelled section, the main fault has, to a certain extent, two planar faults separated with a small bend. The lower area has a slight higher dip compared to the upper half. The whole fault has an overall convex bend.

The best-fit model displays a correlation between the modelled beds and the traced horizons close to the main fault in the Paleozoic, Triassic and Jurassic succession with a minor mismatch in the syncline. On the other hand, the S0 and S2 layers have an apparent mismatch throughout the section. Other fault shapes such as listric (fig.16b) were tested and could not imitate the section. The modelled beds of the listric fault geometry displayed utterly different features in terms of dipping beds and angles.

##### Section BB'

The main fault of section BB' (fig.32) has concave bend based on the seismic features. The best fit was modeled to trail the interpreted beds close to the main fault. The large secondary fault made modelling towards the basin impossible. An overall good fit between the modelled beds and the interpreted beds from Top Paleozoic to Middle – Lower Jurassic, whereas Top Jurassic and the Cretaceous beds show clear mismatch.

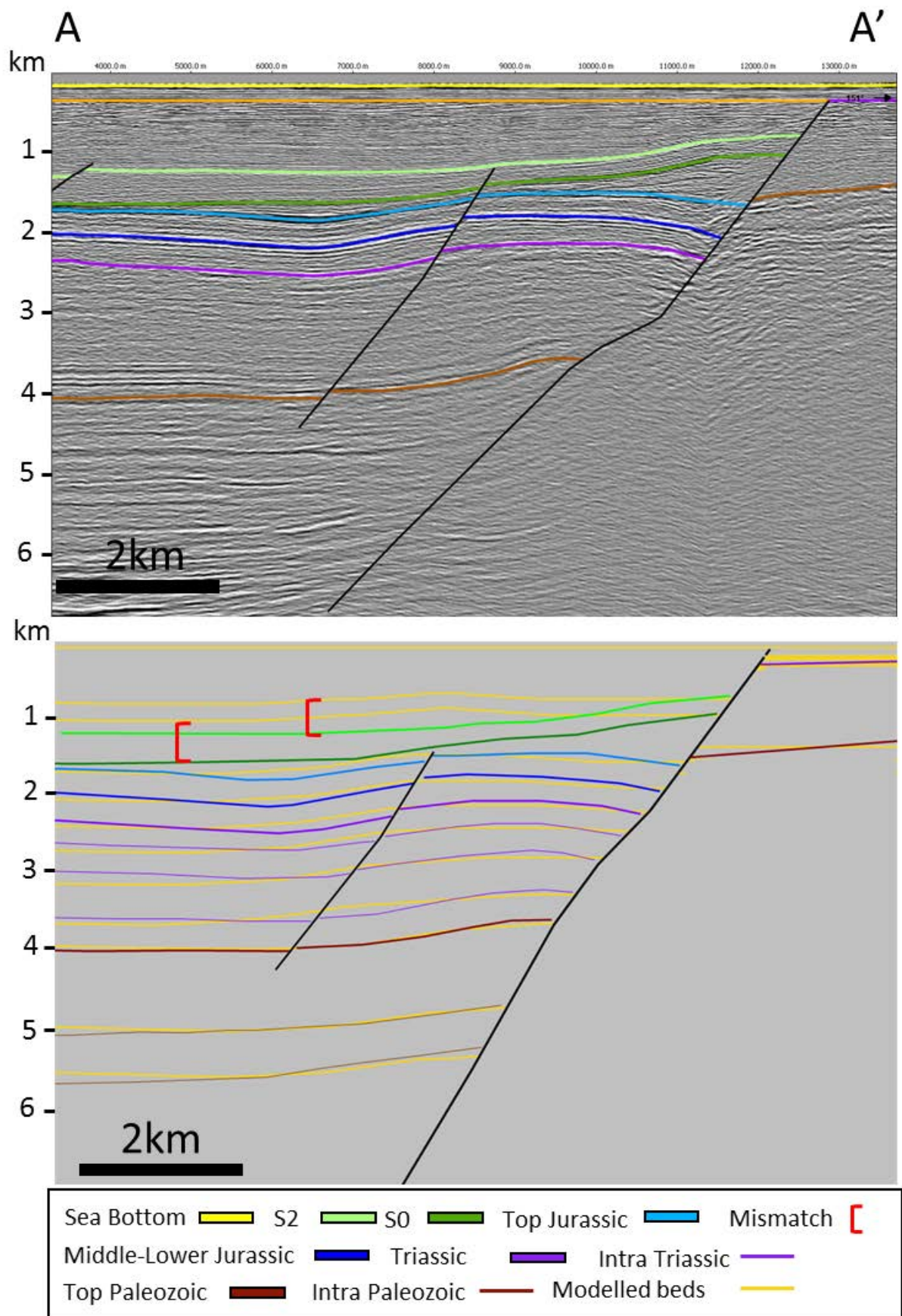


Fig. 31. Upper figure display section AA' of the interpreted top horizons, whereas the underlying show the best-fit modeling result. The section shows an overall good fit until top S0 and S2. See fig.23 for location.

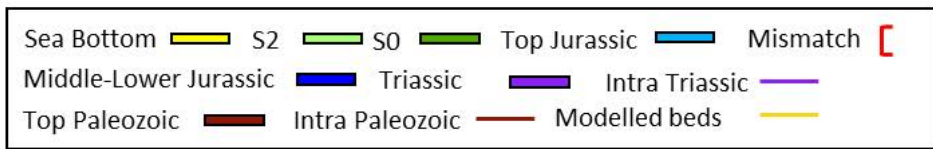
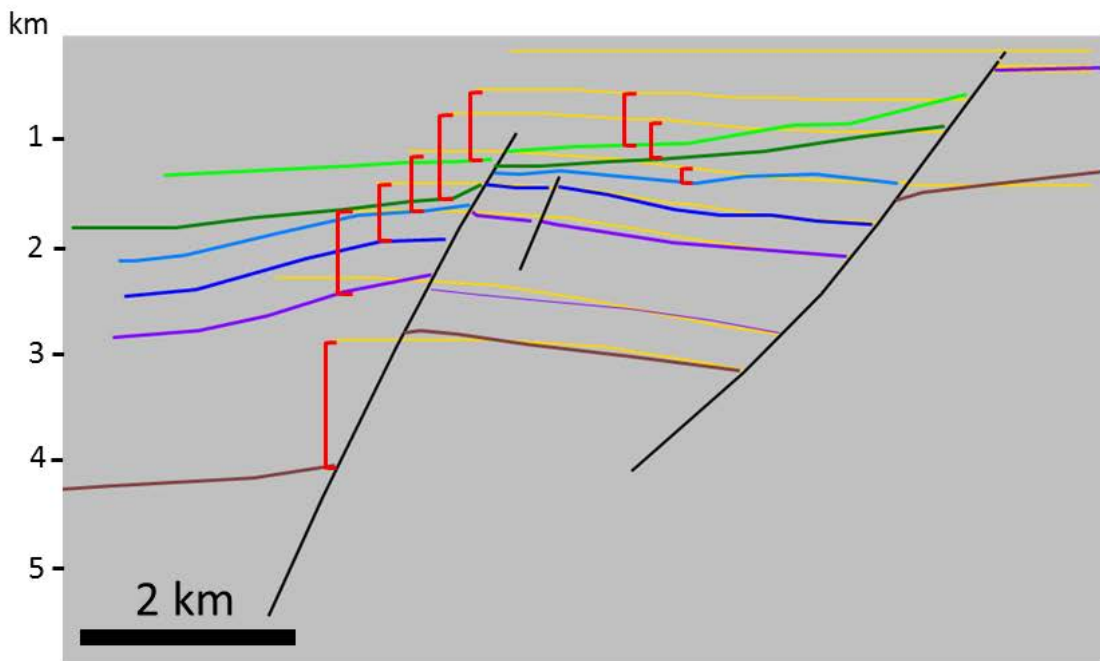
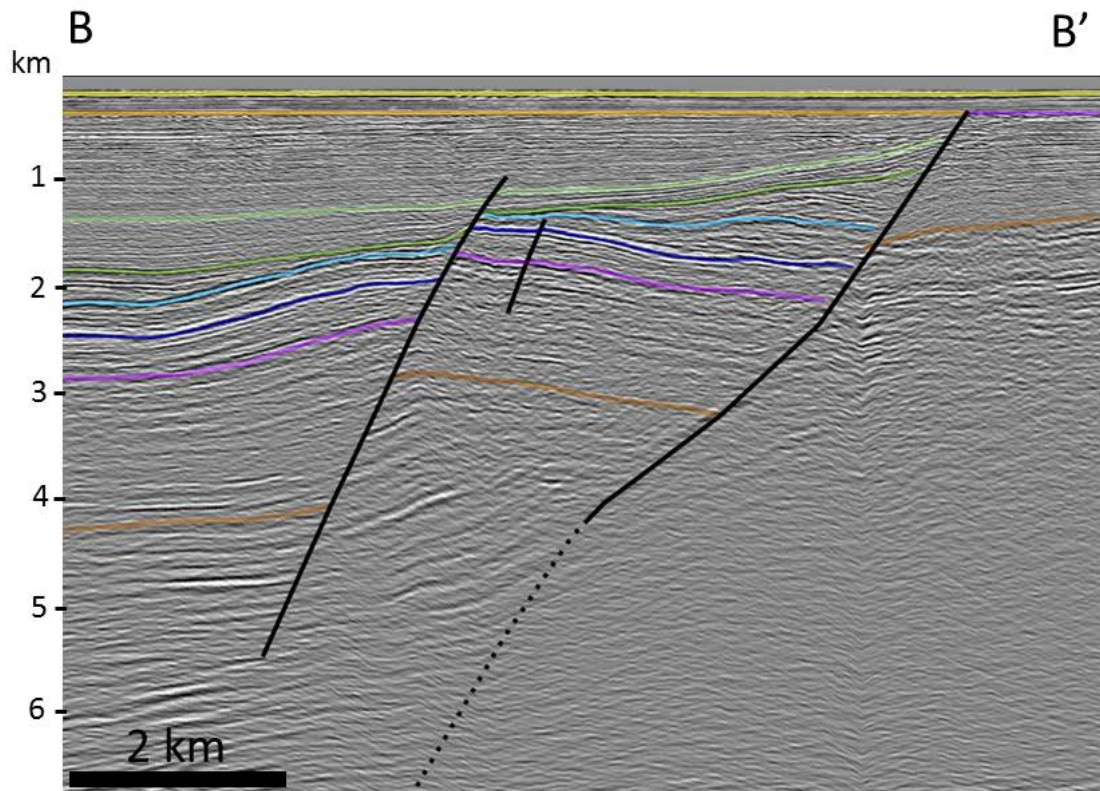


Fig. 32. Upper figure display section AA' of the interpreted top horizons, whereas the underlying show the best-fit modeling result. The best-fit model has limitations basinward close to the secondary fault. See fig.23 for location.

### Section CC'

The interpreted main fault in section CC' (fig.33) has a somewhat listric shape in the upper part, which coincide with modelled fault. The lower fault section changes downwards to a concave bend where the modelled beds between the Paleozoic and Lower – Middle Jurassic seem to fit the interpreted horizons. However, the section consists of a second fault in the hanging wall, which displays a mismatch between the Paleozoic, Triassic and Jurassic succession. This fault was problematic to incorporate into the forward modelling due to the non-horizontal horizons and was therefore neglected. The S0 and S2 have different appearances than the estimated beds and do not show resemblances between each other.

### Section DD'

The horizons in the hanging-wall of section DD' (fig.34) have good continuity with little disturbance and are easy to trace towards the main fault. The distinctive anticline fold can be observed approximately 6.5 km downwards. The interpret fault show characteristics of two separated fault at different depths, where the upper section display similarities towards a listric fault shape. The modelled fault show some concave fault bend (listric features) in the upper part, before changing towards a convex fault bend. The best-fit modelled beds correlates well with the both the Jurassic, Triassic, and Paleozoic units closer to the fault plane, whereas the mismatch rises significantly basinwards where the interpreted beds are located further down in the structure. The mismatch between horizons also increases downwards. The S2 and S0 units show disparity with to the modelling.

A second interpretation with two faults, where one fault segment is located in the upper section with a listric shape and is separated by a second deeper situated fault. The modelled horizons of the listric segment follow the interpret horizons relatively well close to the fault but are limited in extent towards the basin. The Top Paleozoic internal horizons follow the folding above the most deep-seated fault somewhat decent.

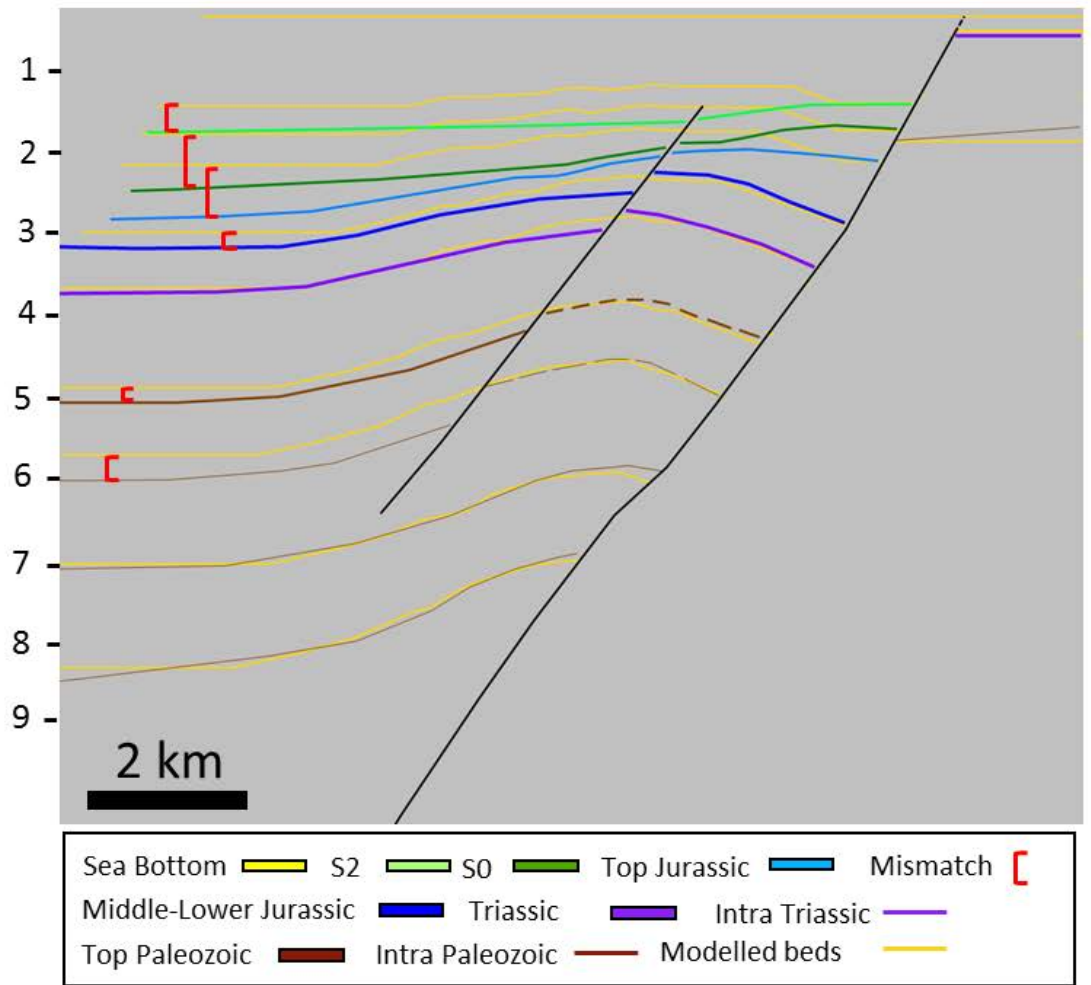
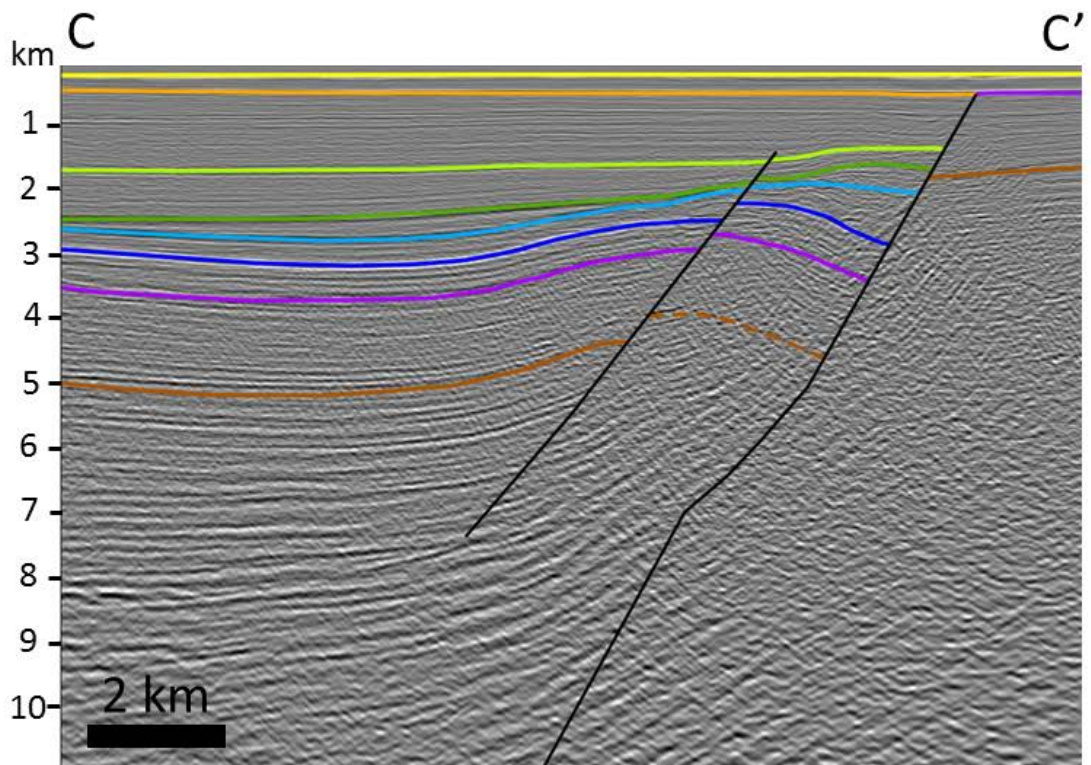


Fig. 33. Upper figure displaying the interpret CC' section, while the lower figure shows the comparison of the modeled beds and interpret intra and top horizons of the best-fit model. An overall good best-fit model. See fig.23 for location.

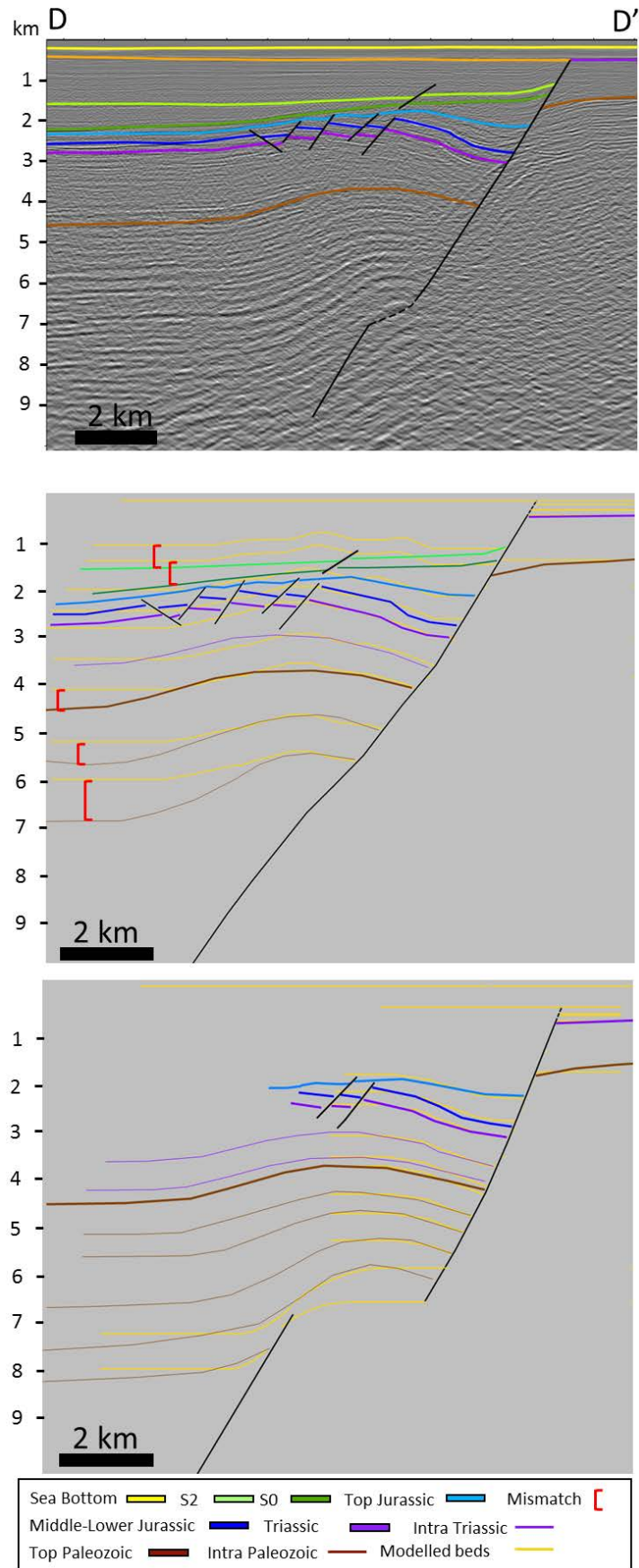


Fig. 34. Upper figure displaying the interpreted DD' section, while the middle figure shows the comparison of the modeled beds and interpret intra and top horizons of the best-fit model. The lowermost figure shows alternative modeling. Both modeling have limitations. See fig.23 for location.

### Section EE'

Section EE' (fig.35) do not show the characteristic anticline shape, as mention earlier. The seismic horizons are well visible in the hanging wall of the main fault. The fault displays an overall concave bend, where the uppermost fault plane is more planar. There is a relatively good match between the modelled beds and the traced horizons. However, the model has a minor mismatch towards the basin. In addition, the modelled S0 and S2 show considerably mismatch with the interpreted horizons in the model.

### Section FF'

Section FF' (fig.36) has similarities with a planar fault plane but has small variations in geometry. The uppermost fault plane has appearances of a convex bend where the lower part is more planar. The modelled beds trail the traced horizons with noteworthy precision between all of the units. The subsidiary faults have little displacement, which does not affect the overall bedding geometry

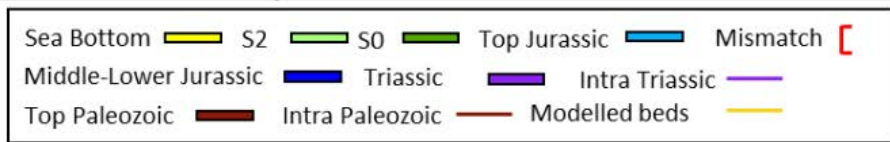
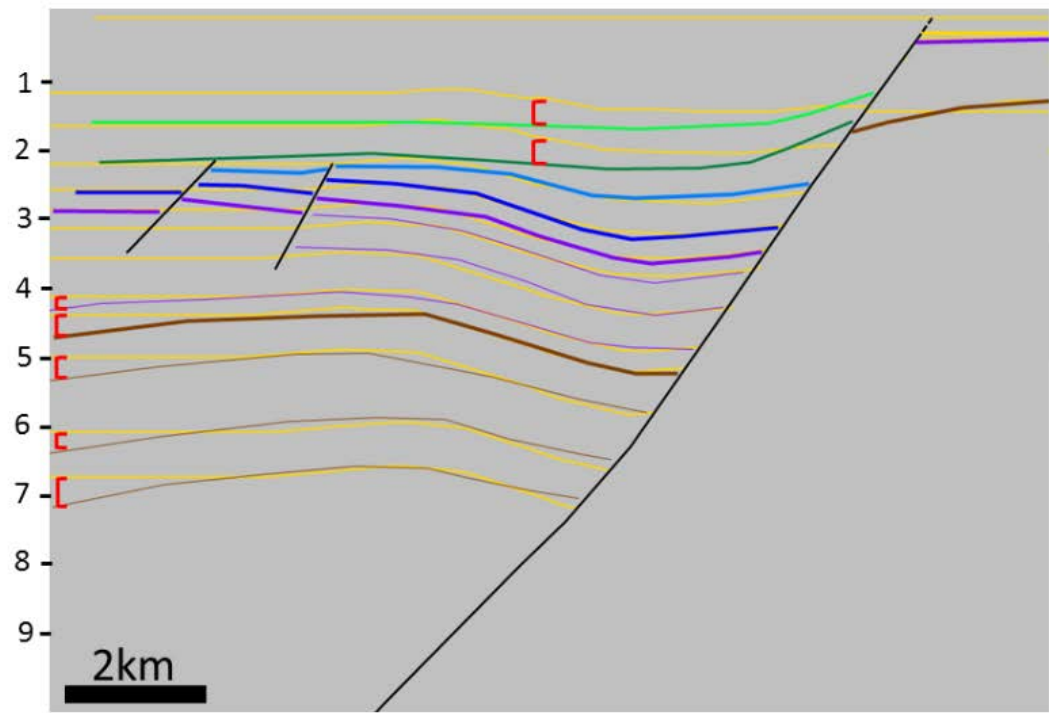
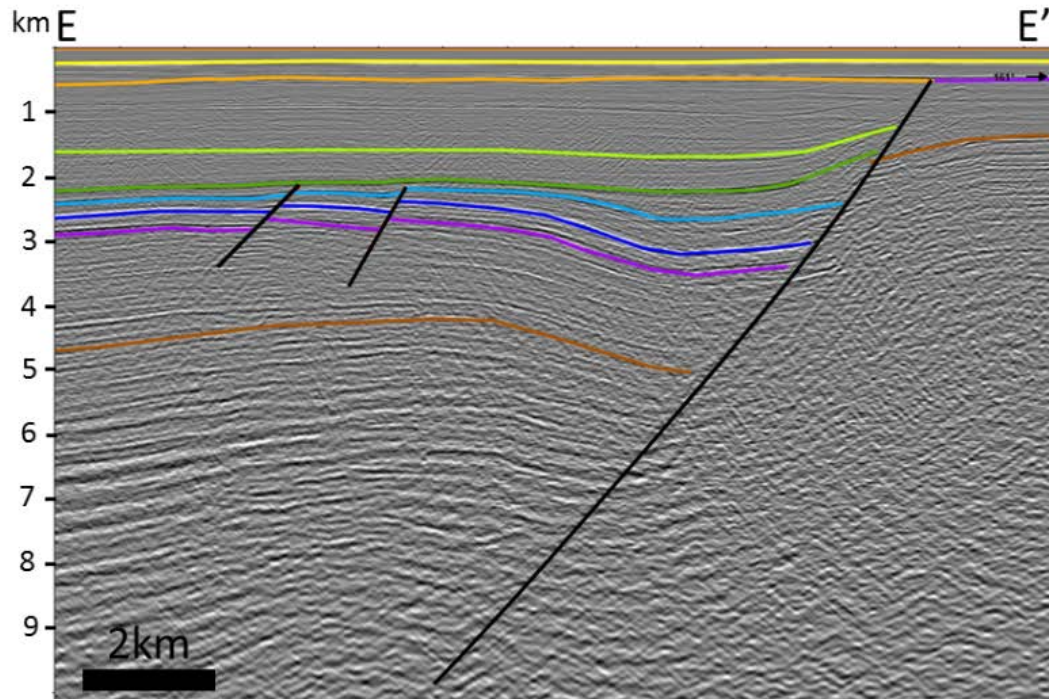


Fig. 35. Upper figure displaying the interpret EE' section, while the lower figure shows the comparison of the projected beds and interpret intra and top horizons of the best-fit model. The best-fit model shows an overall good correlation. See fig.23 for location.



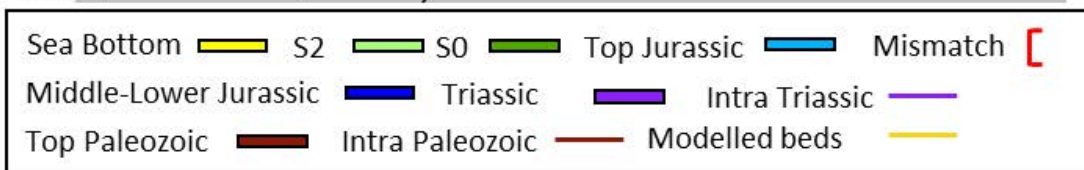
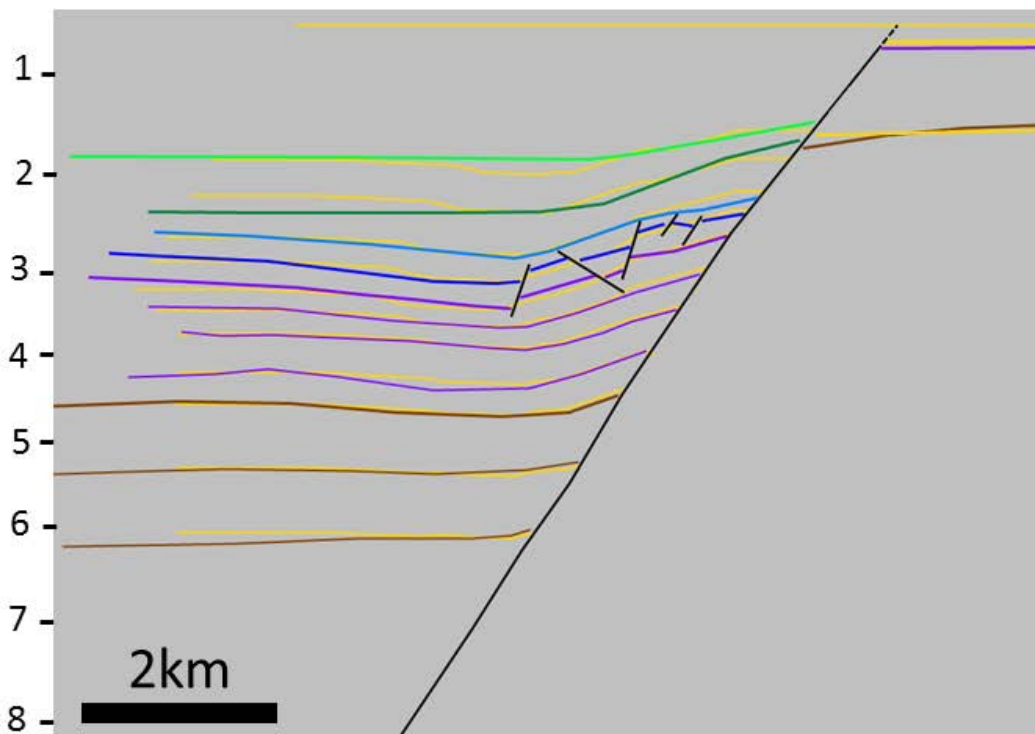
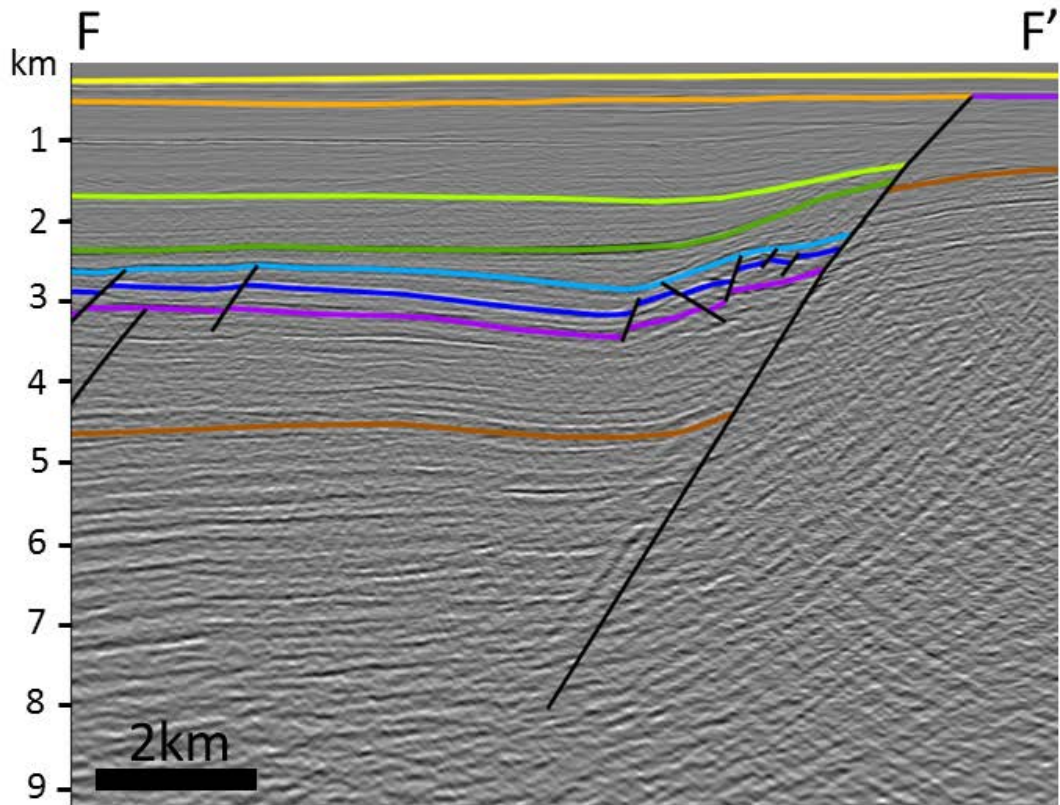


Fig. 36. Upper figure displaying the interpret FF' section, while the lower figure shows the comparison of the projected beds and interpret intra and top horizons of the best-fit model. See fig.23 for location.

## 4.4 Wells

The interval of interest is the Knurr Fm (fig37), which is partially equivalent to sequence 0 (Marin et al., 2017). The thickness of the formation differs significantly throughout the area. The thinnest unit of Hekkingen Fm (i.e., Upper Jurassic) is located in well 7119/12-2. Slightly thicker packages are located in well 7120/10-1 and 7119/12-1, whereas well 7120/10-2 do not offset the base of Hekkingen Formation. The thinnest section of S0 is located in well 7120/10-1 and well 7119/12-1 (i.e., ~40 m), while the thickest units are located in 7119/12-2 and 7120/10-2 (i.e., ~200 m and ~ 380 m respectively). The GR-log motifs are nevertheless different between the thickest sections. The GR-readings for well 7119/12-1 is relatively high throughout, while some changes are observed in 7120/10-1. Well 7119/12-2 consist of relatively high GR-responses whereas well 7120/10-2 changes throughout the interval. The lower section of well 7120/10-2 display low, but erratic readings before changing to consistent high responses.

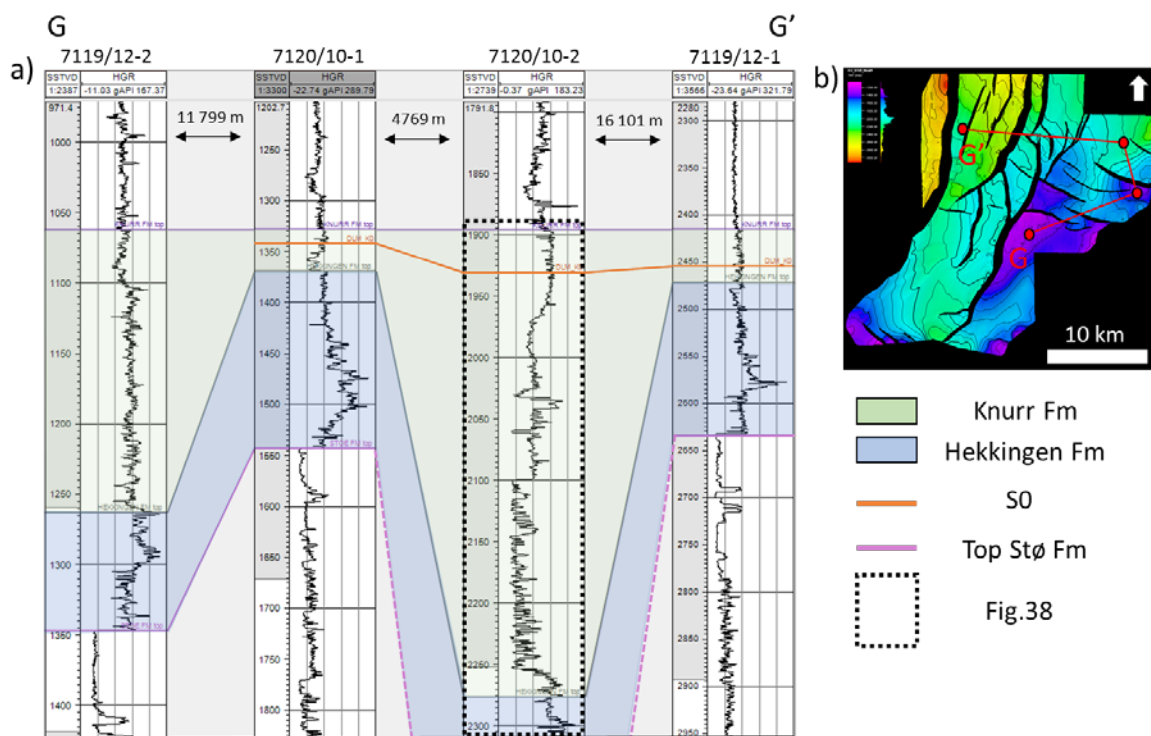


Fig. 37.a) Well correlation of four wells in the area display thickness differences between Hekkingen Fm and S0. (b) Time structural map for the top Stø Fm. GG' show the correlated trend.

Using the gamma ray of well 7120/10-2 (fig.38), sequence 0 can be divided into a lower (2100 – 2255m) and upper section (1930 – 2100m) based on the log motifs. The lowermost section (2200 – 2255m) consist of serrate log pattern of relatively low GR-responses, before changing towards lower and more consistent log motifs (2100 – 2255 m). From 2100 until the top (i.e., 1900m) much higher GR-responses are present only separated by two smaller sections (i.e., at 2060m and 2030m) of low responses.

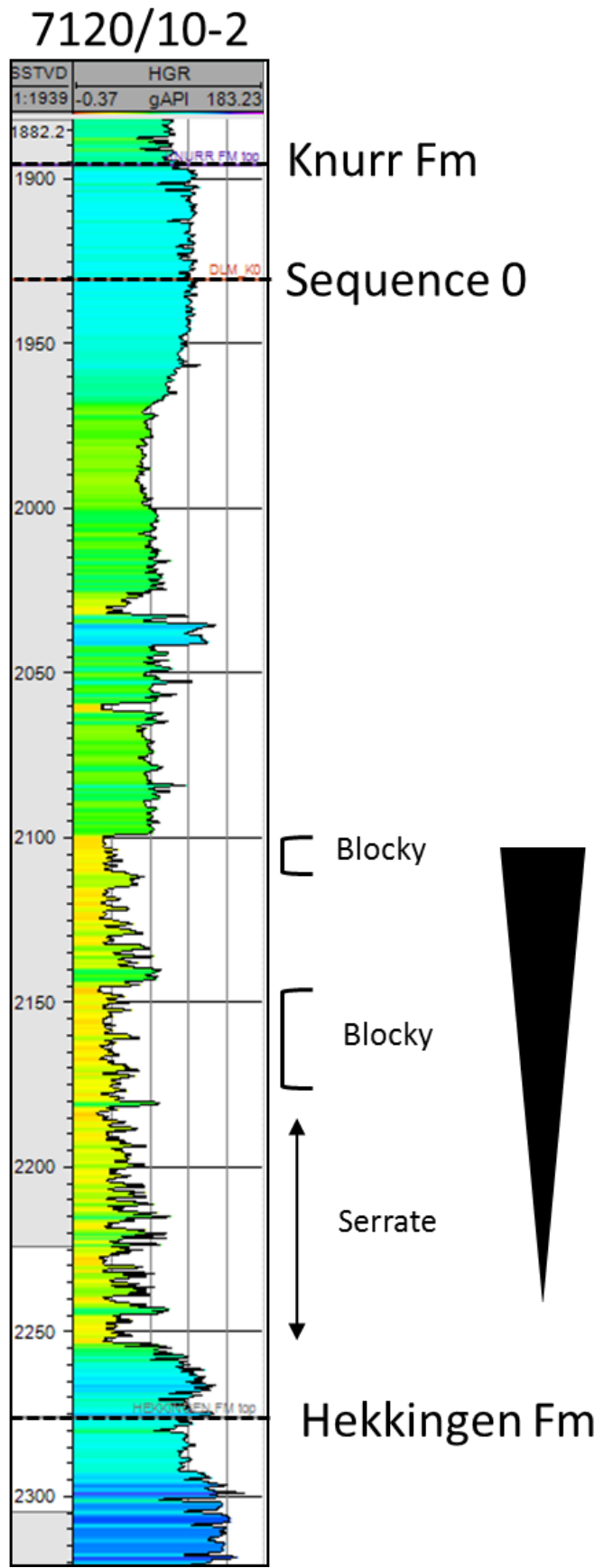


Fig. 38. GR response within the Knurr Fm. Green and blue color indicate an increase in GR-response, whereas yellow and orange points to low responses.

#### 4.5 Iso-slices and rms amplitude

Fig.39a and b display five iso-proportional slices of rms amplitude of the sequence 0 close to well 7120/10-2. The rms amplitude highlight the magnitude of the amplitude response in red. High amplitude reflections are prominent in the footwall of the north-eastern fault throughout all of the slices where the thinnest unit of S0 exist in fig.39 and 40.

A large area (4x5km) with a distinctive increase in amplitude are dominating the north-western areas of fig. 39c. Medium to low rates of increased amplitude is noticeably in the center, while medium to high amplitudes is present in the hanging wall of the most north-eastern fault. In fig.39d, the concentrated regions of amplitude response east of the well, have diminished into low amplitude responses. Medium rates of concentration are more prominent west of the well with minor zones of high amplitude response. These trends are also evident in the south. Some high amplitude reflection tendencies are observed in the hanging wall of the two eastern faults.

Fig.40a display a large area of approximately 3x4 km dimension with high amplitude concentrated responses immediate east of the well. Some medium amplitude responses are located in the middle, whereas no noticeable variation in the west. The central areas of fig.40b show higher amplitude reflections tendencies that are displayed as elongated tubes (see stippled lines), whereas the northern part consists of overall higher response, especially an area around the well. Northwest of the well, medium amplitude dominates. Little responses in the south-western region are noticeable. Fig.40c show little amplitude differences around the well. Areas east and on the western margins of the slice have highest responses. In addition, the hanging wall in the northeast show areas of high concentration of responses (see stippled lines).

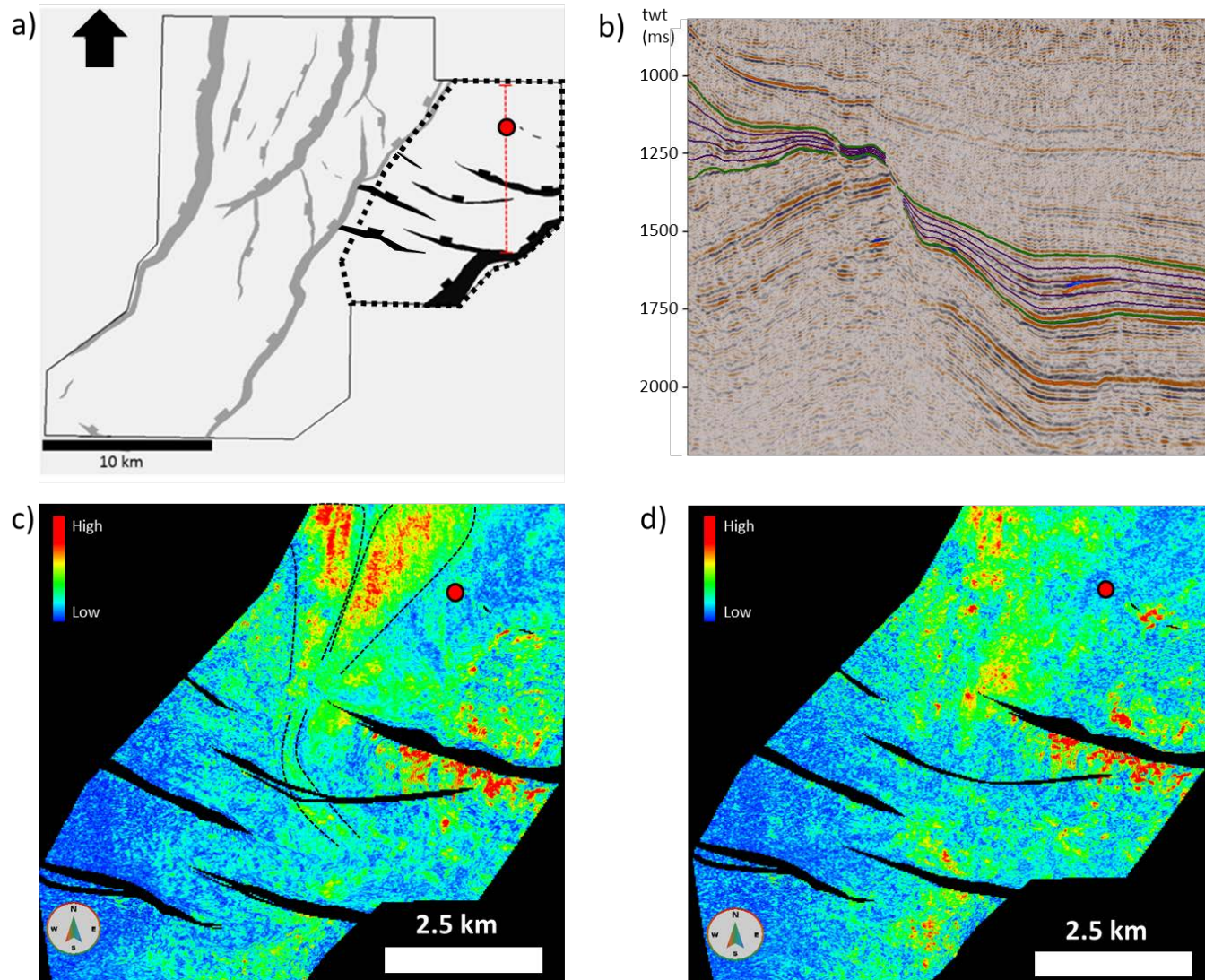


Fig. 39. a) Location of the area that underwent iso-slices and rms attribute. b) Cross section of the traced iso-slices within the S0 interval. NB, the polarity is reversed in this section c) Iso-slice of lowermost area. d) Isoslice of the lower part. Well 7120/10-2 location is marked with a red circle and stippled lines indicate geological features.

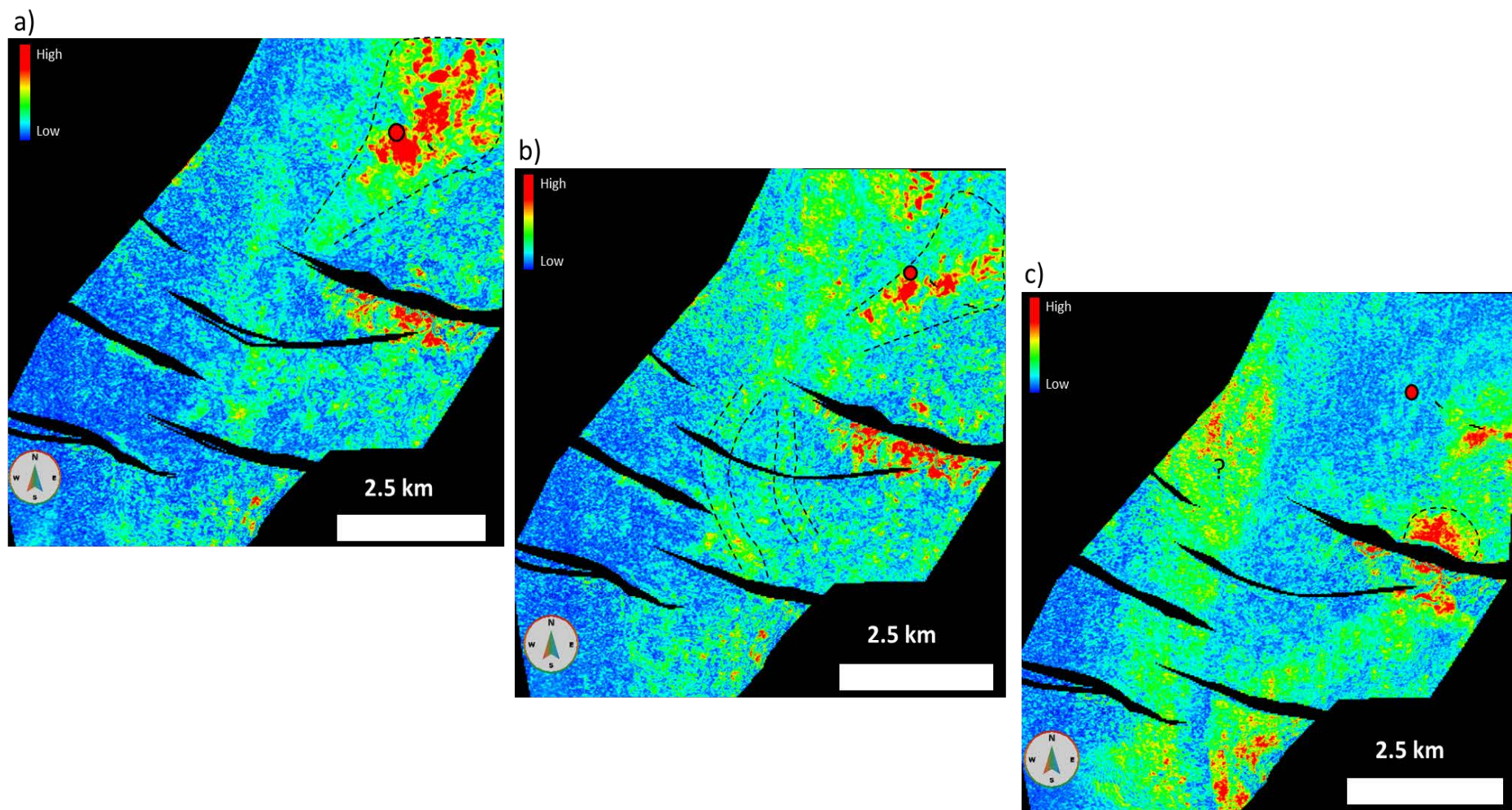


Fig. 40. Iso-slices of the S0 interval. a) Middle part b) Upper part. c) Uppermost part. Well 7120/10-2 location is marked with a red circle and stippled lines indicate geological features. See fig.39 for location.

## 5. Interpretation

### 5.1 Late Jurassic to Early Cretaceous extension and structural styles

From the observation, the structural architecture of the study area has been influenced differently by the structural trends (fig.18-20). The most influential fault in the southwestern part of the Hammerfest Basin is the ENE – WSW striking fault (fig.23) that consist of a massive throw displacement varying from ~ 2km in the seismic cube towards ~ 3km along the selected composite sections (fig. 27-30). The fault corresponds with the Troms-Finnmark Fault Complex and is a basin-platform delineating structure that changes geometries northeastwards along the fault boundary. This indicates that the fault-fold system has affected the hanging wall geometry differently alongside the same fault zone. The fault has influenced the southeastern part of the study area with an anticlinal structure, which is interpreted to continue approximately 25 km northeastwards outside the seismic 3D cube (fig.23) based on the similar anticline and syncline features (i.e width, amplitude etc.) in section CC' (fig.27) and DD' (fig.28). The missing Jurassic and Cretaceous succession indicate that the Finnmark Platform has undergone severe erosion.

The second most influential fault population in terms of displacement is the NNE – SSW trend, which is evident in the central and northwestern part of the seismic cube (fig.17 and 19). This fault trend coincides with the Ringvassøy-Loppa Fault Complex. E – W subsidiary fault trend in the seismic cube were likely developed in response to the master fault (fig.20), since they are not observable in the other areas, except close to the main fault on the eastern side. However, the regional map (fig.11) of the Hammerfest Basin consist of an E – W striking faults which could suggest that they are a result of a more regional event.

The Triassic and Lower – Middle Jurassic units have constant thickness through the sections, indicating pre-rift deposition of sediments (fig.24-30). However, thicker units (~300-400m) of Lower – Middle Jurassic sediments present in the southern part (fig. 24, 25, and 27) compared to the most northeastern regions (~200m; fig.28-30), suggest that along the southern area Troms-Finnmark Fault Complex, greater accommodation space, and sediment supply were present. The initiation of the faulting seemed to start in the Late Jurassic, where small growth strata are present toward the fault planes of the major fault and the NNE – SSW faults (fig.18). The thickest units of the Upper Jurassic growth strata are located towards the main fault (fig.27 and 28) indicating that the fault activity was influential in the area. The considerably thicker strata towards the fault plane from the time-thickness map of the Upper Jurassic is supporting this interpretation (fig.21). The horst (fig.19) has very thin units of Hekkingen and S0 (fig.37),

suggesting that the structure was a structural high during the Late Jurassic with limited sediment accumulation, which was most likely exposed to some erosion.

The S0 unit is relatively thin throughout the region, where it is often much thinner towards the footwall margins of the subsidiary faults (fig.19 and 20). This is also seen in the thickness map (fig.25a), which indicate that the footwall area had restrictions in terms of deposition of sediments, lack of subsidence, uplift or these areas was exposed to some erosion. Nevertheless, the S0 significantly thickens towards the main fault plane in the hanging wall of the southernmost study areas with the characteristic wedge shape (fig.24 and 25). This suggests that the hanging-wall of the main fault started to subside during the deposition of S0 and much faster compared to adjacent basin areas in the 3D seismic. Similar growth strata packages are observed in areas further northeast in section CC' (fig.27) and DD' (fig.28) indicating that the areas were subjected to similar processes in terms of deformation. Whereas, section EE' (fig.29) and FF' (fig.30) have smaller wedge characteristics points towards an area with less tectonic activity, where subsidence and accommodation space are more limited compared to the southwestern region.

Lack of growth wedges in S2 towards the main fault indicates that the fault activity weaned before this sequence started. This is supported by the constant increased in thickness towards the basin, which is consistent with a monocline development that later was breached (fig.24 and 25), which indicates reactivation of the main fault during later tectonic activity. Also, the fault offset is more prominent in the Jurassic period and S0 unit (fig.17) than S2, pointing towards a more quiet period in terms of tectonic activity during the deposition of the S2 units. The exception is the Ringvassøy-Loppa Fault Complex (NNE – SSW). In contrast to the little fault activity along the Troms-Finnmark Fault Complex during the deposition of the S2 unit, the fault activity intensifies towards the northwestern region of the seismic cube (fig.19). Sequence 2 increases significantly in thickness in the hanging-wall of the NNE – SSW faults (fig.22b), indicating that the area was subjected to increased fault activity and subsidence.

## 5.2 Anticline development and fault geometry

The pre-growth strata and the symmetrical axial plane and no dip discordance between the Triassic and Lower – Middle Jurassic units (fig.24) indicates that the anticline development initiated after these periods. The thickness variation of the time-thickness map of Upper Jurassic (fig.21) where the slight thickness increase follows the syncline trend and the thickness decrease follows the anticline trend, can point toward the initiation stage of the anticline development. The transition from Upper Jurassic to Lower Cretaceous is marked by an unconformity, which



will affect the thickness variation in both time-thickness maps (i.e., Upper Jurassic and S0). This is evident in the thickness variation in the Hekkingen formation (i.e., Upper Jurassic) and Sequence 0 (i.e., Knurr) well correlation (fig.37). Nevertheless, the stratigraphic onlaps onto the anticline (fig.26) within sequence 0, suggest that topographic differences existed during the early stages of Valanginian age. The sequence 0 has growth wedges towards the main fault and is also thickening in the syncline relative to the anticline. This suggests that the deposition is syn-kinematic growth, which indicates that the anticline structure already existed in some way during deposition.

The dipping orientation of the different units in section AA' – DD' (fig.24, 25, 27, and 28) show similar features, indicating that these areas were subjected to the same mechanisms. However, the synthetic dipping beds of Cretaceous succession and the antithetic dipping beds in the Paleozoic, Triassic, and Jurassic suggest that the units were affected differently. This is supported by the forwards modelling results, where the modelled beds of S0 and S2 differ compared to the underlying beds, except for section FF' (fig.36).

Composite section of AA' – EE' (fig.24-29) show similar features as the roll-over geometry in the Paleozoic, Triassic and Jurassic succession, which is associated with a listric fault shape (fig.1c and 2c). However, a typical listric fault shape (fig.16b) without a characteristic bend in the forward modelling, do not recreate the interpreted horizons with the anticline structure. The modelling result from the section AA' (fig.31), CC' (fig.33) and DD' (fig.34), together with the distinctive 'flat' feature in section DD' at the depth ~6500 m reveal the presence of a ramp-flat-ramp with listric geometry in the upper fault segment. The modelled beds in AA' and CC' display good correlation with a small mismatch, while DD' do not recreate the whole section. The 'flat' is located in the sedimentary units (i.e., carbonates) above older basement rocks in the Permian.

Section BB' (fig. 32) and CC' (fig.33) are influenced by secondary faulting which was not implemented in the modelling, making the correlation in the distal areas of the hanging wall to lack and mismatch, but they follow the overall trend of the interpreted horizons. Section EE' (fig.35) and FF' (fig.36) has substantially different hanging wall geometries, where the forward modelling fits the interpreted section relatively well. Section EE' exert a concave fault bend, which gives an overall listric shape and the bedding showing characteristics towards a classical rollover (fig.1c). However, section FF' is more planar with a slight convex fault bend in the upper area, creating synthetic dipping beds indicating different deformation mechanisms. The

subsidiary faulting in the hanging-wall along the Troms-Finnmark Fault Complex appears to have occurred during different periods due to varied growth wedges between the units. The secondary fault in fig.24 and 25 seem to be active in S2 because of substantial thickness differences between the hanging-wall and footwall, whereas the underlying successions have similar thicknesses. Then again, the secondary fault in section CC' (fig.27) has growth wedge already in the Upper Jurassic, which is also seen in the other subsidiary faults (fig.28-30). Contemporaneously to these fault movements, the faulting has created narrow grabens and half-grabens.

### 5.3 Stratigraphy

It is known that gamma-ray logs can reflect grain size trends where high GR-readings usually correlate with finer sediments such as clay and lower readings recognizes coarser homogenous sediments. Though there are many exceptions, Marin et al. (2018) analyzed the eight-meter core from depth 2128 – 2135m in well 7120/10-2 (fig.10) and concluded that the sandstone interval within the S0 was deposited in a turbiditic environment, which was correlated with low GR-motifs. Some of the high amplitude response of the rms attribute show similarities with geological bodies such as fan geometries and have been interpreted to be turbidite lobes. Based on the vertical thickness (150m) of the relatively low GR-responses (fig.37) and lateral extent of the lobes from the stratigraphic attribute maps (fig. 39 and 40), the unit corresponds to a feature submarine system according to Grundvåg et al. (2014).

The erratic GR-responses in the lower area (2200 – 2250m) implies the presence of stacked lobe sections with varying thicknesses in distal to fringe setting. This is supported by fig.39c, where the attribute map display resemblance towards lobe features on the western side of well 7120/10-2. The transition from serrate log patterns towards more blocky features (2180m – 2100m) is consistent with a proximal setting. Also, the coarsening upward sequence suggest that the system shifted and prograded closer to the well. This is seen in fig.40a where the highest responses are located close to the well, but the lobe is located more east compared to the underlying lobe features (fig.40c). Higher amplitude responses resemble a potential channel system along the terrace between the E – W trending faults (fig.39 and 40), which is supported by bidirectional onlapping in the syncline (fig.26). The lack of rms responses in the uppermost sequence (fig.40c) corresponds with high GR-readings indicating that sediment supply became either constrained or prograded further into the basin. The intense amplitude increases in the hanging-wall (fig.40c) of the most north-eastern fault, could be other mass transport deposits such as slumps or debris flow.

## 5 Discussion

### 5.1 Comparison with other mechanisms and extensional fault-fold systems

The hanging wall geometry of an extensional-related fold system is directly related to the style of deformation and has many origins (fig.1 and 2), and the bedding geometries of different units provide insight into fault development and fault processes (Gawthorpe & Leeder, 2000; Lewis et al., 2015). General fault and fold geometries in the study area are comparable with several other physical conceptual models and other extensional fault-fold systems (Withjack et al., 1990; McClay & Scott, 1991; Xiao & Suppe, 1992; Schlische, 1995; Rotevatn & Jackson, 2014; Vasquez et al., 2018), even though the study location, deformation scale and experiment material (i.e., clay and sands) are different.

The Goliat anticline is located approximately 30 km north-eastwards from the study area. The area has been extensively studied due to their hydrocarbon findings in Jurassic and Triassic successions. The anticline is a massive structure with a width exceeding 15-20 km at its widest. Mulrooney et al. (2017) identified multiple crest levels of crystalline basement (i.e., varied geometry at depth), which favored two discrete segments as the mechanism for the anticline development (fig.4d). In addition, the two fault segments in Goliat are separated by a distance of 10 km beneath the anticline and has an amplitude height at around 600 m. Nevertheless, similar features are not observed in the study area. The seismic reflectors are recognizable and continuous parallel further out in the basin, and no large lateral Paleozoic terrace structure is located under the anticline. The dimension exceeds the study area, where the fold width and amplitude are ~ 5km and ~ 300m. Therefore, the two anticlines appear to have been developed by different mechanisms during the establishment of the basin.

#### 5.1.1 Roll-over and ramp-flat-ramp

The interpreted composite lines AA' to EE' (fig.24, 25, 27, 28 and 29) show roll-over characteristics (fig.1c and 2c) in the Upper Paleozoic, Triassic, and Jurassic rocks. These features are strongly linked to listric fault geometry (McClay et al., 1991; Xiao & Suppe, 1992). From the forward modelling, the sections from AA' to EE' (fig.31 to 35) display a listric fault shape within these successions with an overall good correlation. However, based on the forward modelling in section AA' and CC' (fig.31 and 33), the listric fault changes downwards to a prominent bend in the Upper Paleozoic succession. This bend had to be implemented in order to recreate the anticline structure, which has a positive relief compared to its reference point. This type of structure is inconsistent with general models of a roll-over (McClay & Scott, 1991), where an overall listric fault is present. Nevertheless, this bend implies that the fault shape is

prone to a ramp-flat-ramp structure (fig. 2d) in the upper Paleozoic succession, where the upper fault segment has a listric character. Analogue models of ramp-flat-ramp experiments from McClay and Scott (1991) are consistent with the anticline and syncline development in the study area. In addition, similar ramp-flat-ramp structure with a steep listric upper fault segment has created comparable anticline structure other places in the SW Barents Sea such as Fingerdjupet subbasin (Serck & Braathen, 2019).

Even though the forward modelling display a relatively good correlation with the interpreted beds throughout the sections until the Cretaceous units due to syn-rift (i.e. wedge) in the S0, it had limitations in recreating section BB' (fig.32) and DD' (fig.34). Modelling two separate faults to reconstruct the structure is intricate because the software is limited and do not have the capability in recreating an overall good fit throughout these sections. However, the seismic features in DD' (fig.34) display characteristics of a 'flat' (fig.34), which is related with dip-linkage (Lewis, Jackson, & Gawthorpe, 2013; Rotevatn & Jackson, 2014) between two laterally different faults that eventually links as the faults propagate.

Vasquez et al. (2018) also showed with analogue modelling (fig.41) that a broad spectrum of folding occurred, such as ramp-flat-ramp, when interbedded layers of brittle and ductile materials were exposed to extension regimes. The forced fold developed above the 'flat' and is characterized by a décollement layer, where the ductile/weak layer controlled the development of 'flats' in the ramp-flat-ramp system. This kind of physical model is applicable to section DD', where the flat develops in the upper Paleozoic rocks. It is possible that the weaker units in the upper parts of Paleozoic created a ramp-flat-ramp system between a deep propagating fault and an overlying splay fault in the cover sequence. This fault structure has also been observed in the NW shelf of Australia (Deng & McClay, 2019), where the 'step' has developed in the mechanically weaker shale unit above the basement fault.

The best-fit models demonstrate how the composite sections significantly vary along the Troms-Finnmark Fault Complex. This is seen in section EE' (fig.29) and FF' (fig.30). The anticline structure has diminished northeast (fig.23), and the forward modelling of EE' (fig.35) show the characteristic roll-over geometry with an overall listric fault shape with slightly synthetic dipping beds. From section FF' (fig.36), a more planar fault is envisaged to have influenced the hanging-wall where steeper synthetic dipping bedding is present. An explanation for developing synthetic dipping beds is breached monoclines (fig.1a; Withjack et al., 1990; Ferril et al., 2005) as the fault propagates, where the rate of the fault propagation is relatively slow with respect to the rate of fault displacement (Ferril et al., 2005). The displacement rate

as the fault propagates upwards into the cover affects the bedding angles (Hardy & McClay, 1999), which could imply a lower propagation-to-slip ratio for both EE' and FF' section compared to the southeastern region.

The synthetic dipping beds in S0 and S2 above the roll-over geometries in fig. 24, 25, 27, 28 and 29 are most probably related to the thick syn-rift wedge that exists within the S0. Also, reactivation of the Troms-Finnmark Fault Complex during later rifting stages likely breached the monocline and influenced the bedding orientation when propagating upwards at a later stage. Reactivation of the fault complex, coincide with the regional studies in the Hammerfest Basin (Gabrielsen et al., 1990; Mulrooney et al., 2017). The S0 and S2 units display misfits with the modelling due to the relative thick syn-kinematic growth packages seen in the composite sections. The anticline structure is mainly situated within the Jurassic and Triassic. Therefore the forward modelling was limited to the pre-growth strata.

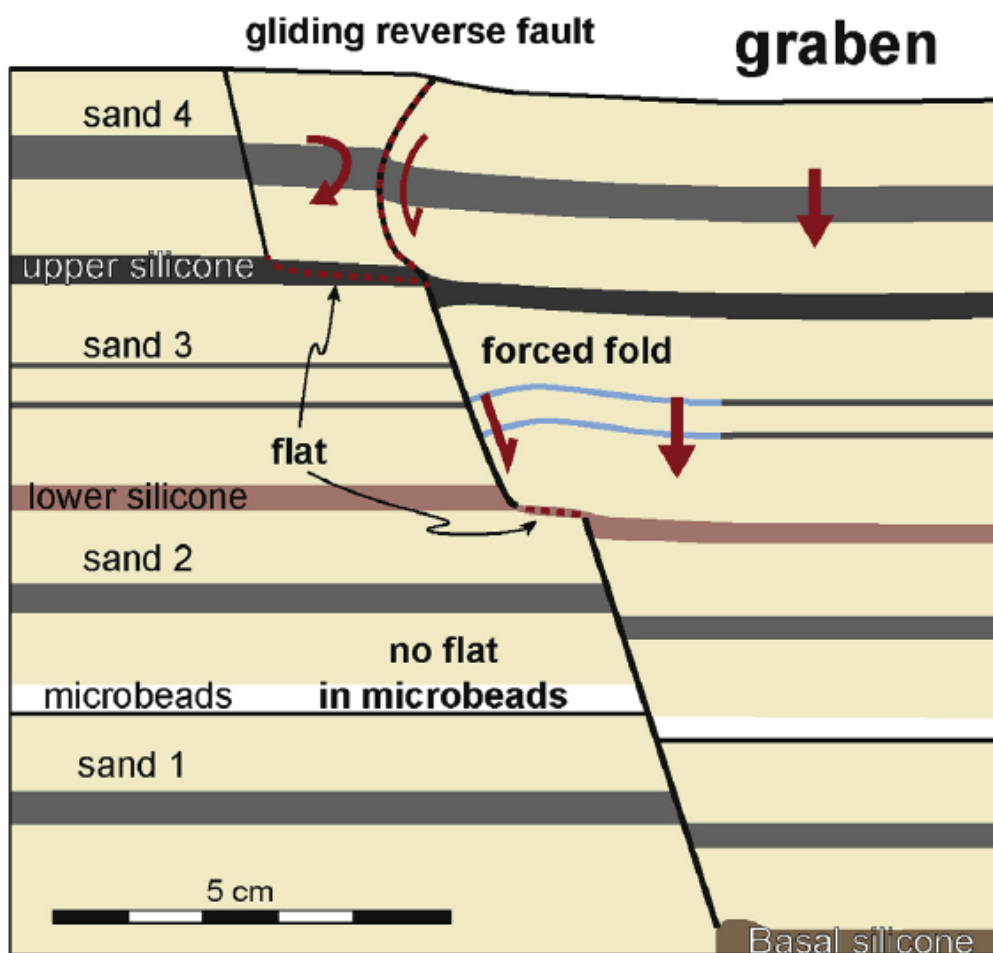


Fig. 41. Forced fold (i.e., anticline) develops above the 'flat' in relation to extensional movements. (Vazquez et al., (2018)

### 5.1.2 Inversion

Based on the anticline development in the hanging wall of normal faults, one may suspect that the anticline was formed as a result of compression (fig.1f). In addition, an alternative interpretation of the synthetic dipping growth packages seen in section DD' (fig.28 and 34) could be inverted depocentre-growth wedges (fig.1f; Allmendinger, 1998). Several authors (Rønnevik et al., 1982; Riis et al., 1986; Gabrielsen and Færseth, 1989, Gabrielsen et al., 1997; Indrevær et al., 2015, 2016) suggested that the bounding structural elements of the Hammerfest Basin, including Troms Finnmark Fault Complex, Asterias Fault Complex, and Ringvassøy-Loppa Fault Complex have been affected by inversion during Early Cretaceous. Since the areal extent of the anticline is relatively large, around 30-35km and these wedges are present in all of the composite sections (fig.24, 25 and 27 to 30), a reasonable assumption would have to be that the area had to undergo a somewhat regional compressional stage to develop the anticline. However, the long regional rifting history (Gabrielsen et al., 1990; Faleide et al., 1993) of the Hammerfest Basin contradicts this possibility, where only minor local inversion (Indrevær et al., 2016; Mulrooney et al., 2017) has been detected along the Troms-Finnmark Fault Complex. Additionally, the other fault populations (i.e., NNE – SSW, and E – W) in the study area exhibit no indication of inversion structure (fig. 19 and 20) that probably would be evident in more significant compressional stages.

### 5.1.3 Other mechanisms

Compaction: Skuce (1996) showed that compaction over planar fault could result in a rotation of the upper fault plane section, where the formation of the concave bend could create a large anticlinal structure (fig.1e). It is realistic that the thick succession of overlying Cretaceous sediment influenced the hanging wall geometry in some way, but it is highly unlikely if the differential compaction was the primary mechanism in developing the anticline structure. The stratigraphic onlaps (fig.26) are strong indicators that the structure was developed before the thick Cretaceous-Paleogene succession was deposited. Rotevatn and Jackson (2014) had a similar structure (i.e. listric and fault linkage; fig.42) as the study area, and they made a reasonable assumption, that the succession between the layers should be relatively homogenous considering the length scale (approximately 30 km). They argued that if compaction was the main mechanism in developing the anticline, why would it only form anticlines along with parts and not on the whole fault system. This could also be applied for the study area, where the deposition of homogenous fine-grained sediments during the Early Cretaceous dominated (fig.8 and 9; Mørk et al., 1999).

Transverse folds: Transverse folds (fig.1d) are related to isolated surface-breaching faults where hanging wall syncline plunges towards the fault, and the footwall plunges away from the fault. The majority of these folds form as a result of along-strike variations in fault displacement where synclines form at displacement maxima. The anticlines develop near the displacement minima, typically near fault segment boundaries (Schlische, 1995). The deformations of the anticline and syncline axes along the Troms-Finnmark Fault Complex are parallel to the fault, which makes transverse folding unlikely to be the primary mechanism in the study area.

Drag: In drags, the folds occur immediately before faulting caused by frictional resistance (Barnett et al., 1987; Schlische, 1995). These folds develop when the strain field of the beds are 'dragged' closed to the propagating fault. In normal drags, the fault creates synclines in the hanging wall and anticlines in the footwall. The mechanism is similar to fault propagation fold Mitra, 1993, whereas drag folds are usually smaller in scale (Khalil and McClay, 2002). The scale of anticlinal development reaches up to ~5 km in width and ~ 30 km in length, making frictional drag unlikely. Deng and McClay (2019) also investigated an extensional-related fold system comprised of an anticline followed by a syncline. They discarded the drag folds as driving mechanism due to the areal extent of their area (>5km in width and >50 km length) which exhibit similar anticlinal structure in the study area. The regional extent of the synthetic dipping beds should discard the drag folds, but rather affected by the fault-propagation fold mechanism.

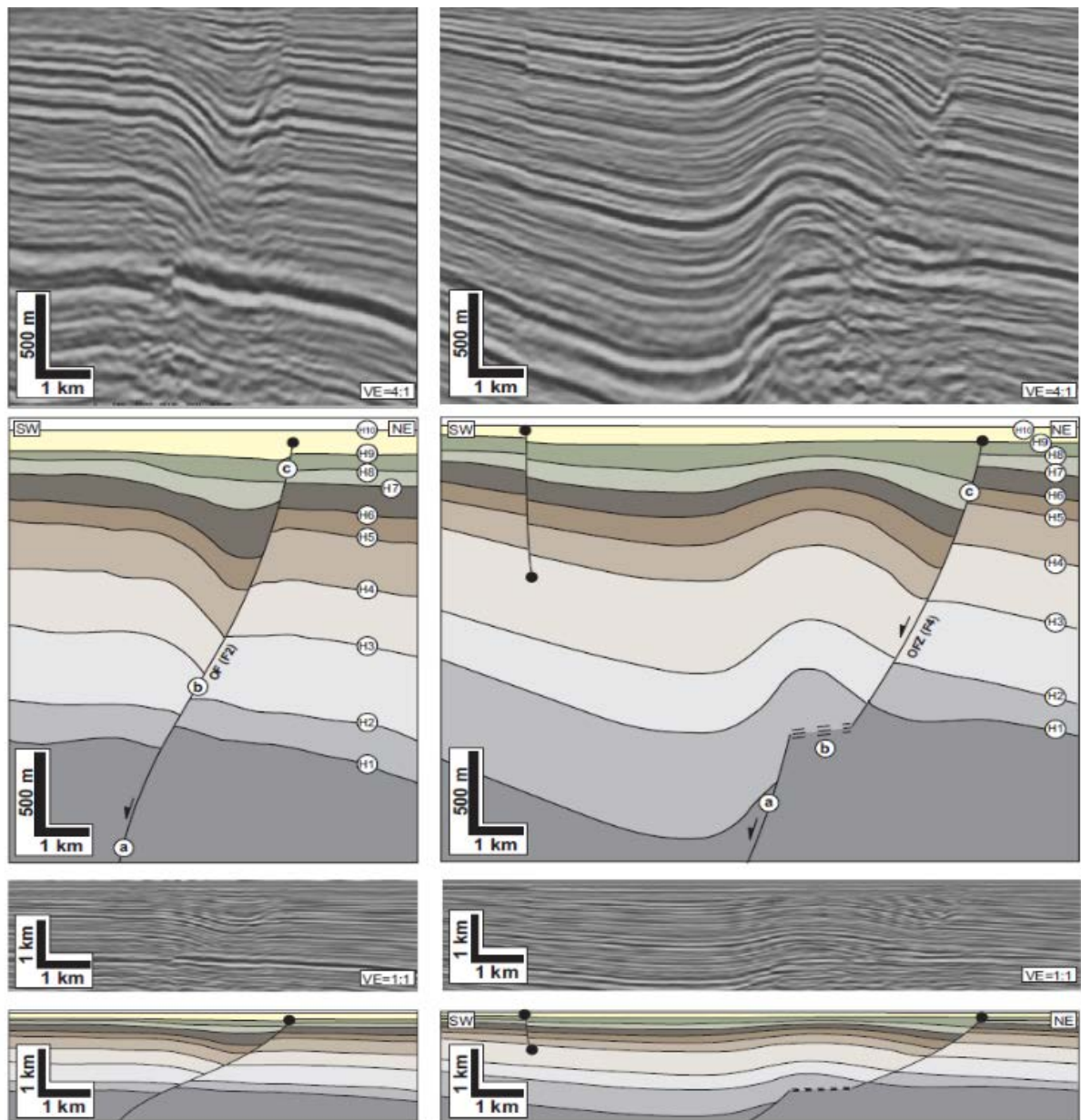


Fig. 42. Section illustrating the structural style associated along October Fault Zone in Gulf of Suez. From Rotevatn and Jackson (2014)



## 5.2 Evolutionary model along Troms-Finnmark Fault Complex

Different fault-fold styles may coexist along different parts of the same fault zone (Deng and McClay, 2019; Rotevatn and Jackson, 2014; Serck and Braathen, 2019), which is documented in the study area. Based on the forward modelling and the interpreted seismic features, a conceptual 3D model was done (fig.43) for the hanging wall deformation of the Troms-Finnmark Fault Complex in the southwestern-most area of the Hammerfest Basin. The proposed model shows the extensive fault system consisting of a through-going fault segment at deep levels, which is influenced by folding weaker stratigraphic cover.

Late Paleozoic rifting event has previously been described to set precursors for the Troms-Finnmark Fault System along the Hammerfest Basin (Gabrielsen et al., 1990). Little observation in the Paleozoic succession is due to the poor seismic quality in the deeper offsetting Troms-Finnmark Fault Complex. Therefore, the lack of possible growth packages close to the fault makes it difficult to determine if the late Paleozoic rifting event set precursors for fault development. However, both the forward modelling and the massive throw displacement indicates that the faults offset deep down in the Paleozoic with a high dip angle, which most likely is basement involved.

The studied fault system has a generally ramp-flat-ramp geometry in the south-western, where the fault geometry changes significantly along the NNE – SSW strike (fig.43). This can perhaps relate to the fault initiation, fault interaction, and later fault linkages of the developing fault complex due to varying strike along the Hammerfest Basin (fig.11 and 23). Even though regional stratigraphy has not been the focus of this thesis, it may be a factor affecting the lateral changing fault geometry. Studies (Walsh et al., 2003; Lohr et al., 2008) have shown that the fault propagates differently due to material properties, which could influence mechanically weaker stratigraphy differently along the strike. Nevertheless, the various fault geometries from the forward modelling along the Troms-Finnmark Fault Complex show evidence for the different kinematic evolution of the fault-fold system.

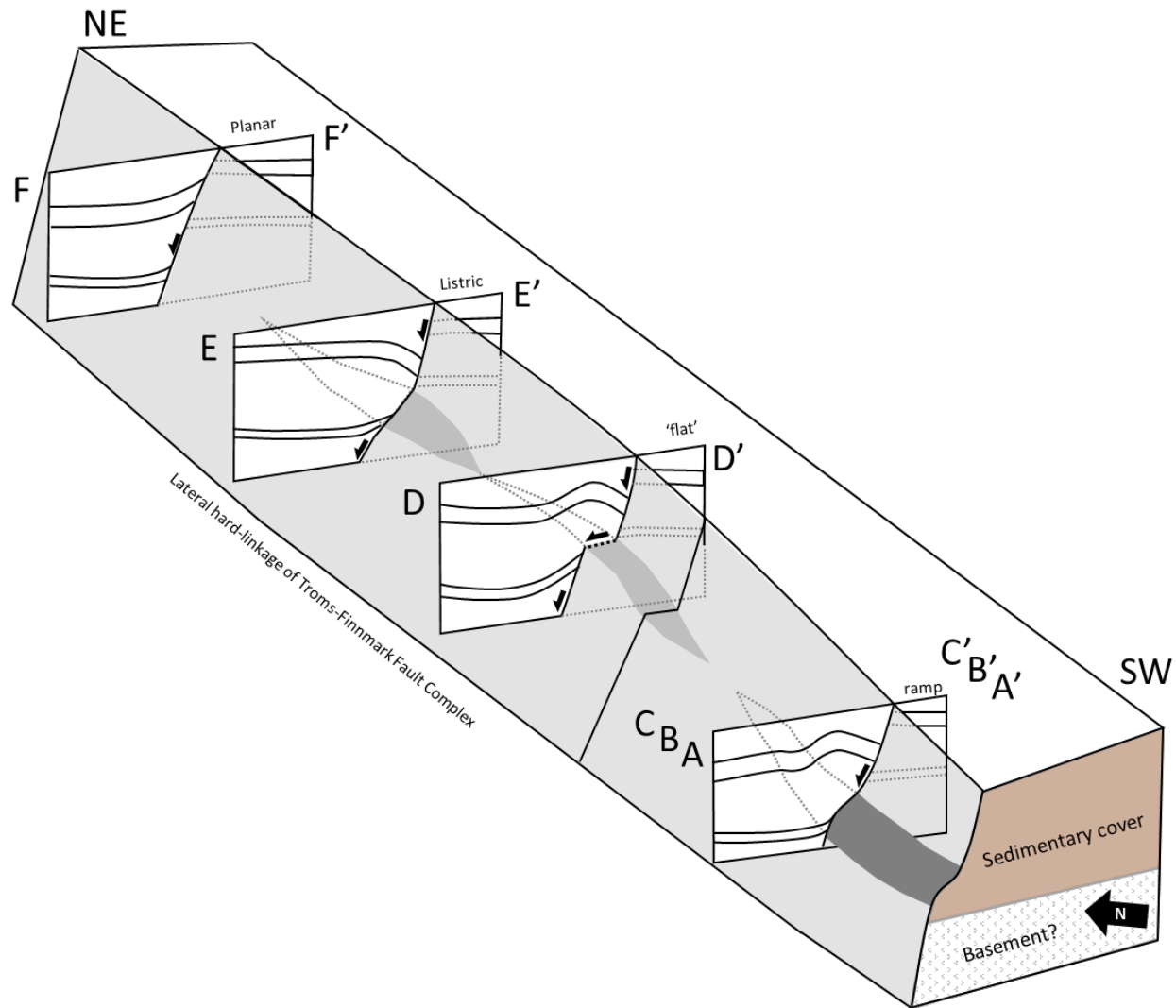


Fig. 43. Conceptual 3D model of the fault-related hanging wall deformation of the Troms-Finmark Fault Complex in the southwestern-most area of Hammerfest Basin. Section AA', BB' and CC is located in a ramp-flat-ramp structure', whereas DD' is located in a flat. Section EE' is situated in a listric fault shape, while FF' has a more planar fault structure.

### 5.3 Anticline and syncline development and its impact on coarse-grained sediments

Based on the interpretation of the alternating turbidite lobes and the forming of the syncline, a conceptual model has been proposed (fig.44). The low GR-responses in well 7120/10-2 of S0 is comprised of several stacked lobe complexes that evolved during the Valangian age when the main faulting was active.

The Finnmark Platform was the primary source of coarse-grained sediments during the deposition of S0 (Selda, 2005, Marin et al., 2017), where the eroded Late Triassic to Middle Jurassic sediments were reworked in a shoreline on a low relief hinterland before deposited as fans in the Hammerfest Basin (Marin et al., 2017). The thick units of coarse-grained sediments in well 7120/10-2 without large intervals of interbedded shales suggest that the turbidite system had continuous access to sediment source. The tectonic activity and the extensive erosion on the Finnmark Platform around the time of deposition, are most likely main factors contributing to the thick wedge-shaped packages of S0. This is supported by Seldal (2005), which interpreted that the thin unit of S0 with irregular log motif in well 7120/10-1 (fig.37a) is located in a distal part of a wedge fan containing sandstones. Based on the stratigraphic attribute maps, the syncline seemed to control the transportation direction of the turbidite deposition (fig.44).

The earliest turbidite sediments (fig.39c) were deposited in a northward direction, suggesting that the syncline was in an early stage of development and did not impact the basinward areas (fig.44). However, the interpreted channel located in the syncline in between the terrace of the E – W trending faults could indicate that the faults were active and that the incision rate of the channel was lower than the rate of fault-related uplift. Therefore, the channel was deflected. The sediment feeder system appears to come from several places, where the primary source came from the Finnmark Platform, other uplifted blocks in the area and the S0 sandstone wedge (fig.18 and 44) due to the channels orientations seen in fig. 39c and fig.40b.

The large lobe feature located eastwards (fig.40a) suggest that the transportation of the coarse-grained sediments shifted direction from north to northeast. In addition, the change towards the present syncline structure transformed the system from distal/fringe to a proximal/axis setting relative to the well. These interpretations imply that the turbidite system was most likely influenced by the evolving syncline adjacent to the anticline. High gamma-ray responses of well 7120/10-2 in the upper half of S0 could suggest that the system shifted basinward by following the syncline where higher amplitude responses are located east of the well.

Within the S0, the coarse-grained architecture in well 7120/10-2 is absent in the upper section, with only minor irregularities in the GR-motifs (fig.38). This can indicate that the turbidites got deposited further basinwards following the syncline, and the high tectonic activity along Troms-Finmark Fault Complex continued providing sediments throughout the sequence stage.

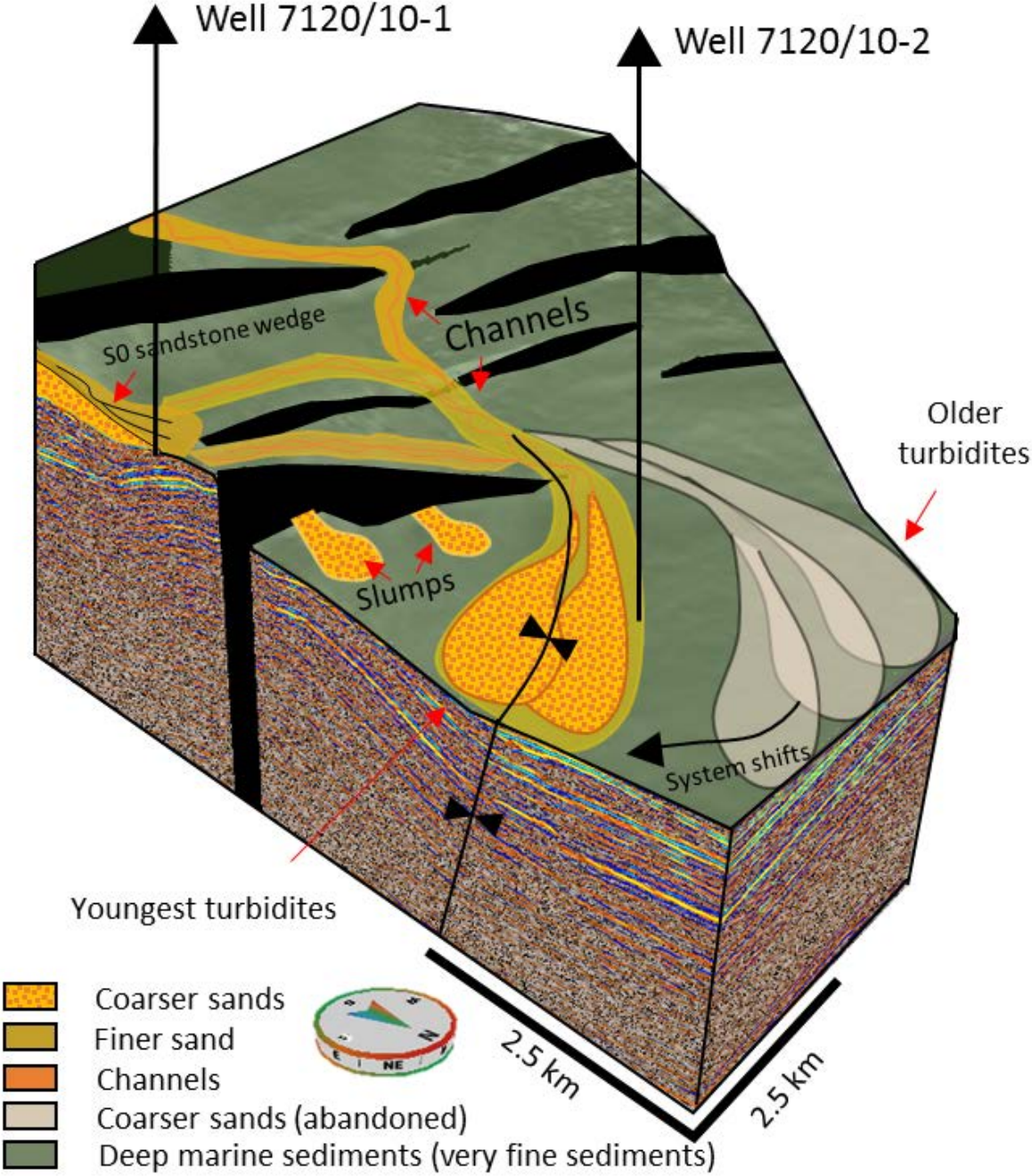


Fig. 44. Conceptual model of how the turbidite system shifted from a northern direction towards a northeastern due to the syncline development.

## Conclusion

This study has documented how the extensional fault and fold growth impacted the sedimentary infill during successive rifting along the southern parts of the Hammerfest Basin. Sedimentary packages give valuable information about fault activity and fold growth, where forward modeling provides insight about the fault morphology in deeper areas where seismic quality varies.

The study has improved the knowledge about the extensional fault-related folds along the southern parts of the Troms-Finnmark Fault Complex, and the main findings are:

- i. The fault geometry changes along the ENE – WSW striking fault in the southern parts of the Hammerfest Basin, where the fault shape is directly involved in developing the anticline structure.
- ii. Based on the forward modeling, the anticline-syncline structure have arisen from a ramp-flat-ramp geometry, controlled by a listric shape in the upper segment.
- iii. The Late Jurassic – Early Cretaceous rifting period developed the structure, where significant topography changes were evident during the early stages of Valanginian age (i.e, S0).
- iv. The continuation of the syncline development influenced the major turbidite system close to well 7120/10-2 to shift from a northern towards a north-eastern direction.
- v. The sediment infill was situated adjacent to the anticline and constrained to the E – W terrace, which controlled the channel orientation.

## Future work

The forward modeling is a good tool in finding probable fault geometry but has definite limitations when secondary faulting with significant offset is present. Also, the modeling reconstructed the sections to fit the structures in the pre-growth succession where the structure was prominent. Therefore, the syn-growth packages were neglected. One can improve the quality control of the fault geometry in the composite section by taking the best-fit modeled fault and incorporate it in a restoration. The restoration will then account for the syn-rift sediments and provide confirmation about the fault shape validity for each section.

## References

- Allmendinger, R. W. (1998). Inverse and forward numerical modeling of trishear fault-propagation folds. *Tectonics*, 17(4), 640-656.
- Anell, I., Braathen, A., Olaussen, S., & Osmundsen, P. T. (2013). Evidence of faulting contradicts a quiescent northern Barents Shelf during the Triassic. *First Break*, 31(6), 67-76.
- Anell, I., Midtkandal, I., & Braathen, A. (2014). Trajectory analysis and inferences on geometric relationships of an Early Triassic prograding clinoform succession on the northern Barents Shelf. *Marine and petroleum geology*, 54, 167-179.
- Barnett, J. A. M., Mortimer, J., Rippon, J. H., Walsh, J. J., & Watterson, J. (1987). Displacement Geometry in the Volume Containing a Single Normal Fault. *American Association of Petroleum Geologists (AAPG) Bulletin*, 71(8), 925-937.
- Berglund, L. T., Augustson, J., Færseth, R., Gjeldberg, J., & Ramberg-Moe, H. (1986). The evolution of the Hammerfest Basin. *Habitat of Hydrocarbons on the Norwegian Continental Shelf. Norwegian Petroleum Association. Graham & Trotman*, 319-338.
- Chopra, S., & Marfurt, K. J. (2007). *Seismic Attributes for Prospect Identification and Reservoir Characterization*. Tulsa: Society of Exploration Geophysicists and European Association of Geoscientists and Engineers.
- Conneally, J., Childs, C., & Nicol, A. (2017). Monocline formation during growth of segmented faults in the Taranaki Basin, offshore New Zealand. *Tectonophysics*, 721, 310-321.
- Corfield, S., & Sharp, I. R. (2000). Structural style and stratigraphic architecture of fault propagation folding in extensional settings: a seismic example from the Smørbukk area, Halten Terrace, Mid-Norway. *Basin Research*, 12(3-4), 329-341.
- Deng, H., & McClay, K. (2019). Development of extensional fault and fold system: Insights from 3D seismic interpretation of the Enderby Terrace, NW Shelf of Australia. *Marine and petroleum geology*, 104, 11-28.
- Etris, E. L., Crabtree, N. J., Dewar, J., & Pickford, S. (2001). True depth conversion: more than a pretty picture. *CSEG recorder*, 26(9), 11-22.
- Faleide, J. I., Bjørlykke, K., & Gabrielsen, R. H. (2010). Geology of the Norwegian Continental Shelf. In K. Bjørlykke (Ed.), *Petroleum Geoscience: From Sedimentary Environments to Rock Physics* (pp. 467-499).
- Faleide, J. I., Gudlaugsson, S. T., & Jacquart, G. (1984). Evolution of the western Barents Sea. *Marine and petroleum geology*, 1(2), 123-150.
- Faleide, J. I., Tsikalas, F., Breivik, A. J., Mjelde, R., Ritzmann, O., Engen, Ø., . . . Eldholm, O. (2008). Structure and evolution of the continental margin off Norway and the Barents Sea. *Episodes*, 31(1), 82-91.
- Faleide, J. I., Vågnes, E., & Gudlaugsson, S. T. (1993). Late Mesozoic - Cenozoic evolution of the southwestern Barents Sea in a regional rift - shear tectonic setting. *Marine and petroleum geology*, 10(3), 186-214.
- Ferril, D. A., Morris, A. P., Sims, D. W., Waiting, D. J., & Hasegawa, S. (2005). Development of Synthetic Layer Dip Adjacent to Normal Faults. *AAPG Bulletin*, 85, 125-138.
- Ford, M., Veslund, C. L. C. D., & Bourgeois, O. (2007). Kinematic and geometric analysis of fault-related folds in a rift setting: The Dannemarie basin, Upper Rhine Graben, France. *Journal of Structural Geology*, 29(77), 1811-1830.
- Fossen, H., Pedersen, R. B., Bergh, S., & Andresen, A. (2008). Creation of a mountain chain. In I. B. Ramberg, I. Bryhni, A. Nøttvedt, & K. Rangnes (Eds.), *The Making of a Land, Geology of Norway* (pp. 179-231). Trondheim: Norwegian Geological Association.
- Gabrielsen, R. H. (1984). Long-lived fault zones and their influence on the tectonic development of the southwestern Barents Sea. *Journal of the Geological Society, London*, 141(4), 651-662.
- Gabrielsen, R. H., & Færseth, R. B. (1989). The inner shelf of North Cape, Norway and its implications for the Barents Shelf-Finnmark Caledonide boundary. A comment. *Norwegian Journal of Geology*, 69, 57-62.

- Gabrielsen, R. H., Færseth, R. B., Jensen, L. N., Kalheim, J. E., & Riis, F. (1990). Structural elements of the Norwegian continental shelf. Part 1: The Barents Sea Region. *Norwegian Petroleum Directorate Bulletin*, 6, 47.
- Gawthorpe, R. L., Fraser, J. A., & Collier, R. E. L. (1994). Sequence stratigraphy in active extensional basins: implications for the interpretation of ancient basin-fills. *Marine and petroleum geology*, 11(6), 642-658.
- Gawthorpe, R. L., Jackson, C. A. L., Young, M. J., Sharp, I. R., Moustafa, A. R., & Leppard, C. W. (2003). Normal fault growth, displacement localisation and the evolution of normal fault populations: the Hammam Faraun fault block, Suez rift, Egypt. *Journal of Structural Geology*, 25(6), 883-895.
- Gawthorpe, R. L., & Leeder, M. R. (2000). Tectono-sedimentary evolution of active extensional basins. *Basin Research*, 12, 195-218.
- Gawthorpe, R. J., Sharpe, I., Underhill, J. R., & Sanjev, G. (1997). Linked sequence stratigraphic and structural evolution of propagating normal faults. *Geology*, 25(9), 795-798.
- Gernigon, L., Brönnner, M., Roberts, D., Olesen, O., Nasuti, A., & Yamasaki, T. (2014). Crustal and basin evolution of the southwestern Barents Sea: From Caledonian orogeny to continental breakup. *Tectonics*, 33(4), 347-373.
- Glørstad-Clark, E., Birkeland, E. P., Nystuen, J. P., Faleide, J. I., & Midtkandal, I. (2011). Triassic platform-margin deltas in the western Barents Sea. *Marine and petroleum geology*, 28(7), 1294-1314.
- Glørstad-Clark, E., Faleide, J. I., Lundschieen, B. A., & Nystuen, J. P. (2010). Triassic seismic sequence stratigraphy and paleogeography of the western Barents Sea area. *Marine and petroleum geology*, 27(7), 1448-1475.
- Grundvåg, S. A., Johannessen, E. P., Hansen, W. H., & Plink-Bjørklund, P. (2014). Depositional architecture and evolution of progradationally stacked lobe complexes in the Eocene Central Basin of Spitsbergen. *Sedimentology*, 61(2), 535-569.
- Hardy, S., & McClay, K. (1999). Kinematic modelling of extensional fault-propagation folding. *Journal of Structural Geology*, 21(7), 695-702.
- Hedberg, H. D. (1926). The Effect of Gravitational Compaction on the Structure of Sedimentary Rocks. *AAPG Bulletin*, 10, 1035-1072.
- Henriksen, E., Ryseth, A. E., Larssen, G. B., Heide, T., Rønning, K., Sollied, K., & Stoupakova, A. V. (2011). Tectonostratigraphy of the greater Barents Sea: implications for petroleum systems. *Geological Society London, Memoirs*, 35(1), 163-195.
- Indrevær, K., Faleide, J. I., Gabrielsen, R. H., Mulrooney, M., & Braathen, A. (2015). Inversion along the Troms-Finnmark Fault Complex, SW Barents Sea - Structural Character and Timing. Oral Presentation, AAPG 3P Artic Meeting, October, 2015, Stavanger.
- Indrevær, K., Gabrielsen, R. H., & Faleide, J. I. (2016). Early Cretaceous synrift uplift and tectonic inversion in the Loppa High areas, southwestern Barents Sea, Norwegian shelf. *Journal of the Geological Society*, 174(2), 242-254.
- Jackson, J., & Leeder, M. (1994). Drainage systems and the development of normal fault: an example from Pleasant valley, Nevada. *Journal of Structural Geology*, 16(8), 1041-1059.
- Jakobsson, M., Mayer, L., Coackley, B., Dowdeswell, J. A., Forbes, S., Friedman, B., . . . Schenke, H. W. (2012). The international bathymetric chart of the Arctic Ocean (IBCAO) Version 3.0. *Geophysical Research Letters*, 39(12).
- Johannessen, E. P., & Nøttvedt, A. (2008). Norway encircled by coastal plains and deltas. In I. B. Ramberg, I. Bryhni, A. Nøttvedt, & K. Rangnes (Eds.), *The Making of a Land, Geology of Norway* (pp. 356-383). Trondheim: Norwegian Geological Association.
- Klausen, T. G., Nyberg, B., & Helland-Hansen, W. (2019). The largest delta plain in Earth's history. *Geology*, 47(5), 470-474.
- Lewis, M. M., Jackson, C. A. L., & Gawthorpe, R. L. (2013). Salt-influenced normal fault growth and forced folding: The Stavanger Fault System, North Sea. *Journal of Structural Geology*, 54, 156-173.

- Lewis, M. M., Jackson, C. A. L., Gawthorpe, R. L., & Whipp, P. S. (2015). Early synrift reservoir development on the flanks of extensional forced folds: A seismic-scale outcrop analog from the Hadahid fault system, Suez rift, Egypt. *AAPG Bulletin*, 99(6), 985-1012.
- Lohr, T., Krawczyk, C. M., Oncken, O., & Tanner, D. C. (2008). Evolution of a fault surface from 3D attribute analysis and displacement measurements. *Journal of Structural Geology*, 30(6), 690-700.
- Mahajan, A., Gabrielsen, R. H., & Faleide, J. I. (2014). Structural evolution using 3D seismic of Hoop Fault Complex, SW Barents Sea Norway. *Conf. Arct. Energy Conf. Tromso, Vol. NGF Abstr. Proc*, 2.
- Marín, D., Escalona, A., Grundvåg, S. A., Olaussen, S., Sandviks, S., & Sliwinska, K. K. (2017). Unravelling key controls on the rift climax to post-rift fill of marine rift basins: insights from 3D seismic analysis of the Lower Cretaceous of the Hammerfest Basin, SW Barents Sea. *Basin Research*, 30(4), 587-612.
- Martinsen, O., & Nøttvedt, A. (2008). Norway rises from the sea. In I. B. Ramberg, I. Bryhni, A. Nøttvedt, & K. Rangnes (Eds.), *The Making of a Land, Geology of Norway* (pp. 442-479). Trondheim: Norwegian Geological Association.
- Maurin, J. C., & Niviere, B. (1999). Extensional forced folding and décollement of the pre-rift series along the Rhine Graben and their influence on the geometry of the syn-rift sequences. *Geological Society London*, 169(1), pp.73-86.
- McClay, K. R., & Scott, A. D. (1991). Experimental models of hangingwall deformation in ramp-flat listric extensional fault system. *Tectonophysics*, 188(1-2), 85-96.
- McClay, K. R., Waltham, D. A., Scott, A. D., & Abousetta, A. (1991). Physical and seismic modelling of listric normal fault geometries. *Geological Society London, Special Publication*, 56(1), 231-239.
- Mitra, S. (1993). Geometry and Kinematic Evolution of Inversion Structures. *AAPG Bulletin*, 77(7), 1159-1191.
- Mulrooney, M. J., Leutscher, J., & Braathen, A. (2017). A 3D structural analysis of the Goliat field, Barents Sea, Norway. *Marine and petroleum geology*, 86, 192-212.
- Mørk, A., Dallmann, W., Dypvik, H., Johannessen, E., Larsen, G., Nagy, J., . . . Worsley, D. (1999). Mesozoic lithostratigraphy. In W. K. Dallman (Ed.), *Lithostratigraphic Lexicon of Svalbard. Upper Paleozoic to Quaternary Bedrock. Review and Recommendation for Nomenclature use* (pp. 127-214). Tromsø: Norwegian Polar Institute, Tromsø.
- NPD. (2019). Norwegian Petroleum Directorate Factpages; Barents Sea - Lower Cretaceous plays. Retrieved from <https://www.npd.no/en/facts/geology/plays/barents-sea/upper-jurassic-to-lower-cretaceous-plays/>
- Nystuen, J. P., Müller, R., Mørk, A., & Nøttvedt, A. (2008). From desert to alluvial plain - from land to sea. In I. B. Ramberg, I. Bryhni, A. Nøttvedt, & K. Rangnes (Eds.), *The Making of a Land, Geology of Norway* (pp. 330-355). Trondheim: Norwegian Geological Association.
- Nøttvedt, A., & Johannessen, E. P. (2008). The source of Norway's oil wealth. In I. B. Ramberg, I. Bryhni, A. Nøttvedt, & K. Rangnes (Eds.), *The Making of a Land, Geology of Norway* (pp. 384-417). Trondheim: Norwegian Geological Association.
- Ohm, S. E., Karlsen, A., & Austin, T. J. F. (2008). Geochemically driven exploration models in uplifted areas: Examples from the Norwegian Barents Sea. *AAPG Bulletin*, 92(9), 1191-1223.
- Prosser, S. (1993). Rift-related linked depositional systems and their seismic expression. *Geological Society Special Publication*, 71(1), 35-66.
- Ravnås, R., & Steel, R. J. (1997). Contrasting styles of Late Jurassic syn-rift turbidite sedimentation: a comparative study of the Magnus and Oseberg areas, northern North Sea. *Marine and petroleum geology*, 14(4), 417-449.
- Rotevatn, A., & Jackson, C. A. L. (2014). 3D structure and evolution of folds during normal fault dip linkage. *Journal of the Geological Society*, 171(6), 821-829.



- Rykkelid, E., & Fossen, H. (2002). Layer rotation around vertical fault overlap zones: observations from seismic data, field examples, and physical experiments. *Marine and petroleum geology*, 19(2), 181-192.
- Rønnevik, H., Beskow, B., & Jakobsen, H. P. (1982). Structural and stratigraphic evolution of the Barents Sea. *Arctic Geology and Geophysics: Proceedings of the Third International Symposium on Arctic Geology. Memoir*, 8, 431-440.
- Rønnevik, H., & Jacobsen, H. P. (1984). Structural highs and basins in the western Barents Sea. *Petroleum Geology of the North European Margin*, 19-32.
- Sattar, N., Juhlin, C., Koyi, H., & Ahmad, N. (2017). Seismic stratigraphy and hydrocarbon prospectivity of the Lower Cretaceous Knurr Sandstone lobes along the southern margin of Loppa High, Hammerfest Basin, Barents Sea. *Marine and petroleum geology*, 85, 54-69.
- Schlische, R. W. (1995). Geometry and Origin of Fault-Related Folds in Extensional Settings *AAPG Bulletin*, 79, 1661-1678.
- Seldal, J. (2005). Lower Cretaceous: The next target for oil exploration in the Barents Sea. *Geological Society, London, Petroleum Geology Conference series*, 6(1), 231-240.
- Serck, C. S., & Braathen, A. (2019). Extensional fault and fold growth: impact on accommodation evolution and sedimentary fill. *Basin Research*, 1-24.
- Skuce, A. (1996). Forward modelling of compaction above normal faults: an example from the Sirte Basin, Libya. *Geological Society London, Special Publication*, 99(1), 135-146.
- Smelror, M., Petrov, O. V., Larssen, G. B., & Werner, S. C. (2009). Geological history of the Barents Sea. *Geological Survey of Norway*, 1-135.
- Sund, T., Skarpmes, O., Nørgård-Jensen, L. N., & Larsen, R. M. (1986). Tectonic Development and Hydrocarbon Potential Offshore Troms, Northern Norway. *AAPG Bulletin*, 68(7-8), 615-627.
- Vasquez, L., Nalpez, T., Ballard, J. F., Veslud, C. L. C. D., Simon, B., Dauteuil, O., & Bernard, X. D. (2018). 3D geometries of normal faults in a brittle-ductile sedimentary cover: Analogue modelling. *Journal of Structural Geology*, 112, 29-38.
- Walsh, J., Bailey, W. R., Childs, C., Nicol, A., & Bonson, C. G. (2003). Formation of segmented normal faults: a 3-D perspective. *Journal of Structural Geology*, 25(8), 1251-1262.
- Withjack, M. O., Olson, J., & Peterson, E. (1990). Experimental Models of Extensional Forced Folds. *AAPG Bulletin*, 74, 1038-1054.
- Worsley. (2008). The post-Caledonian development of Svalbard and the western Barents Sea. *Polar Research*, 27(3), 298-317.
- Worsley, & Nøttvedt, A. (2008). Vast lowland plains, coal and salt. In I. B. Ramberg, I. Bryhni, A. Nøttvedt, & K. Rangnes (Eds.), *The Making of a Land, Geology of Norway* (pp. 304-329). Trondheim: Norwegian Geological Association.
- Xiao, H., & Suppe, J. (1992). Origin of Rollover. *AAPG Bulletin*, 76, 509-529.
- Ziegler, W. H., Doery, R., & Scott, J. (1986). Tectonic habitat of Norwegian oil and gas. *Habitat of Hydrocarbons on the Norwegian Continental Shelf*, 3-19.